Chiral Dynamics of Baryons in the Perturbative Chiral Quark Model

DISSERTATION

zur Erlangung des Grades eines Doktors
der Naturwissenschaften

der Fakultät für Mathematik und Physik
der Eberhard-Karls-Universität zu Tübingen

vorgelegt von

Kem Pumsa-ard

aus Bangkok, Thailand

2006

Tag der mündlichen Prüfung:	27 Juli 2006
Dekan:	Prof. Dr. Peter Schmid
1. Berichterstatter:	Prof. Dr. Dr. h.c. mult. Amand Fäßler
2. Berichterstatter:	Prof. Dr. Thomas Gutsche

ABSTRACT

In this work we develop and apply variants of a perturbative chiral quark model (PCQM) to the study of baryonic properties dominantly in the low-energy region. In the PCQM baryons are considered in leading order as bound states of valence quarks with a nontrivial structure, while the sea-quark excitations are contained in a cloud of pseudoscalar mesons as imposed by chiral symmetry requirements. Since the valence quark structure dominates, pseudoscalar or chiral effects are treated perturbatively. In a first step we consider a noncovariant form of the PCQM, where confinement is modelled by a static, effective potential and chiral corrections are treated to second order, in line with similar chiral quark models. We apply the PCQM to the study of the electromagnetic form factors of the baryon octet. We focus in particular on the low-energy observables such as the magnetic moments, the charge and magnetic radii. In addition, the electromagnetic $N-\Delta$ transition is also studied in the framework of the PCQM, where meson cloud contributions play a decisive role. In the chiral loop calculations we consider a quark propagator, which is restricted to the quark ground state, or in hadronic language to nucleon and delta intermediate states, for simplicity. At this stage reasonable results can be achieved, where the role of the meson cloud, in particular for the $N-\Delta$ transition, is clearly elaborated. We furthermore include the low-lying excited states to the quark propagator, which influences the result at the level of 15%. In particular, the charge radius of the neutron and the transverse helicity amplitudes of the $N-\Delta$ transition are considerably improved by this additional effect. In a next step we develop a manifestly Lorentz covariant version of the PCQM, where in addition higher order chiral corrections are included. The full chiral quark Lagrangian is motivated by and in analogy to the one of Chiral Perturbation Theory (ChPT). This Lagrangian contains a set of low energy constants (LECs), which are parameters encoding short distance effects and heavy degrees of freedom. We evaluate the chiral Lagrangian to order $O(p^4)$ and to one loop to generate the dressing of the bare quark operators by pseudoscalar mesons. In addition we include the vector meson degrees of freedom in our study. Projection of the dressed quark operators on the baryonic level serves to calculate the relevant matrix elements. The main result of this technique is that the effects of the meson cloud and of the bare valence quarks factorize in the baryon matrix elements. In a first application of this scheme, we resort to a parameterization of the valence quark form factors in the electromagnetic sector. Constraints on these quark form factors are set by symmetries and by matching to model-independent predictions of ChPT. Physical applications are worked out for the masses and the magnetic moments of the baryon octet, the meson-nucleon sigma terms and the electromagnetic form factors of the nucleon. We demonstrate in particular that the meson cloud plays a vital role to explain the detailed structure of the electromagnetic form factors for momenta transfers up to 0.5 GeV^2.

ZUSAMMENFASSUNG

In dieser Arbeit entwickeln und untersuchen wir verschiedene Formen eines perturbativen, chiralen Quarkmodells (PCQM) zur Beschreibung baryonischer Eigenschaften im Niederenergiebereich. Im PCQM werden die Baryonen in führender Ordnung als gebundene Zustände von Valenzquarks mit nichttrivialer Struktur beschrieben. Zusätzliche Seequarkanregungen werden durch energetisch niedrigliegende, pseudoskalare Mesonen erzeugt, wobei die Ankopplung an die Quarks durch die chirale Symmetrie festgelegt ist. Da die Valenzquarks die Struktur der Baryonen dominieren, werden pseudoskalare oder chirale Effekte störungstheoretisch behandelt. Im ersten Schritt betrachten wir eine nicht-kovariante Form des PCQM, in welcher der Farbeinschluss (Confinement) durch ein statisches, effektives Potenzial modelliert und chirale Korrekturen bis zur zweiten Ordnung behandelt werden. In einer ersten Anwendung berechnen wir die elektromagnetischen Formfaktoren der Oktett-Baryonen, wobei Niederenergieobservable wie die magnetischen Momente, die Ladungs- und Magnetisierungsradien am zuverlässigsten beschrieben werden. Zusätzlich studieren wir die elektromagnetischen $N-\Delta$ Übergänge, wo die pseudoskalaren Mesonbeiträge eine entscheidende Rolle zur Erklärung der experimentellen Daten spielen. In den auftretenden Schleifendiagrammen der chiralen Korrekturen betrachten wir zunächst einen Quarkpropagator, welcher nur den Grundzustand, d.h. in hadronischer Sprache den N und Δ Zwischenzustand, beinhaltet. Mit dieser Vereinfachung können die Daten vernünftig beschrieben werden, wobei die Rolle der mesonischen Beiträge, insbesondere für den $N-\Delta$ Übergang, wesentlich ist. Der Einbezug niedrigliegender, angeregter Zustände im Quarkpropagator führt zu Beiträgen der Grössenordnung von bis zu 15%. Insbesondere der Ladungsradius des Neutrons und die transversalen Helizitätsamplituden der $N-\Delta$ hängen entscheidend von diesen zusätzlichen Beiträgen ab. Im nächsten Schritt entwickeln wir eine manifest Lorentz kovariante Version des PCQM, wobei chirale Korrekturen höherer Ordnung berücksichtigt werden können. Die vollständige, dynamische Beschreibung, welche in einer chiralen Lagrange-Funktion der Valenzquarks formuliert wird, steht in Analogie zur chiralen Störungstheorie (ChPT). Die Lagrange-Funktion enthält einen Satz von Niederenergiekonstanten (LECs), welche die kurzreichweitigen Effekte und die Beiträge schwerer Freiheitsgrade parametrisieren. Die chirale Lagrange-Funktion wird zur Ordnung $O(p^4)$ und in der Einschleifen-Näherung ausgewertet, um die durch die chiralen Effekte angezogenen Quarkoperatoren auszuwerten. Zusätzlich werden die Vektormesonen einbezogen. Durch Projektion der effektiven Quarkoperatoren auf baryonische Zustände werden die relevanten Matrixelemente der hadronischen Übergänge berechnet. Das Hauptergebnis dieser Technik ist, dass die Beiträge der Mesonen und der nackten Valenzquarks in den Amplituden faktorisieren. In einer ersten Anwendung dieses Modells greifen wir auf eine Parametrisierung der Formfaktoren der Valenzquarks zurück, welche im elektromagnetischen Sektor relevant sind. Diese Formfaktoren werden durch zusätzliche Symmetrien und durch Anpassung an modellunabhängige Vorhersagen der ChPT eingeschränkt. Anwendungen dieses chiralen

Quarkmodells werden für die Massen und magnetischen Momente des Baryonenoktetts, für die Meson-Nukleon Sigmaterme und die elektromagnetischen Formfaktoren des Nukleons ausgearbeitet. Insbesondere wird gezeigt, dass die chiralen Korrekturen eine entscheidende Rolle spielen, um die detaillierte Struktur der elektromagnetischen Formfaktoren für Impulstransfers bis zu 0.5 GeV^2 zu erklären.

Contents

1 Introduction **1**

2 Basics of the strong interaction **7**

2.1 The QCD Lagrangian 7

2.2 Chiral symmetry 10

2.3 Chiral symmetry breaking 13

2.4 Chiral perturbation theory 15

3 Electromagnetic structure of the nucleon **19**

3.1 Evidences of the nucleon structure 19

3.2 Elastic electron-nucleon scattering 20

3.3 Electromagnetic nucleon form factors 23

4 Perturbative chiral quark model **30**

4.1 Effective Lagrangian 31

4.2 Quark wave functions 33

4.3 Calculational technique 34

4.4 Renormalization 36

4.5 Physical applications 47

4.5.1 Electromagnetic form factors of the baryon octet 48

4.5.2 Electromagnetic $N - \Delta$ transition 55

4.6 Summary 61

5 Lorentz covariant chiral quark model **63**
5.1 Effective Lagrangian 63
5.1.1 Chiral Lagrangian 63
5.1.2 Inclusion of vector mesons 67
5.2 Dressing of quark operators 68
5.3 Matching to ChPT 72
5.4 Nucleon mass and meson-nucleon σ-terms 75
5.4.1 Nucleon mass 75
5.4.2 Pion-nucleon σ-terms 81
5.5 Physical applications 82
5.5.1 Baryon masses and meson-nucleon sigma-terms 82
5.5.2 Magnetic moments of the baryon octet 84
5.5.3 Nucleon electromagnetic form factors 90
5.5.4 Strong vector meson-nucleon form factors 103
5.6 Summary 106

6 Summary **108**

A Basic notions of the SU(3) group **112**

B Solutions of the Dirac equation for the effective potential **114**

C Renormalization of the nucleon charge in the PCQM **117**

D Electromagnetic $N - \Delta$ transition in the PCQM **119**

E Calculational technique of quark-meson loop diagrams **123**

F Loop Integrals **127**

G Electromagnetic meson-cloud form factors **133**

H Meson-nucleon sigma-terms **140**

Chapter 1

Introduction

Proton and neutron, as the basic building blocks of the atomic nuclei, play an important role in physics. The understanding of their properties and structure will probably lead us to a deeper understanding of the mechanism of the strong interaction in nature. Since the masses of the proton ($M_p = 938.27$ MeV) and the neutron ($M_n = 939.57$ MeV) are nearly identical, one considers both of them as two different states of the same particle, namely, the nucleon. Experiments point out that the nucleon is not a point-like particle but contains a subtle structure. First evidence came from the measurement of the magnetic moment of the proton in which a strong deviation from the value of the point-like particle, hence an anomalous magnetic moment, was observed. A detailed knowledge of the spatial distribution of the electromagnetic current in the nucleon was achieved by elastic electron scattering on the nucleon which started in the fifties. Deep inelastic scatterings of electrons on the nucleon, originally performed in the late sixties, lead to the evidence for point-like scattering centers in the nucleon and consequently to the knowledge of quark and gluon degrees of freedom. Other evidence for the structure of the nucleon comes from the rich excitation spectrum of the nucleon. Compton scattering is a further tool to determine the electromagnetic response or polarizabilities of the nucleon. The searching for and the determination of the structure of the nucleon is one vital task in nuclear and particle physics. Among all the fundamental interactions, the electromagnetic interaction of the nucleon gives an utmost information. This leads to the knowledge of the electromagnetic structure of the nucleon which tells us how the charge and the current are distributed within the nucleon. The subject is actively studied both on theoretical and experimental sides. Recently [1, 2, 3], experiments utilizing polarized beams and targets significantly improved the previous data based on the Rosenbluth separation technique. The ongoing programs for the complete measurement of the electromagnetic form factors of the nucleon at laboratories around the world will lead to more precise data, which is important for the theoretical study.

Besides the nucleon many other strongly interacting particles, hadrons, are

observed both in scattering and in cosmic ray experiments. Amount to these numerous number of particles, one originally faced a difficulty in order to classify them. Group theory plays an important role in such a classification, especially the SU(3)-flavor group which can fit the observed low-lying baryons into the octet and decuplet. The original idea proposed by Gell-Mann [4] and, independently, by Zweig [5] suggests that there could be particles having quantum numbers associated with the fundamental representation of SU(3). By assigning u, d and s quarks and their antiparticles $\bar{u}$, $\bar{d}$ and $\bar{s}$ as the fundamental representations $\mathbf{3}$ and $\bar{\mathbf{3}}$ of SU(3), respectively, hadrons can be constructed from these representations. The quark hypothesis was at first a purely mathematical tool for classifying the zoo of subatomic particles. However, evidences, for example in deep inelastic electron scattering, point to the existence of quarks as real particles. Therefore, the strongly interacting hadrons are believed to be built up from the combinations of quarks and antiquarks. In a minimal configuration, baryons are composed of three valence quarks whereas mesons are composed of a quark-antiquark pair. These quark-antiquark combinations are constructed such that the correct quantum numbers associated with the corresponding hadrons are achieved. For the nucleon, the quark flavor contents of the proton and the neutron are uud and udd, respectively. In addition, experiments reveal the existence of heavier quarks, i.e. the c, b and t quarks so that at the present time we have six quark flavors along with their antiquarks.

Despite many attempts, the quark, which is considered as a particle with a fractional electric charge, was never observed in an asymptotically free state in nature. From this fact it is deduced that there exists a mechanism, named confinement, preventing that free quarks exist. This point is directly connected to a new degree of freedom called "color", originally introduced to restore the Pauli exclusion principle in the Δ^{++} system with the quark content uuu. Traditionally, we label the color degrees of freedom as "red", "blue" and "green" for each quark flavor. The non-observation of free quarks is therefore consistent with the proposal that hadrons contain no net color i.e they are color singlets.

The color degrees of freedom play a crucial role in the strong interaction, which goes beyond the usual labelling of quarks in hadrons to obtain a color singlet. The color charges are considered as the fundamental representation of the gauge group $SU(3)$, raising them to dynamical degrees of freedom. Local gauge invariance under the color SU(3) leads to the fundamental theory of strong interaction called Quantum Chromodynamics (QCD). QCD is believed to be the correct theory for describing the physics of the strong interaction. The basic particles in QCD are quarks and their interactions are mediated by exchange of gluons which are the gauge quanta of the color fields. Two important properties of QCD are the asymptotic freedom and the color confinement. The asymptotic freedom is related to the experimental result that in the high energy regime or at small distances the interaction between the quarks is small. In this regime the coupling constant between quarks and gluons is therefore small and a perturbative method can be

applied to evaluate QCD. However, in the low energy regime where the strong running coupling constant is large, at the order of one, the perturbative method cannot be applied and one has to deal with a non-perturbative approach.

In QCD the quark masses are scale dependent, they are also called running quark masses. At the scale of 1 GeV, the masses of the light quarks (u, d and s quarks) are rather small compared to the nucleon mass [6, 7]. When we neglect the small quark masses and consider light quarks as massless particles, another global symmetry arises in the strong interaction which is rather important in the low energy regime. This is the so-called chiral symmetry. Since the spectrum of the hadrons, at least in the known sector, does not display parity doublets, we believe that the chiral symmetry is spontaneously broken and as a consequence there must exist massless particles called the Goldstone bosons. Pions, although massive, are interpreted as the Goldstone bosons of the spontaneously broken chiral symmetry because their masses are small compared to the nucleon mass. The finite value for the pion mass is due to the explicit breaking of chiral symmetry when the quarks acquire their small, but physical mass values.

Since the non-perturbative aspect of the nucleon structure cannot be solved analytically from QCD, one has to use alternative ways in order to study the nucleon structure. Different approaches were proposed, for example, QCD sum rule, lattice QCD, $1/N_c$ expansion, etc. However, the most convenient language for the treatment of light hadrons at small energies is Chiral Perturbation Theory (ChPT) [8, 9, 10], which is considered as an effective field theory of the strong interaction. ChPT is based on a chiral expansion of the QCD Green functions, i.e. an expansion in powers of the external hadron momenta and quark masses. ChPT works perfectly in the meson sector, as was proved in Ref. [9, 10], especially in the description of pion-pion interactions. In Ref. [11] a manifestly Lorentz invariant form of baryon ChPT was suggested. However, in the baryonic sector of ChPT a new scale parameter associated with the nucleon mass shows up and the formulation of a consistent chiral expansion of matrix elements is lost. In particular, the chiral expansion of the loop diagrams starts at the same order as the tree-level diagrams. This leads to an inconsistency in the perturbation theory, i.e. the higher order graphs contribute to the low-order ones and the physical quantities require renormalization at every order of the expansion. The method called Heavy Baryon Chiral Perturbation Theory (HBChPT) [12] overcomes the problems of chiral power counting by keeping track of power counting at every step of the calculation. The drawback of HBChPT is that it is based on the nonrelativistic expansion of the nucleon propagator which results in the lack of manifest Lorentz covariance. Another problem for HBChPT is that the nonrelativistic expansion of the pion-nucleon scattering amplitude generates a convergence problem of the perturbative series in part of the low-energy region.

A new method for the study of baryons in ChPT was suggested in Refs. [13, 14, 15, 16]. It is based on the infrared dimensional regularization of loop diagrams [13], which exploits the advantages of the two frameworks formulated in

Refs. [11] and [12], while avoiding their disadvantages. Alternatively, an equivalent formulation of baryon ChPT based on the method called extended on-mass-shell renormalization was suggested in Refs. [17, 18, 19]. A successful application of the improved versions of baryon ChPT to nucleon properties has been performed, for example, in Refs [13, 18, 19, 20, 21]. The multi-nucleon sector in baryon ChPT was studied in Ref. [22]. The consistent inclusion of vector mesons in baryon ChPT has been done in Ref. [18], which helped to successfully improve the momentum behavior of the nucleon form factors up to approximately 0.4 GeV^2 as shown in Ref. [19]. Note, that ChPT is formulated on the hadronic level, therefore the important features of low-energy QCD, such as confinement and hadronization are not addressed in ChPT.

Alternatively, physical insights into the structure and interactions of hadrons can be gained by model building, that is phenomenology. By taking into account assumed properties of QCD, like chiral symmetry and confinement, many models of the nucleon were proposed. Chiral quark models describe the elementary baryon, the nucleon, as a bound state of valence quarks supplied by the sea-quark excitation in form of the pions. If the valence quark content dominates the nucleon, pion contributions can be treated perturbatively. The origin of this kind of models is the MIT bag model [23]. In the MIT bag model the three valence quarks are confined in a spherical region called a bag. However, chiral symmetry is violated in the MIT bag model due to the confinement mechanism. The cloudy bag model [24] restores chiral symmetry to the MIT bag model by allowing the confined quarks to interact with the pion fields at the surface of the bag. The contributions arising from the pion cloud contribute significantly to the physical observables. Similar to the cloudy bag model, chiral quark models were developed [25, 26] where the unphysical sharp boundary of the bag is replaced by a finite surface thickness of the quark core. Confinement is introduced through a static quark potential of general form with adjustable parameters. The perturbative technique allows a fully quantized treatment of the pion field up to a given order in accuracy. Although formulated on the quark level, with confinement put in phenomenologically, perturbative chiral quark models are formally close to ChPT formulated on the hadron level. Alternatively, when the pion cloud is assumed to dominate the nucleon structure this effect has to be treated non-perturbatively. Refs. [27] are examples of the non-perturbative approach, where the chiral quark soliton model was derived. This model is based on the concept that the QCD instanton vacuum is responsible for the spontaneous breaking of chiral symmetry which in turn leads to an effective chiral Lagrangian at low energy. On the phenomenological level the chiral quark soliton model tends to be advantageous in the description of the nucleon spin structure, that is for large momentum transfers, but is comparable to the original perturbative chiral quark models in the description of low-energy nucleon properties.

As a further development of chiral quark models with a perturbative treatment of the pion cloud, we recently developed the so-called Perturbative Chiral

Quark Model (PCQM) for the description of low-energy properties of baryons. This approach is based on the work by Gutsche and Robson [26, 28]. In the PCQM baryons are considered as bound states of valence quarks surrounded by a cloud of pseudoscalar mesons, as imposed by chiral symmetry requirements. The confinement of the quarks in the PCQM arises from a static potential implying noncovariance. Starting with the SU(3)-flavor version of the quark fields means that by chiral symmetry we have already taken into account the pseudoscalar octet mesons (π, K, η) as the Goldstone bosons. This is an extension of other chiral quark models which usually considered only the pion cloud. By treating these pseudoscalar meson as small fluctuations around the three-quark core, the perturbative method can be applied in terms of an expansion of the small current quark masses ($\hat{m}$, m_s) and the expansion parameter $1/F$, where F is the pion decay constant in the chiral limit. To simplify the calculation in the PCQM the quark propagator in loop diagrams is restricted to the ground state, which in hadronic language refers to intermediate N and Δ states. Following this truncation of the quark propagator, several successful applications within the framework of the PCQM have been performed. Examples of previous applications based on this truncation are σ-term physics [29], the electromagnetic structure of the nucleon [30], $\pi - N$ scattering [31] and the strange nucleon form factors [32].

A further improvement of the PCQM was achieved by including the low-lying quark excitations in the quark propagator relevant in loop calculations. This was done in the study of the electromagnetic $N - \Delta$ transitions [33]. Excited state quark propagators contribute at the level of 15% to the electromagnetic $N - \Delta$ helicity amplitudes, $A_{1/2}(Q^2 = 0)$ and $A_{3/2}(Q^2 = 0)$. Other applications by including the excited quark states contributions were done in the PCQM as well. Examples are the electromagnetic form factors of the octet baryons [34], an updated analysis of the meson-nucleon σ-terms [35], the nucleon axial charge [36] and the nucleon polarizabilities [37]. All of these applications point to the same conclusion that the quark excited state contributions to the loop diagrams are crucial.

In a next step we performed a further formulation of the PCQM in a manifestly Lorentz covariant approach [38, 39]. The main idea is to dress the quark operators by using the chiral Lagrangian taken from baryon ChPT. The physical observables are obtained from these dressed quark operators by calculating the matrix elements projected on the baryonic level. Constraints of the model can be fixed by using the symmetries of the system and the matching to the original ChPT. Other Low Energy Constants (LECs) which cannot be fixed emerge as parameters of the model which in turn are adjusted by considering various physical observables. We emphasize here the study of the electromagnetic properties of the nucleon and the baryon octet. Physical applications of this approach are the baryon octet masses, the meson-nucleon σ-terms, the magnetic moments of the octet baryon, the electromagnetic form factors of the nucleon and the coupling of vector mesons to the nucleon.

In the course of this thesis we will proceed as follows. In Chapter 2 we will give a brief introduction to the concept of chiral symmetry in the strong interaction. The electromagnetic structure of the nucleon and its corresponding form factors will be presented in Chapter 3. In Chapter 4 we outline the construction of the PCQM based on the non-covariant approach and discuss the physical applications. These are the magnetic moments and the electromagnetic form factors of the octet baryons and the electromagnetic $N - \Delta$ transitions. Chapter 5 will contain the fully covariant treatment of the PCQM which is the improved version of our model. Physical applications concern properties like the meson-nucleon σ-terms, the mass of the nucleon, the octet baryon magnetic moments, the electromagnetic form factors of the nucleon and the strong coupling of vector mesons to the nucleon. Finally, we will give the summary of this work in Chapter 6.

Chapter 2

Basics of the strong interaction

The elementary theory of the strong interaction is Quantum Chromodynamics (QCD). QCD is a local gauge theory which describes the interaction of quarks and gluons. The quarks and gluons possess color which is the basic quantum number associated with QCD. Actually, conservation of color means that QCD is invariant under $\mathrm{SU}(3)_c$ color transformations. Another important symmetry of the QCD Lagrangian is chiral symmetry. This symmetry is approximate and is fulfilled in the limit of massless quarks. Approximate chiral symmetry is widely manifest in low-energy hadron phenomenology and is therefore an important constraint in the derivation of phenomenological approaches motivated by QCD. In this chapter we briefly discuss the basic notions of the QCD Lagrangian and the aspects of chiral symmetry, including its explicit and spontaneous breaking. Finally, the effective field theory for the strong interaction at low energies– Chiral Perturbation Theory (ChPT)– will be briefly reviewed.

2.1 The QCD Lagrangian

In QCD, the matter fields are the quark fields $q_f^c(x)$ which are Dirac particles with two specific quantum numbers, color (c) and flavor (f). Their free Lagrangian is written as

$$\mathcal{L} = \bar{q}_f^i(x)\,(i\,\not{\partial} - m_f)\,q_f^i(x)\,. \tag{2.1}$$

Here we employ the slash notation: $\not{\partial} \equiv \partial_\mu \gamma^\mu$. For each quark flavor $f = u,\, d,\, s,\, c,\, b$ and t, it contains three additional quantum numbers, the color charge, $i = r,\, g,\, b$.

Originally, the need for the color degrees of freedom arose due to the fact that the Pauli exclusion principle is not valid in the construction of the quark model. As an explicit example, let us consider the spin-flavor wave function of the Δ^{++} baryon which is

$$\left|\Delta^{++}, J_z = \frac{3}{2}\right\rangle = |u\ \uparrow\rangle|u\ \uparrow\rangle|u\ \uparrow\rangle. \tag{2.2}$$

This spin-flavor wave function is composed of three u-quarks with spin-projection $s_z = 1/2$ which are identical to each other. However, assumes that the spatial part of the wave function is symmetric for a ground state configuration, this certainly violates the Pauli exclusion principle. To remedy this, other quantum numbers as color must be introduced to each quark to make them differ from each other. Nevertheless, the color degree of freedom plays a more rigorous role in the strong interaction, since the color group $\mathrm{SU}(3)_c$ acts as the gauge group of the strong interaction.

The color charges of the quarks form a fundamental representation related to the generators of $\mathrm{SU}(3)_c$ i.e. the Gell-Mann matrices λ_a^c. The explicit forms of λ_a^c are shown in Appendix A. The free Lagrangian of Eq. (2.1) is invariant under the "global" transformation of the color degrees of freedom,

$$\begin{aligned} q_f^i(x) &\mapsto U[\theta]q_f^i(x), \\ U[\theta] &= \exp\left(-i\sum_{a=1}^{8}\frac{\lambda_a}{2}\theta_a\right) \equiv \exp\left(-i\frac{\lambda_a}{2}\theta_a.\right), \end{aligned} \tag{2.3}$$

where $\theta = (\theta_1, \ldots, \theta_8)$ are arbitrary constants (for aspects of the $\mathrm{SU}(3)_c$ group see Appendix A). Note, that the summation over the same indices is implied.

The requirement of the local gauge invariance principle can be applied to the free Lagrangian of the matter fields to generate the interaction of the matter fields with the gauge fields which are the mediators of the interaction. In Quantum Electrodynamics (QED) it is the photon which is the gauge field of the electromagnetic interaction. Considering QED as a prototype, interactions in QCD can be constructed by extension of the global transformations to the "local" transformations

$$q_f^i(x) \mapsto U[\theta(x)]q_f^i(x), \tag{2.4}$$

where $\theta(x)$ is now space-time dependent. In order to maintain the invariance of the Lagrangian of Eq. (2.1) under this local gauge transformation one has to introduce the gauge fields which interact with the quark fields. The usual way is to replace

the normal space-time derivative, $\partial_\mu q_f^i(x)$, of the free quark Lagrangian by the so-called "covariant derivative", $D_\mu q_f^i(x)$,

$$\partial_\mu q_f^i(x) \to D_\mu q_f^i(x). \tag{2.5}$$

This covariant derivative is constructed such that it has the same transformation property as the quark fields, i.e.

$$\begin{aligned} D_\mu q_f^i(x) &\mapsto U[\theta(x)] D_\mu q_f^i(x) \\ &= \exp\left(-i\frac{\lambda_a}{2}\theta_a(x)\right) D_\mu q_f^i(x). \end{aligned} \tag{2.6}$$

Eq. (2.6) can be fulfilled by the introduction of the gauge fields $\mathcal{A}_\mu^a(x)$ in the covariant derivative

$$D_\mu q_f^i(x) = (\partial_\mu - ig\mathcal{A}_\mu(x))\, q_f^i(x), \tag{2.7}$$

where $\mathcal{A}_\mu(x) = \lambda_a \mathcal{A}_\mu^a(x)/2$ and g is a coupling constant. These $\mathcal{A}_\mu^a(x)$ are the gluon fields which serve as the gauge fields of the strong interaction. The transformation of the gluon fields under the gauge group $\mathrm{SU}(3)_c$ is

$$\mathcal{A}_\mu(x) \mapsto U[\theta(x)]\mathcal{A}_\mu(x)U^\dagger[\theta(x)] - \frac{i}{g}\partial_\mu U[\theta(x)]U^\dagger[\theta(x)]. \tag{2.8}$$

As in QED, the field strength tensor $\mathcal{G}_{\mu\nu,a}(x)$ can be defined in QCD as well. The explicit form for $\mathcal{G}_{\mu\nu,a}(x)$ is

$$\mathcal{G}_{\mu\nu,a}(x) = \partial_\mu \mathcal{A}_{\nu,a}(x) - \partial_\nu \mathcal{A}_{\mu,a}(x) + g f_{abc}\mathcal{A}_{\mu,b}(x)\mathcal{A}_{\nu,c}(x), \tag{2.9}$$

where f_{abc} are the structure constants of SU(3) as shown in Eq. (A.7). The difference with respect to QED is the presence of the last term in Eq. (2.9) originating from the non-Abelian properties of SU(3). The transformation of the field strength tensor is simpler if one defines the tensor $\mathcal{G}_{\mu\nu}(x)$ such that

$$\mathcal{G}_{\mu\nu}(x) \equiv \frac{\lambda_a}{2}\mathcal{G}_{\mu\nu,a}(x) \mapsto U[\theta(x)]\mathcal{G}_{\mu\nu}(x)U^\dagger[\theta(x)]. \tag{2.10}$$

The free gluonic Lagrangian can be written as

$$\mathcal{L} = -\frac{1}{4}\mathcal{G}_{\mu\nu,a}(x)\mathcal{G}_a^{\mu\nu}(x) = -\frac{1}{2}\mathrm{Tr}(\mathcal{G}_{\mu\nu}(x)\mathcal{G}^{\mu\nu}(x)). \tag{2.11}$$

The full QCD Lagrangian is therefore

$$\mathcal{L}_{QCD} = \sum_{f=u,d,s,c,b,t} \bar{q}_f^i(x)\,(i\not{D} - m_f)\,q_f^i(x) - \frac{1}{4}\mathcal{G}_{\mu\nu,a}(x)\mathcal{G}_a^{\mu\nu}(x). \tag{2.12}$$

Finally we note that in addition to the coupling between the quarks and gluons, gluon fields also interact with themselves. This is a consequence of the non-Abelian nature of the group SU(3). Due to Eq. (2.9) and Eq. (2.11) there exist the three- and four-gluonic self-coupling terms which are proportional to g and g^2, respectively. This is not the case for the electromagnetic fields in QED, but in QCD the gluon fields are "charged" i.e. they carry "color", whereas the photon carries no (electric) charge.

2.2 Chiral symmetry

In the limit where the light quark masses vanish, the QCD Lagrangian of Eq. (2.12) has another important symmetry. This is the so-called "chiral symmetry". This symmetry is only approximate since in reality quarks possess a small but finite mass. Let us first consider the quark masses related to the light and the heavy quarks. The sector of light quarks is composed of the u, d and s quarks with the estimated masses [43]

$$m_u = 1.5 - 4 \text{ MeV}, \quad m_d = 4 - 8 \text{ MeV} \quad \text{and} \quad m_s = 80 - 130 \text{ MeV}. \tag{2.13}$$

The c, b and t quarks are considered as heavy quarks with masses ≥ 1 GeV. In the low-energy regime the heavy quarks do not play a role due to their large masses. Since the u, d and s quarks are much lighter than the hadronic mass scale of 1 GeV this suggests that one can treat the current quark masses as a small perturbation. Therefore, for the low-energy regime and in the chiral limit, where m_u, m_d, $m_s \to 0$, the appropriate QCD Lagrangian becomes

$$\mathcal{L}_{QCD}^0 = \sum_{f=u,d,s} \bar{q}_f^i(x) i\not{D} q_f^i(x) - \frac{1}{4}\mathcal{G}_{\mu\nu,a}(x)\mathcal{G}_a^{\mu\nu}(x). \tag{2.14}$$

The symmetry of the Lagrangian (2.14) can be made explicit if one decomposes the quark fields in terms of left- and right-handed components. This can be achieved through the projection operators P_R and P_L defined by

$$P_R = \frac{1}{2}(1+\gamma_5), \quad P_L = \frac{1}{2}(1-\gamma_5). \tag{2.15}$$

With these operators the right- and left-handed components of the quark fields can be written as

$$q^i_{R,f}(x) = P_R q^i_f(x), \quad q^i_{L,f}(x) = P_L q^i_f(x). \tag{2.16}$$

Consequently, Eq. (2.14) can be rewritten as

$$\mathcal{L}^0_{QCD} \;=\; \bar{q}_R(x) i \not{D} q_R(x) + \bar{q}_L(x) i \not{D} q_L(x) - \frac{1}{4}\mathcal{G}_{\mu\nu,a}(x)\mathcal{G}^{\mu\nu}_a(x), \tag{2.17}$$

where we represent the right- and left-handed quark fields in terms of the column vectors

$$q_R = \begin{pmatrix} q_{R,u} \\ q_{R,d} \\ q_{R,s} \end{pmatrix}, \quad q_L = \begin{pmatrix} q_{L,u} \\ q_{L,d} \\ q_{L,s} \end{pmatrix}, \tag{2.18}$$

and we simplify the notation by dropping the color index. The respective space on which the operators of (2.17) act should be clear from the context. We consider the "global" unitary transformation of the quark fields of Eq. (2.18) with

$$q_L \mapsto U_L q_L, \quad q_R \mapsto U_R q_R, \tag{2.19}$$

and

$$U_L = \exp\left(-i\frac{\lambda_a}{2}\theta^L_a\right), \qquad U_R = \exp\left(-i\frac{\lambda_a}{2}\theta^R_a\right), \tag{2.20}$$

where $\theta^{L(R)}_a$ are independent, real parameters. The group of this transformation is denoted by $\mathrm{SU}(3)_L\times\ \mathrm{SU}(3)_R$. Obviously, Eq. (2.17) is invariant under such transformations and hence is referred to as the "chiral symmetry" of QCD. Since U_L and U_R contain altogether 16 real parameters, the symmetry, due to Noether's theorem, results in 16 conserved currents associated with the transformation of Eq. (2.19). These conserved currents are

$$R^\mu_a = \bar{q}_R\gamma^\mu\frac{\lambda_a}{2}q_R, \qquad L^\mu_a = \bar{q}_L\gamma^\mu\frac{\lambda_a}{2}q_L, \tag{2.21}$$

with

$$\partial_\mu R^\mu_a = 0, \qquad \partial_\mu L^\mu_a = 0. \tag{2.22}$$

Instead of working with the left- and right-handed currents, one conventionally considers the linear combinations

$$\begin{aligned} V_a^\mu &= R_a^\mu + L_a^\mu = \bar{q}\gamma^\mu \frac{\lambda_a}{2} q, \\ A_a^\mu &= R_a^\mu - L_a^\mu = \bar{q}\gamma^\mu \gamma_5 \frac{\lambda_a}{2} q, \end{aligned} \tag{2.23}$$

together with

$$\partial_\mu V_a^\mu = 0, \qquad \partial_\mu A_a^\mu = 0. \tag{2.24}$$

These are the vector and axial currents. Note, that a simple phase transformations of q_L and q_R also results in an invariance of $\mathcal{L}^0_{QCD}$. The corresponding group of transformations are referred to as $\mathrm{U}(1)_V$ and $\mathrm{U}(1)_A$, if q_R and q_L transform with the same and the opposite phases, respectively. Consequently, there exist two additional conserved currents

$$V^\mu = \bar{q}\gamma^\mu q, \qquad A^\mu = \bar{q}\gamma^\mu \gamma_5 q, \tag{2.25}$$

with $\partial_\mu V^\mu = \partial_\mu A^\mu = 0$.

Up to now all considerations relate to classical fields, where all the vector and axial currents are conserved. When extending the symmetry considerations to quantum fields, special care must be taken for the singlet axial-vector A^μ, since it is no longer conserved. Instead, extra terms arise, referred to as "anomalies", which presented as

$$\partial_\mu A^\mu = \frac{3g^2}{32\pi^2} \epsilon_{\mu\nu\rho\sigma} \mathcal{G}_a^{\mu\nu} \mathcal{G}_a^{\rho\sigma}, \tag{2.26}$$

where $\epsilon_{\mu\nu\rho\sigma}$ is the totally antisymmetric tensor with $\epsilon_{0123} = 1$. Furthermore, non-vanishing current quark masses will contribute to Eq. (2.26) as well, which we will see later. Moving from the level of classical to quantum fields the global $\mathrm{U}(3)_R \times \mathrm{U}(3)_L$ symmetry of $\mathcal{L}^0_{QCD}$ is reduced to a global $\mathrm{SU}(3)_R \times \mathrm{SU}(3)_L \times \mathrm{U}(1)_V$ symmetry.

Finally, after quantization, we note that corresponding to the conserved currents V_a^μ, A_a^μ and V^μ we have the conserved charge operators Q_V^a, Q_A^a and Q_V. These operators form the algebra

$$\begin{aligned} [Q_V^a, Q_V^b] &= i f_{abc} Q_V^c, \\ [Q_V^a, Q_A^b] &= i f_{abc} Q_A^c, \\ [Q_A^a, Q_A^b] &= i f_{abc} Q_V^c, \\ [Q_V^a, Q_V] &= [Q_A^a, Q_V] = 0. \end{aligned} \tag{2.27}$$

The algebra which is constructed from the currents themselves is known as "current algebra". In the predawn of QCD, where the elementary origin of chiral symmetry was not understood yet, current algebra was already applied to the study of low-energy hadronic processes.

2.3 Chiral symmetry breaking

Previously, we have shown that in the chiral limit the Lagrangian $\mathcal{L}^0_{QCD}$ has a $\mathrm{SU}(3)_R \times \mathrm{SU}(3)_L \times \mathrm{U}(1)_V$ symmetry which results in the conserved charge operators Q^a_V, Q^a_A and Q_V. If $\mathcal{H}^0_{QCD}$ is the Hamiltonian corresponding to $\mathcal{L}^0_{QCD}$, this means that

$$[H^0_{QCD}, Q^a_V] = [H^0_{QCD}, Q^a_A] = [H^0_{QCD}, Q_V] = 0. \tag{2.28}$$

By considering the symmetry of the vacuum state $|0\rangle$, above symmetry of the Lagrangian can be realized in two modes. The first realization relies on the assumption that the vacuum has exactly the same symmetry as the Lagrangian. As a consequence the vacuum state is annihilated by the conserved charge operators

$$Q^a_V|0\rangle = Q^a_A|0\rangle = 0. \tag{2.29}$$

This realization in which the Lagrangian and the vacuum share the same symmetry is called the "Wigner-Weyl" mode of chiral symmetry. As a consequence the hadronic spectrum of positive and negative parity states built upon the vacuum is degenerate resulting in parity doublets. However, this is not the case in the observed spectrum of hadrons, e.g. the light pseudoscalar ($J^\pi = 0^-$) mesons have masses much lower than those of the lightest scalar ($J^\pi = 0^+$) mesons.

Another realization of chiral symmetry is achieved when the vacuum state of the system does not share the symmetry of the Lagrangian. This realization is called the Nambu-Goldstone mode of chiral symmetry and the symmetry is said to be "hidden" or "spontaneously broken". Since the approximate validity of SU(3) flavor symmetry suggests that $Q^a_V|0\rangle = 0$, in the Nambu-Golstone realization we are left with

$$Q^a_A|0\rangle \neq 0. \tag{2.30}$$

As a result of the spontaneously broken symmetry there exist massless particles the so-called "Goldstone bosons", as evident from Goldstone's theorem. In nature, chiral symmetry is realized in the Nambu-Goldstone mode, since the observed hadron spectrum contains the rather light pseudoscalar mesons (π, K, η) in comparison to

the scale set by the nucleon mass of ~ 1 GeV. Hence the low-lying pseudoscalar mesons are interpreted as Goldstone bosons. The finite but small masses of the π, K and η mesons arise from the fact that the quarks have a nonvanishing current mass. Then, "explicit" symmetry breaking due to the quark masses is responsible for the finite masses of the π, K and η mesons. Therefore, the SU$(3)_R\times$ SU$(3)_L\times$ U$(1)_V$ symmetry is spontaneously broken down to the SU$(3)_V\times$ U$(1)_V$ symmetry.

The spontaneous breaking of chiral symmetry is closely related to the nonvanishing of the order parameter, the "quark condensate", which is defined as

$$\langle 0|\bar{q}q|0\rangle \equiv \langle \bar{q}q\rangle = \langle \bar{u}u\rangle + \langle \bar{d}d\rangle + \langle \bar{s}s\rangle. \tag{2.31}$$

The condition $Q_V^a|0\rangle = 0$ suggests that $\langle \bar{u}u\rangle = \langle \bar{d}d\rangle = \langle \bar{s}s\rangle = 0$, whereas $Q_A^a|0\rangle \neq 0$ results in

$$\langle \bar{u}u\rangle = \langle \bar{d}d\rangle = \langle \bar{s}s\rangle \neq 0. \tag{2.32}$$

The spontaneous breaking of chiral symmetry induces a rearrangement of the ground state such that it is populated by scalar quark-antiquark pairs with nonzero expectation values.

Up to now we have considered the Lagrangian $\mathcal{L}^0_{QCD}$ for massless quarks and also discussed the scenario of the spontaneously broken chiral symmetry. Nevertheless, the current quark masses, although, they are small, do not vanish. The finite values of the quark masses give rise to explicit breaking of chiral symmetry due to the presence of a quark mass term in the QCD Lagrangian

$$\mathcal{L}_M = -\bar{q}(x)\mathcal{M}q(x), \tag{2.33}$$

where $\mathcal{M} = \mathrm{diag}(m_u, m_d, m_s)$ is the quark mass matrix. Including the explicit quark mass terms the divergence of the various currents becomes

$$\begin{aligned}
\partial_\mu V_a^\mu &= i\bar{q}\left[\mathcal{M}, \frac{\lambda_a}{2}\right] q, \\
\partial_\mu A_a^\mu &= i\bar{q}\left\{\mathcal{M}, \frac{\lambda_a}{2}\right\} \gamma_5 q, \\
\partial_\mu V^\mu &= 0, \\
\partial_\mu A^\mu &= 2i\bar{q}\mathcal{M}\gamma_5 q + \frac{3g^2}{32\pi^2}\epsilon_{\mu\nu\rho\sigma}\mathcal{G}_a^{\mu\nu}\mathcal{G}_a^{\rho\sigma},
\end{aligned} \tag{2.34}$$

where the anomaly of Eq. (2.26) is taken into account for completeness. Note, that V^μ is always conserved, whereas V_a^μ is only conserved when all the quark masses are equal. However, A_a^μ is not conserved and this is the microscopic origin of the so-called Partially Conserved Axial-vector Current (PCAC).

2.4 Chiral perturbation theory

Unfortunately, perturbative methods in QCD cannot be applied directly to hadronic systems in the low-energy regime due to the large coupling constant. However, phenomena in the low-energy region can be studied in terms of Effective Field Theory (EFT). The idea of the EFT was originally proposed by Weinberg [8] in 1979 stating that "... if one writes down the most general possible Lagrangian, including all terms consistent with assumed symmetry principles, and then calculates matrix elements with this Lagrangian to any given order of perturbation theory, the result will simply be the most general possible S-matrix consistent with analyticity, perturbative unitarity, cluster decomposition and the assumed symmetry principles." The link between QCD and the EFT can be employed through the generating functional. In the presence of external fields the QCD Lagrangian in Eq. (2.14) reads

$$\mathcal{L}_{ext} = \mathcal{L}^0_{QCD} + \bar{q}\gamma^\mu(v_\mu + \gamma_5 a_\mu)q - \bar{q}(s - i\gamma_5 p)q, \tag{2.35}$$

where, v_μ, a_μ, s and p are the external fields concerning vector, axial vector, scalar and pseudoscalar currents, respectively. The generating functional Z is related to $\mathcal{L}_{ext}$ and can be considered as the vacuum to vacuum transition amplitude in the presence of external fields i.e.

$$\begin{aligned} \exp(iZ[v,a,s,p]) &= \langle 0|T\exp\left[i\int d^4x\mathcal{L}_{ext}(x)\right]|0\rangle \\ &= \langle 0_{\text{out}}|0_{\text{in}}\rangle_{v,a,s,p}. \end{aligned} \tag{2.36}$$

In terms of EFT with some asymptotic hadron fields as the relevant degrees of freedom rather than the quark and gluon fields, the low-energy representation of the generating functional Z can be obtained by the use of an effective Lagrangian $\mathcal{L}_{eff}$. In the path-integral formalism this can be written as

$$\exp(iZ[v,a,s,p]) = N\int[dU]\exp\left(i\int d^4x\mathcal{L}_{eff}(U,v,a,s,p)\right), \tag{2.37}$$

where U is a matrix containing the asymptotic fields. This leads to the development of Chiral Perturabation Theory (ChPT) [8, 9, 10, 11], which is the EFT of strong interactions at low energies.

ChPT was first applied to the study of the system of Goldstone bosons which originate from the spontaneous breaking of chiral symmetry of the QCD Lagrangian. As mention earlier, instead of considering the quark and gluon fields as the elementary degrees of freedom of the theory, the active degrees of freedom

in ChPT are the asymptotically observed states, the hadrons. In the mesonic sector, the effective Lagrangian is composed of the string of terms as

$$\mathcal{L}_{eff} = \mathcal{L}_2 + \mathcal{L}_4 + \mathcal{L}_6 + \cdots , \tag{2.38}$$

where the subscripts refer to the order in the momentum and quark mass expansion. The lowest-order effective Lagrangian $\mathcal{L}_2$ which contains two derivatives and one quark mass term is

$$\mathcal{L}_2 = \frac{F^2}{4}\mathrm{Tr}\left[D_\mu U (D^\mu U)^\dagger + \chi U^\dagger + U\chi^\dagger\right] . \tag{2.39}$$

The matrix U contains the Goldstone boson fields. The covariant derivative D^μ is composed of the usual derivative and terms concerning the coupling of the Goldstone boson fields to external fields. The current quark mass is hidden in the definition of χ, i.e. $\chi = 2B(s + ip)$, where B is related to the quark condensate parameter and F, in the SU(2) sector, is the pion decay constant in the chiral limit. Higher-order terms in the Lagrangian can be constructed and each term contains coefficients, the so-called Low Energy Constants (LEC). In case one could solve the fundamental theory from first principles, one can map the LECs of the EFT to the fundamental parameters of the underlying theory. However, since QCD cannot be solved analytically in the low-energy region, we consider the LECs as free parameters, which at this point can be extracted from physical observables.

After the most general effective Lagrangian is constructed one also needs a method to classify the order of the diagram built from the effective Lagrangian. Weinberg's power counting scheme offers such a method for labelling the specific order D, the chiral dimension, of the diagram of interest and it can be obtained from

$$D = 2 + 2N_L + \sum_{k=1}^{\infty} 2(k-1)N_{2k}, \tag{2.40}$$

where N_L is the number of independent loop momenta and N_{2k} is the number of vertices originating from the Lagrangian $\mathcal{L}_{2k}$. In ChPT loop diagrams also contain a divergent part, which has to be renormalized. However, ChPT is not a renormalizable theory in the traditional sense since the infinities cannot be reabsorbed into parameters of the lowest-order Lagrangian, e.g. B and F. A consistent removal of infinities can be done by redefinition of the fields and the LECs.

The extension to include the nucleon in ChPT is also possible and was done in Ref. [11]. In the SU(2) sector, the effective Lagrangian describing the interaction of π and N can be written as

$$\mathcal{L}_{\pi N} = \mathcal{L}^{(1)}_{\pi N} + \mathcal{L}^{(2)}_{\pi N} + \cdots . \tag{2.41}$$

The lowest order Lagrangian $\mathcal{L}_{\pi N}^{(1)}$ is of the form

$$\mathcal{L}_{\pi N}^{(1)} = \bar{\psi}_0 \left(i\gamma^\mu \partial_\mu - m_0 - \frac{1}{2}\frac{\overset{\circ}{g}_{A_0}}{F_0}\gamma^\mu\gamma_5\tau^a\partial_\mu\pi_0^a \right)\psi_0, \tag{2.42}$$

where ψ_0 and $\vec{\pi}_0$ denote a doublet and a triplet of bare nucleon and pion fields, respectively. The constants m, $\overset{\circ}{g}_A$ and F denote the nucleon mass, the axial-vector coupling and the pion decay constant in the chiral limit, which arise after renormalization. The new scale associated with the mass of the nucleon, which does not vanish in the chiral limit as opposed to the case of the Goldstone bosons, brings a new difficulty when demanding consistency in the power counting of the specific diagram. Namely, loop diagrams involving the nucleon contribute also to lower order diagrams and therefore a consistent perturbative picture collapses.

The first attempt to remedy this deficiency was formulated in terms of the Heavy Baryon Chiral Perturbation Theory (HBChPT). The basic idea of HBChPT is the separation of the nucleon momenta into a part which is close to the on-shell kinematics and a soft residual part, i.e. $p = mv + k_p$ where $v^2 = 1$, $v^0 \leq 1$. The nucleon field is then expressed in terms of

$$\psi(x) = e^{-imv\cdot x}(\mathcal{N}_v + \mathcal{H}_v), \tag{2.43}$$

where $\mathcal{N}_v = e^{imv\cdot x}\frac{1}{2}(1+\not{v})\psi$ and $\mathcal{H}_v = e^{imv\cdot x}\frac{1}{2}(1-\not{v})\psi$. As a consequence in HBChPT the power counting as in the mesonic sector is restored. The disadvantages of HBChPT are that higher order terms in the Lagrangian due to the $1/m$ expansion become increasingly complicated and not all the scattering amplitudes resulting from such a Lagrangian show the correct analytic behavior in the low-energy region.

Recently, the formulation of the manifestly Lorentz-invariant baryon ChPT was developed in Refs. [13, 14, 15, 16]. It is constructed to utilize the advantages of the mesonic ChPT and HBChPT while at the same time avoiding their disadvantages. The technique associated with this formulation is the so-called "infrared regularization" as presented in Appendix B. The basic idea of this technique is to separate the loop integral containing the nucleon into two parts, an infrared singular and regular part. The infrared singular part contains fractional powers of the meson masses, whereas the infrared regular part involves fractional powers of the nucleon mass. The power counting is valid for the infrared singular part, but not for the infrared regular part. One therefore surmounts the problem of power counting by absorbing the infrared regular part into a redefinition of the LECs. Another renormalization technique is also available as proposed in Refs. [17, 18, 19], namely, the "Extended On-Mass-Shell" (EOMS) formalism.

The mesonic ChPT, especially in the $\pi\pi$ interaction, has achieved impressive success as the EFT of the strong interaction at low energies. In baryonic ChPT, the recent development of the manifestly Lorentz-invariant technique has tremendously improved the previous analysis of ChPT. The electromagnetic form factors of baryons as well as other baryonic properties have been studied in Refs. [13, 18, 19, 20, 21]. Extension to multi-nucleon processes is also possible as shown in Ref. [22]. The further inclusion of vector mesons in baryon ChPT successfully improved the description of the electromagnetic nucleon form factors up to approximately $Q^2 \sim 0.4$ GeV^2 as shown in Ref. [19]. Open questions concerning the inclusion of other additional degrees of freedom like the $\Delta(1232)$ resonance are currently studied with the hope to further extend the kinematic region, where ChPT is applicable.

Chapter 3

Electromagnetic structure of the nucleon

In this chapter we will review some facts concerning the electromagnetic structure of the nucleon. The important tool to investigate the charge and current distributions within the nucleon and the properties of its resonances is electron-nucleon scattering. Both elastic and inelastic electron-nucleon scattering is used as a probe to study the subtle structure of the nucleon. The elastic channel is important for the global properties of the charge and the current distributions in the nucleon. On the other hand, the inelastic channel reveals information concerning nucleon resonances. Here we restrict ourselves to the case of elastic electron-nucleon scattering since in recent years the new polarization measurements significantly improved the quality of the data which previously were extracted by the Rosenbluth separation technique. First, we briefly review evidences for the nucleon structure. Next, we will discuss elastic electron-nucleon scattering and the definitions of various nucleon form factors. Finally, the electromagnetic form factors of the nucleon will be presented.

3.1 Evidences of the nucleon structure

Evidences for the existence of an inner structure of the nucleon with strong deviations from the point-like Dirac particle are revealed from essentially two aspects. The first aspect comes from the experiments in 1933 by Frisch and Stern [40] and Estermann and Stern [41] in measuring the magnetic moments of deuteron and proton. Their first result for the magnetic moment of the proton was between 2 to 3 times the nuclear magneton. This strong deviation from the value of one nuclear magneton for a point-like, spin-$\frac{1}{2}$ particle suggested that the proton is not a

point-like particle but has some finite structure. The results for the magnetic moment of the deuteron also indicated that the neutron has a structure as well. More accurate values of the proton and deuteron magnetic moments were measured by Kellogg *et al.* [42] which resulted in $\mu_p = 2.785 \pm 0.02$ and $\mu_D = 0.855 \pm 0.006$ in units of nuclear magnetons. Nowadays, the very precise values for the magnetic moments of the nucleon are [43]

$$\begin{aligned} \mu_p &= 2.792847351 \pm 0.000000028 \mu_N, \\ \mu_n &= -1.9130427 \pm 0.0000005 \mu_N. \end{aligned}$$

The second evidence of the nucleon structure is the existence of the excited nucleon states or the nucleon resonances. They are well observed especially in the mass region around 1-2 GeV. Their properties can be studied through the use of electromagnetic and strong probes, e.g. electrons, photons and pions. The results of the measurement of the differential cross section obtain from the inelastic electron nucleon scattering with energy transfer below 2 GeV reveal the existence of three pronounced maxima. The first maximum corresponds to the $\Delta(1232)$, the second peak involves the $N^*(1520)$ and $N^*(1535)$ and the third resonance region contains the $N^*(1680)$. Many other resonances are identified and their properties are listed by the Particle Data Group (PDG) [43]. The transition of the nucleon to such resonances, with important information contained in the detailed electric and magnetic multipole decomposition with associated transition form factors, delivers additional crucial constraints for tests of models of the nucleon.

3.2 Elastic electron-nucleon scattering

The lowest-order elastic electron-nucleon scattering process is shown in Fig. 3.1. The four-momenta of the incident and scattered electron are $p = (\epsilon, \vec{p})$ and $p' = (\epsilon', \vec{p}')$, respectively. $P = (E, \vec{P})$ and $P' = (E', \vec{P}')$ are the four-momenta of the nucleon in the initial and final state. The four-momentum transfer carried by a photon is $q = p - p' = P' - P$. The characteristics of this scattering process is such that the square of the four-momentum transfer is space-like, i.e. $q^2 < 0$. Usually one defines a quantity Q^2, which is positive, i.e. $Q^2 = -q^2 > 0$.

The invariant amplitude of this process is of the form

$$\mathcal{M} \sim \bar{u}_e(p')\gamma_\mu u_e(p) \frac{e^2}{q^2} \langle N(P')|J^\mu_{\rm em}(0)|N(P)\rangle, \tag{3.1}$$

where $u_e(p)$, $\bar{u}_e(p')$ refers to the electron Dirac spinors and $\langle N(P')|J^\mu_{\rm em}(0)|N(P)\rangle$ is the nucleon current matrix element. From considerations of Lorentz covariance, charge and parity conservation, the most general form of the nucleon current matrix element is

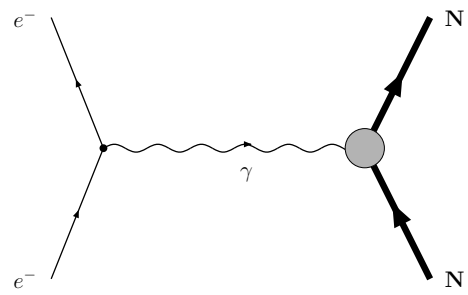

Figure 3.1: Lowest-order electron-nucleon scattering

$$\langle N(P')|J^{\mu}_{\rm em}(0)|N(P)\rangle = \bar{u}_N(P')\left[\gamma^{\mu}F_1^N(Q^2) + \frac{i}{2M_N}\sigma^{\mu\nu}q_{\nu}F_2^N(Q^2)\right]u_N(P), \quad (3.2)$$

where $F_1^N(Q^2)$ and $F_2^N(Q^2)$ are the Dirac and Pauli form factors, respectively. Their normalizations are such that at zero recoil ($Q^2 = 0$) $F_1^N(0)$ is the charge of the nucleon (in units of the elementary charge), whereas $F_2^N(0)$ is the anomalous magnetic moment (κ_N) of the nucleon

$$\begin{aligned} F_1^p(0) &= 1, \quad F_2^p(0) = \kappa_p = 1.793, \\ F_1^n(0) &= 0, \quad F_2^n(0) = \kappa_n = -1.913, \end{aligned} \quad (3.3)$$

where κ_N is given in units of the nuclear magneton.

In the laboratory frame, where the target nucleon is at rest, and neglecting the small mass of the electron, the energy ϵ' of the outgoing electron scattered by an angle θ off the target of mass M is

$$\epsilon' = \frac{\epsilon}{1 + \frac{2\epsilon}{M}\sin^2\frac{\theta}{2}}, \quad (3.4)$$

with the momentum transfer squared as, $Q^2 = 4\epsilon\epsilon'\sin^2\frac{\theta}{2}$. For the simplest case of a spinless, point-like target the differential cross section reduced to the "Mott" differential cross section with the inclusion of the recoil factor ϵ'/ϵ as

$$\left(\frac{d\sigma}{d\Omega}\right)_{\rm Mott} = \frac{\alpha^2}{4\epsilon^2\sin^4\frac{\theta}{2}}\frac{\epsilon'}{\epsilon}\cos^2\frac{\theta}{2}. \quad (3.5)$$

Extension to the case of spin-$\frac{1}{2}$ target particle, but still point-like, leads to the well-known modification of the Mott formula

$$\frac{d\sigma}{d\Omega} = \left(\frac{d\sigma}{d\Omega}\right)_{\text{Mott}} \left[1 + \frac{Q^2}{4M^2} 2\tan^2\frac{\theta}{2}\right]. \tag{3.6}$$

The term proportional to $\tan^2\frac{\theta}{2}$ results in an increase of the differential cross section at backward angles. It is due to the magnetic scattering of the spin of both projectile and target. For a spin-$\frac{1}{2}$ target with an extended structure and an anomalous magnetic moment, as is the case for the nucleon, the differential cross section is referred to as "Rosenbluth cross section" [44]

$$\begin{aligned}\frac{d\sigma}{d\Omega} &= \left(\frac{d\sigma}{d\Omega}\right)_{\text{Mott}} \Bigg[(F_1^N(Q^2))^2 \\ &\quad + \frac{Q^2}{4M_N^2}\left\{(F_2^N(Q^2))^2 + 2(F_1^N(Q^2) + F_2^N(Q^2))^2 \tan^2\frac{\theta}{2}\right\}\Bigg],\end{aligned} \tag{3.7}$$

where $F_1^N(Q^2)$ and $F_2^N(Q^2)$ are the Dirac and Pauli form factors as in Eq. (3.2).

Instead of working with $F_1^N(Q^2)$ and $F_2^N(Q^2)$, it is convenient to consider linear combinations constructed as

$$\begin{aligned}G_E^N(Q^2) &= F_1^N(Q^2) - \frac{Q^2}{4M_N^2} F_2^N(Q^2), \\ G_M^N(Q^2) &= F_1^N(Q^2) + F_2^N(Q^2),\end{aligned} \tag{3.8}$$

which are the "Sachs form factors". With Eq. (3.3) the normalizations for the Sachs form factors of the nucleon are

$$\begin{aligned}&G_E^p(0) = 1, \quad G_M^p(0) = \mu_p = 2.793, \\ &G_E^n(0) = 0, \quad G_M^n(0) = \mu_n = -1.913,\end{aligned} \tag{3.9}$$

where μ_N are the nucleon magnetic moments. As for $F_1^N(Q^2)$ and $F_2^N(Q^2)$, the Sachs form factors can be related to the current matrix elements of Eq. (3.2). The interpretation of the Sachs form factors become simple when we restrict to a specific frame of reference, namely, the "Breit frame". For the elastic electron-nucleon scattering process the Breit frame coincides with the center-of-mass frame. In this particular frame the energy transfer vanishes and thus the photon carries the four-momentum $q^\mu = (0, \vec{q})$ and therefore $Q^2 = \vec{q}^2$. The incoming electron has momentum $\vec{p} = +\vec{q}/2$ and the incoming nucleon has opposite momentum $\vec{P} = -\vec{q}/2$, while in the final state the outgoing electron and nucleon have momenta

$\vec{p}' = -\vec{q}/2$ and $\vec{P}' = +\vec{q}/2$, respectively. In the Breit frame, the corresponding matrix elements of Eq. (3.2) are

$$\begin{aligned}\langle N(\vec{q}/2, s')|J^0_{\rm em}(0)|N(-\vec{q}/2, s)\rangle &= G^N_E(Q^2)\delta_{s's}, \\ \langle N(\vec{q}/2, s')|\vec{J}_{\rm em}(0)|N(-\vec{q}/2, s)\rangle &= G^N_M(Q^2)\chi^\dagger_{s'}\frac{i\vec{\sigma}\times\vec{q}}{2M_N}\chi_s,\end{aligned} \tag{3.10}$$

where s and s' are the spin orientations of the incoming and outgoing nucleon, respectively, while χ_s and $\chi_{s'}$ refer to the two-component Pauli spinors. In terms of the Sachs form factors the Rosenbluth formula for elastic scattering of an electron on the nucleon target becomes

$$\begin{aligned}\frac{d\sigma}{d\Omega} &= \left(\frac{d\sigma}{d\Omega}\right)_{\rm Mott}\left[\frac{(G^N_E(Q^2))^2 + \frac{Q^2}{4M_N^2}(G^N_M(Q^2))^2}{1+\frac{Q^2}{4M_N^2}}\right. \\ &\quad \left. + \frac{Q^2}{2M_N^2}(G^N_M(Q^2))^2\tan^2\frac{\theta}{2}\right]\end{aligned} \tag{3.11}$$

in the one-photon exchange approximation.

3.3 Electromagnetic nucleon form factors

Elastic electron-nucleon scattering is the basic tool in order to extract the electromagnetic form factors of the nucleon. Due to the finite lifetime of the neutron, one faces the difficulty in constructing free neutron targets. Instead, deuteron or ^{3}He targets have been used in which an additional subtraction of the effect due to the presence of the protons is needed in the analysis. As known from early experiments, the electromagnetic form factors of the nucleon, except for the neutron charge form factor $G^n_E(Q^2)$, are well described by the dipole parameterization

$$G^p_E(Q^2) \approx \frac{G^p_M(Q^2)}{\mu_p} \approx \frac{G^n_M(Q^2)}{\mu_n} \approx G_D(Q^2), \tag{3.12}$$

where the dipole form factor is

$$G_D(Q^2) = \frac{1}{[1+Q^2/(0.71\,\mathrm{GeV}^2)]^2}. \tag{3.13}$$

The electromagnetic proton form factors can be directly obtained by measuring the differential cross section of the elastic electron-proton scattering process.

Based on Eq. (3.7) Hofstadter, Bumiller and Croissiaux [45] extracted the Dirac and Pauli form factors of the proton by measuring the differential cross section at different angles but at the same Q^2. They found that $F_1^p(Q^2)$ and $F_2^p(Q^2)$ are less than unity, indicating a finite structure of proton, and are approximately equal to each other up to $Q^2 = 9.3$ fm^{-2} $= 0.36$ GeV^2. Alternatively, Hand, Miller and Wilson [46] suggested the extraction of $G_E^p(Q^2)$ and $G_M^p(Q^2)$ rather than the Dirac and Pauli form factors from the differential cross section by rewritten Eq. (3.11) as

$$\sigma_R \equiv \frac{d\sigma/d\Omega}{(d\sigma/d\Omega)_{\text{Mott}}}\varepsilon(1+\tau) = \tau(G_M^p(Q^2))^2 + \varepsilon(G_E^p(Q^2))^2, \tag{3.14}$$

where σ_R is the reduced cross section, $\tau = Q^2/(4M_p^2)$ and the linear polarization of the virtual photon is

$$\varepsilon = [1 + 2(1+\tau)\tan^2(\theta/2)]^{-1}. \tag{3.15}$$

By fixing Q^2, the plots of the measured quantities σ_R and ϵ for different combinations of (θ, ϵ) can be fitted by a linear polynomial in which the slope is $(G_E(Q^2))^2$ and the intercept on the σ_R-axis is $\tau(G_M^2(Q^2))^2$. This method is referred to as "Rosenbluth separation technique".

However, at large Q^2 the Rosenbluth separation for $G_E^p(Q^2)$ suffers from the increasing systematic uncertainties with increasing values of Q^2. Fig. 3.2 shows the available data for the ratios G_E^p/G_D and $G_M^p/(\mu_p G_D)$ obtained by the Rosenbluth separation. $G_M^p/(\mu_p G_D)$ can be well measured up to $Q^2 \sim 30$ GeV^2, whereas the data for G_E^p/G_D scatter and have large uncertainties for values above $Q^2 \sim 1$ GeV^2. Later we will see that improved data on the electromagnetic proton form factors can alternatively be obtained by polarization experiments.

Akhiezer, Rozentsweig and Shumshkevich [53] already showed in 1958 that a considerable increase in accuracy of the nucleon charge form factor measurement can be achieved by scattering polarized electrons off a polarized nucleon target. Twenty years later Arnold, Carlson and Gross [54] also arrived at the same conclusion. However, it took several decades before such experiments were technically feasible. In the polarization transfer experiment, e.g. $\vec{e}p \to e\vec{p}$, the polarization of the final proton is measured in addition. The longitudinal part P_l parallel to the proton momentum and the transverse part P_t of the proton polarization are given by [54]

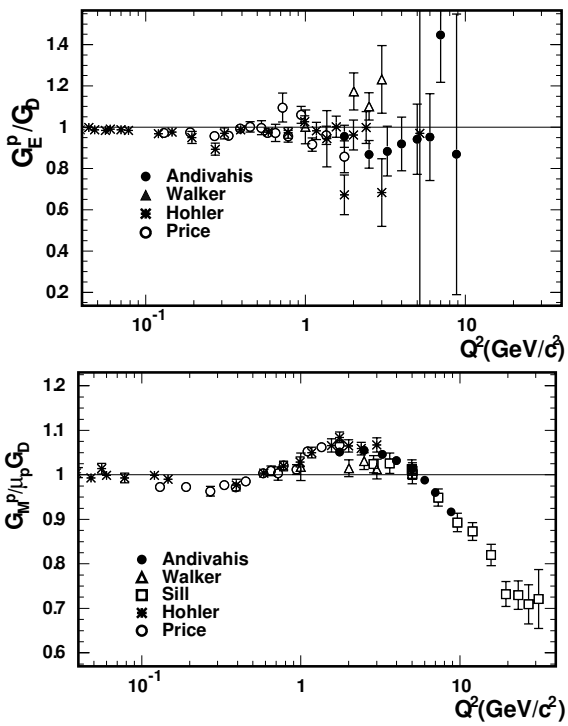

Figure 3.2: *G_E^p/G_D and $G_M^p/(\mu_p G_D)$ obtained by the Rosenbluth method. Data are taken from [47, 48, 49, 50, 51]. The figures are taken from Ref. [52].*

$$
\begin{aligned}
P_l &= \frac{\epsilon+\epsilon'}{M_p I_0}\sqrt{\tau(1+\tau)}(G_M^p)^2\tan^2\frac{\theta}{2}, \\
P_t &= -\frac{2}{I_0}\sqrt{\tau(1+\tau)}G_E^p G_M^p\tan\frac{\theta}{2},
\end{aligned}
\tag{3.16}
$$

with

$$
I_0 = (G_E^p)^2 + \tau\left[1+2(1+\tau)\tan^2\frac{\theta}{2}\right](G_M^p)^2. \tag{3.17}
$$

Both P_l and P_t can be measured by the polarimeter and their ratio gives rise to

$$
\frac{G_E^p}{G_M^p} = -\frac{\epsilon+\epsilon'}{2M_p}\left(\frac{P_t}{P_l}\right)\tan\frac{\theta}{2}. \tag{3.18}
$$

In this way the systematic uncertainties in extracting the ratio of G_E^p/G_M^p are minimized. Figs. 3.3 and 3.4 show the results for the ratio $\mu_p G_E^p/G_M^p$ as measured by the Rosenbluth separation and the polarization experiments, respectively. Obviously, the polarization measurements lead to a significant improvement of the experimental data. An important feature detected by the polarization transfer experiments is the observed linear decline of $\mu_p G_E^p/G_M^p$ as Q^2 increases, shown in Fig. 3.4. From Ref. [59] this observed behavior satisfies the relation

$$\mu_p \frac{G_E^p(Q^2)}{G_M^p(Q^2)} = 1 - 0.13(Q^2 - 0.29 \text{ Gev}^2). \tag{3.19}$$

Since the empirical values for $G_M^p(Q^2)/\mu_p$ closely follow the dipole parameterization $G_D(Q^2)$, the linear decrease of $\mu_p G_E^p/G_M^p$ suggests that $G_E^p(Q^2)$ falls off more rapidly with Q^2 than $G_D(Q^2)$. This is in clear contradiction to the results obtained by the Rosenbluth separation technique as seen in Fig. 3.4. Due to occurence of large systematic errors of $G_E^p(Q^2)$ at large Q^2 with the Rosenbluth extraction, attempts have been made in order to improve the data. A careful reanalysis of the old Rosenbluth data was done by Arrington [63]. Christy *et al.* [64] analyzed the data on elastic electron-proton scattering as part of experiment E99-119 performed in Hall C at Jefferson Lab. Results from a high-precision Rosenbluth extraction especially designed for the measurement in Hall A at Jefferson Lab were reported by Qattan *et al.* [65]. Note that the results of these reanalyses and remeasurements are also shown in Fig. 3.4. All of these recent analyses of the Rosenbluth data showed agreement with the previous Rosenbluth results. Therefore, the origin for the discrepancy of results between Rosenbluth separation and polarization technique must be due to other mechanisms.

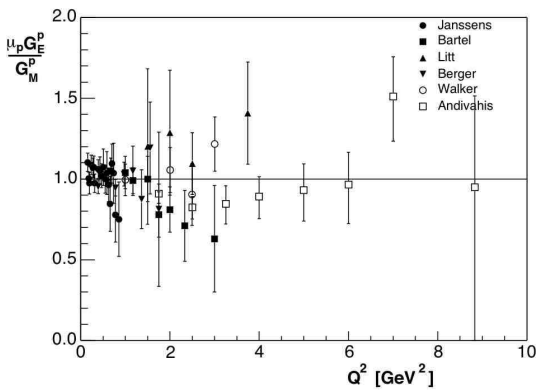

Figure 3.3: *The ratio $\mu_p G_E^p/G_M^p$ obtained from the Rosenbluth separation. Data are taken from Refs. [47, 48, 55, 56, 57, 58]. This figure is taken from Ref. [59].*

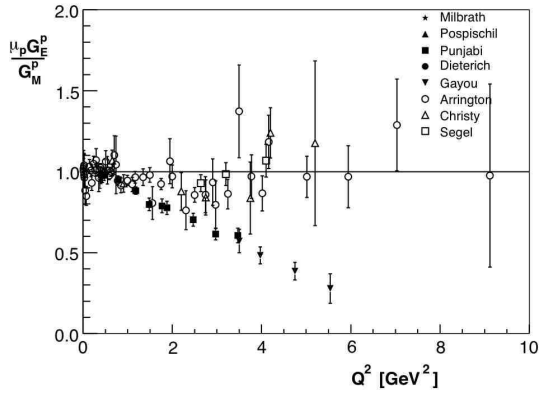

Figure 3.4: *The ratio $\mu_p G_E^p / G_M^p$ obtained from polarization transfer measurements. Data are taken from Refs. [2, 3, 60, 61, 62]. A reanalysis of the Rosenbluth separation in Refs. [63, 64, 65] is also shown here for comparison. This figure is taken from Ref. [59].*

The two-photon exchange (TPE) diagrams are believed to be the source for the disagreement of the measured ratios $\mu_p G_E^p / G_M^p$ originating from the two methods. The TPE diagrams, also called the box diagrams, are shown in Fig. 3.5. After the exchange of the first photon, the intermediate state proton can also be in an excited state, which after the second photon exchange, makes a transition to the ground state. In the previous Rosenbluth separation analysis, these box diagrams were included by using the method of Mo and Tsai [66] with the assumption that one of the photons is a soft photon, while excluding the diagram where both photons are hard. The work by Blunden *et al.* [67] and by Chen *et al.* [68] showed that inclusion of the hard scattering process of TPE significantly improves the Rosenbluth separation with the resulting data moving in the direction of the ones obtained from the polarization measurement.

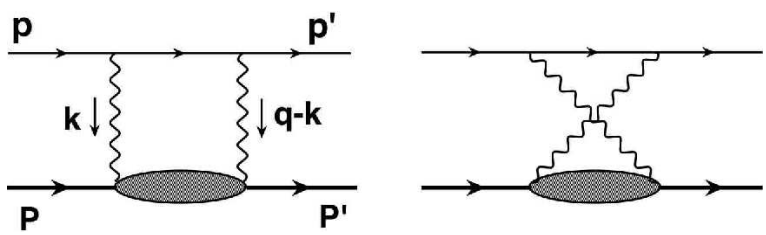

Figure 3.5: Feynman diagrams for the two-photon exchange.

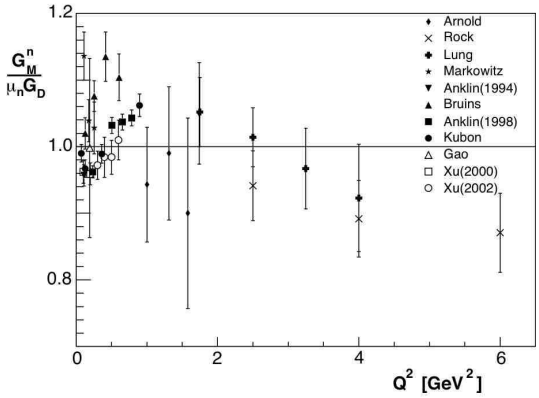

Figure 3.6: *The ratio $G_M^n/(\mu_n G_D)$: data are taken from Refs. [69, 70, 71, 72, 73, 74, 75, 77, 78, 79, 80]. This figure is taken from Ref. [59].*

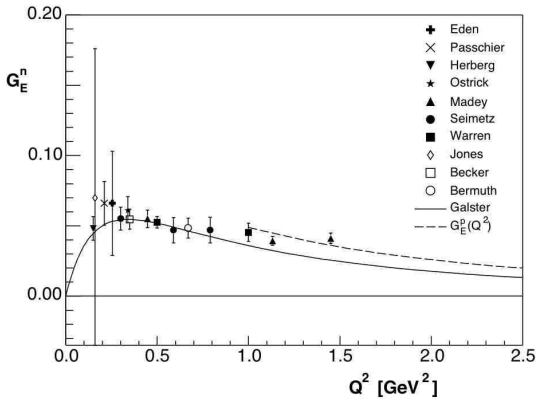

Figure 3.7: *The charge form factor of the neutron: data are taken from Refs. [81, 82, 83, 84, 85, 86, 87, 88, 89, 90, 91, 92, 93]. The Q^2-behavior of G_E^p and the Galster parameterization are also shown here. This figure is taken from Ref. [59].*

Finally, the database of the electromagnetic form factors of the neutron are shown in Figs. 3.6 and 3.7. For G_M^n, early data were obtained from inclusive quasi-elastic scattering off the deuteron which result in sizable systematic uncertainties. A new technique in measuring the ratio of quasi-elastic neutron and proton knock-out from a deuterium target which has little sensitivity to nuclear binding effects, has been pioneered and applied to the region of $Q^2 < 1$ GeV^2 at Mainz [69, 70, 71] and Bonn [72]. Another method for extracting G_M^n is the measurement of a beam asymmetry in the polarization measurement for the ^{3}He target as was done in Refs. [73, 74, 75]. As in the case of G_M^n, the early data for G_E^n were extracted

from the (quasi-) elastic scattering off the deuteron. The more accurate data are obtained from the double-polarization measurements of neutron knock-out from a polarized ^{2}H or ^{3}He target. For values larger than $Q^2 \sim 1$ GeV^2, G_E^n appears to exhibit a Q^2-behavior similar to that of G_E^p. The Q^2-behavior of G_E^p is also shown in Fig. 3.7 together with the Galster parameterization [76].

Chapter 4

Perturbative chiral quark model

For the study of the low-energy properties of baryons we recently developed the so-called Perturbative Chiral Quark Model (PCQM). The idea of the PCQM is that a baryon is viewed as a system of three valence quarks, which are confined in space and are surrounded by a cloud of mesons (quark-antiquark pairs), which in turn are treated perturbatively. The meson cloud is interpreted as the additional correction arising from the Goldstone bosons, which naturally arise by the spontaneously broken chiral symmetry. Therefore, physical observables are composed of two contributions, the valence quarks (or the quark core) and the meson cloud. In many observables, as in other quark models, the quark core contributions are supposed to dominate the observables, while the meson cloud gives some corrections. However, there exists also some observables, such as meson-nucleon sigma-terms and the strangeness content of the nucleon, where the meson cloud gives the major contribution. The importance of the meson cloud which significantly contributes to these observables is also observed in the earlier concept of the cloudy bag model [24]. To explore the role of the meson cloud in the low-energy regime is one of the goals we are interested in.

In this chapter we outline the PCQM and give selected physical applications. First, as a starting point of the PCQM, the effective Lagrangian describing the baryonic system which fulfills the appropriate symmetries of the theory will be constructed. Next, the calculational technique and the renormalization of the PCQM will be discussed. Finally, we present the application of the PCQM to the study of the electromagnetic baryon form factors, their magnetic moments and, in addition, the electromagnetic $N - \Delta$ transition.

4.1 Effective Lagrangian

The perturbative chiral quark model is based on an effective chiral Lagrangian describing the valence quarks of baryons as relativistic fermions moving in a self-consistent field (static potential), $V_{\text{eff}}(r) = S(r) + \gamma^0 V(r)$, with $r = |\vec{x}|$, which are supplemented by a cloud of Goldstone bosons (π, K, η). The Lagrangian describing relativistic quarks in this static potential is

$$\mathcal{L}^{(0)}(x) = \bar{\psi}(x)\left[i\partial\!\!\!/ - \mathcal{M} - S(r) - \gamma^0 V(r)\right]\psi(x), \tag{4.1}$$

where $\mathcal{M} = \text{diag}\{\hat{m}, \hat{m}, m_s\}$ is the mass matrix of current quarks. Note, that we restrict to the isospin symmetry limit, $m_u = m_d = \hat{m}$. This Lagrangian is not chirally invariant due to the presence of $\mathcal{M}$ and $S(r)$. By introducing the interaction of the octet of Goldstone pseudoscalar mesons (π, K, η) with quarks, the chiral invariance of the Lagrangian in the limit $\mathcal{M} \to 0$ can be restored. The chiral fields can be represented by the exponential parameterization

$$U = \exp\left[i\frac{\hat{\Phi}}{F}\right], \tag{4.2}$$

where F is the pion decay in the chiral limit. The octet matrix $\hat{\Phi}$ of pseudoscalar mesons is defined as

$$\begin{aligned}\frac{\hat{\Phi}}{\sqrt{2}} &= \sum_{i=1}^{8}\frac{\Phi_i\lambda_i}{\sqrt{2}} \\ &= \begin{pmatrix} \pi^0/\sqrt{2}+\eta/\sqrt{6} & \pi^+ & K^+ \\ \pi^- & -\pi^0/\sqrt{2}+\eta/\sqrt{6} & K^0 \\ K^- & \bar{K}^0 & -2\eta/\sqrt{6} \end{pmatrix}.\end{aligned} \tag{4.3}$$

Therefore, the chirally invariant interaction Lagrangian is introduced as

$$\begin{aligned}\mathcal{L}_{int} &= -\bar{\psi}(x)S(r)\left[\frac{U+U^\dagger}{2} + \gamma^5\frac{U-U^\dagger}{2}\right]\psi(x) \\ &= -\bar{\psi}(x)S(r)\exp\left[i\gamma^5\frac{\hat{\Phi}}{F}\right]\psi(x).\end{aligned} \tag{4.4}$$

Together with the kinetic term of the meson fields

$$\mathcal{L}_\Phi = \frac{F^2}{4}\text{Tr}\left[\partial_\mu U \partial^\mu U^\dagger\right], \tag{4.5}$$

we obtained the chirally invariant Lagrangian

$$\mathcal{L}_{inv}(x) = \bar{\psi}(x)[i\partial\!\!\!/ - \gamma^0 V(r)]\psi(x) + \mathcal{L}_\Phi + \mathcal{L}_{int}. \tag{4.6}$$

Explicitly breaking of chiral symmetry arises from the nonvanishing of the quark mass matrix $\mathcal{M}$. Taking into account explicit chiral symmetry breaking we include in the Lagrangian the term

$$\mathcal{L}_{\chi SB}(x) = -\bar{\psi}(x)\mathcal{M}\psi(x) - \frac{B}{2}\mathrm{Tr}\left[\hat{\Phi}^2(x)\mathcal{M}\right], \tag{4.7}$$

which represents the mass term of quarks and of the octet of Goldstone boson, respectively. $B = -\langle 0|\bar{u}u|0\rangle/F^2$ is the quark condensate constant. The masses of the octet of Goldstone bosons are in the leading order (i.e. linear in the current quark mass)

$$M_\pi^2 = 2\hat{m}B, \quad M_K^2 = (\hat{m} + \hat{m}_s)B, \quad M_\eta^2 = \frac{2}{3}(\hat{m} + 2\hat{m}_s)B. \tag{4.8}$$

Note that Eq. (4.8) corresponds to the "Gell–Mann-Oakes-Renner" relation. In addition, Eq. (4.8) satisfies also the "Gell–Mann-Okubo" relation,

$$4M_K^2 = 3M_\eta^2 + M_\pi^2. \tag{4.9}$$

From Eq. (4.6) and Eq. (4.7), the chirally invariant Lagrangian together with the explicit chiral symmetry breaking terms is of the form

$$\mathcal{L}_{full}(x) \;=\; \mathcal{L}_{inv}(x) + \mathcal{L}_{\chi SB}(x). \tag{4.10}$$

In the calculations, the mesonic degrees of freedom are treated perturbatively, hence we consider the expansion of U with

$$U = \exp\left[i\frac{\hat{\Phi}}{F}\right] = 1 + i\frac{\hat{\Phi}}{F} + \frac{1}{2}\left(i\frac{\hat{\Phi}}{F}\right)^2 + \dots\ . \tag{4.11}$$

The approximate Lagrangian can be obtained from Eq. (4.10) and Eq. (4.11) by this perturbative expansion, i.e. expansion in terms of the coupling $1/F$ up to a specific order in $1/F$. In the physical applications, we will restrict our consideration to the one-loop approximation, i.e. we will perform our calculations to order of

accuracy $o(1/F^2)$. This means that we keep the expansion of U up to terms linear in $\hat{\Phi}$.

Finally, the effective linearized Lagrangian can be summarized as

$$\begin{aligned}\mathcal{L}_{\text{eff}}(x) &= \mathcal{L}_{lin}(x) + \mathcal{L}_{\chi SB}(x) \\ &= \bar{\psi}(x)[i\partial\!\!\!/ - S(r) - \gamma^0 V(r)]\psi(x) \\ &\quad + \frac{1}{2}[\partial_\mu \Phi_i(x)]^2 - \bar{\psi}(x) S(r) i\gamma^5 \frac{\hat{\Phi}(x)}{F}\phi(x) \\ &\quad - \bar{\psi}(x)\mathcal{M}\psi(x) - \frac{B}{2}\text{Tr}\left[\hat{\Phi}^2(x)\mathcal{M}\right]. \end{aligned} \tag{4.12}$$

4.2 Quark wave functions

In the basis of potential eigenstates the quark field ψ can be expanded as

$$\psi(x) = \sum_\alpha b_\alpha u_\alpha(\vec{x}) \exp\left(-i\mathcal{E}_\alpha t\right) + \sum_\beta d_\beta^\dagger v_\beta(\vec{x}) \exp\left(i\mathcal{E}_\beta t\right), \tag{4.13}$$

where the sets of quark $\{u_\alpha\}$ wave functions with the corresponding single quark energies $\{\mathcal{E}_\alpha\}$ and antiquark $\{v_\beta\}$ wave functions with the single antiquark energies $\{\mathcal{E}_\beta\}$ in orbits α and β are solutions of the Dirac equation with the static potential $V_{\text{eff}}(r)$. The single quark annihilation and antiquark creation operators are denoted by the expansion coefficients b_α and $d_\beta^\dagger$, respectively. The Dirac equation for the quark wave functions $u_\alpha(\vec{x})$ is

$$\left[-i\gamma^0\vec{\gamma}\cdot\vec{\nabla} + \gamma^0 S(r) + V(r) - \mathcal{E}_\alpha\right] u_\alpha(\vec{x}) = 0. \tag{4.14}$$

For a specific form of $V_{\text{eff}}(r)$, Eq. (4.14) can be solved numerically . However, to simplify the problem, a specific form for $V_{\text{eff}}(r)$ will be used with the purpose that the problem can be solved analytically. Therefore, the choice of $V_{\text{eff}}(r)$ that we are going to work with has a quadratic radial dependence of the form

$$S(r) = M_1 + c_1 r^2, \;\; V(r) = M_2 + c_2 r^2, \tag{4.15}$$

with the particular choice

$$M_1 = \frac{1-3\rho^2}{2\rho R}, \;\; M_2 = \mathcal{E}_0 - \frac{1+3\rho^2}{2\rho R}, \;\; c_1 \equiv c_2 = \frac{\rho}{2R^3}, \tag{4.16}$$

where $\mathcal{E}_0$ is the energy of the single quark ground state. This particular choice leads to quark wave functions of the Gaussian type. The analytic forms of u_α are shown explicitly in Appendix B. The parameters ρ and R are related to the ground-state wave function

$$u_0(\vec{x}) = N \exp\left[-\frac{\vec{x}^2}{2R^2}\right] \begin{pmatrix} 1 \\ i\frac{\rho}{R}\vec{\sigma}\cdot\vec{x} \end{pmatrix} \chi_s \chi_f \chi_c, \tag{4.17}$$

where $N = \left[\pi^{3/2}R^3(1+3\rho^2/2)\right]^{-1/2}$ is a normalization constant. χ_s, χ_f and χ_c are the spin, flavor and color quark wave functions, respectively. The parameter ρ is responsible for the relativistic aspect of the wave function, since it is connected with the amplitude of the lower component of the Dirac spinor. The parameter R can be considered as a parameter related to the size of the charge radius of the proton.

In zeroth-order (or $3q$-core) approximation, one can relate ρ to the axial charge of the nucleon g_A by

$$g_A = \frac{5}{3}\left(1 - \frac{2\rho^2}{1+\frac{3}{2}\rho^2}\right), \tag{4.18}$$

and relate R to the charge radius of the proton at the leading order (LO) as

$$\begin{aligned} \langle r_E^2 \rangle_{LO}^p &= \int d^3x u_0^\dagger(\vec{x})\vec{x}^2 u_0(\vec{x}) \\ &= \frac{3R^2}{2}\frac{1+\frac{5}{2}\rho^2}{1+\frac{3}{2}\rho^2}. \end{aligned} \tag{4.19}$$

The physical interpretation and role of ρ in the relativistic quark wave function is clearly seen from Eq. (4.18). If we take the nonrelativistic limit by putting $\rho = 0$, the nonrelativistic quark model result for the axial coupling $g_A = 5/3$ is reproduced. In our calculations we use the value of $g_A = 1.25$ and allow a variation of $\langle r_E^2 \rangle_{LO}^p$ from 0.5 fm^2 to 0.7 fm^2 as done in Ref. [30]. This corresponds to a fixed value of the parameter $\rho = \sqrt{2/13}$. Thus the only free quantity left in the PCQM is the size parameter R with a range of variation given by 0.55 fm $< R < 0.65$ fm.

4.3 Calculational technique

We will apply perturbation theory in calculating the contributions of the meson cloud to the physical observables. The matrix element of an operator $\hat{A}$ can be

calculated from

$$\begin{aligned}\langle B'|\hat{A}|B\rangle &= {}^{B'}\langle\phi_0|\sum_{n=1}^{\infty}\frac{i^n}{n!}\int d^4x_1\ldots \\ &\int d^4x_n T\left[\mathcal{L}_I(x_1)\ldots\mathcal{L}_I(x_n)\hat{A}\right]|\phi_0\rangle_c^B,\end{aligned} \tag{4.20}$$

where the state vector $|\phi_0\rangle$ corresponds to the unperturbed three-quark state ($3q$-core). In order to calculate the matrix element, we project the state vectors onto the respective baryon states as indicated by the superscripts "B'" and "B". Subscript "c" refers that only connected graphs contribute to the matrix element. The perturbation, contained in the interaction Lagrangian $\mathcal{L}_I(x)$, arises from the effective Lagrangian of Eq. (4.12) and is given by

$$\mathcal{L}_I(x) = -\bar{\psi}(x)i\gamma^5\frac{\hat{\Phi}(x)}{F}S(r)\psi(x). \tag{4.21}$$

By applying Wick's theorem with the appropriate propagators for quarks and mesons, Eq. (4.20) can be evaluated in a straightforward manner.

The quark propagator in a binding potential can be written as

$$\begin{aligned}iG_\psi(x,y) &= \langle\phi_0|T\left[\psi(x)\bar{\psi}(y)\right]|\phi_0\rangle \\ &= \theta(x_0-y_0)\sum_\alpha u_\alpha(\vec{x})\bar{u}_\alpha(\vec{y})e^{-i\mathcal{E}_\alpha(x_0-y_0)} \\ &\quad -\theta(y_0-x_0)\sum_\beta v_\beta(\vec{x})\bar{v}_\beta(\vec{y})e^{i\mathcal{E}_\beta(x_0-y_0)}.\end{aligned} \tag{4.22}$$

Both quark and antiquark wave functions contribute to the quark propagator. In Refs. [29, 30, 31, 32] the quark propagator of Eq. (4.22) is truncated by considering the contribution from the ground state quark wave function u_0 only, that is

$$iG_\psi(x,y) \to iG_0\psi(x,y) = \theta(x_0-y_0)u_0(\vec{x})\bar{u}_0(\vec{y})e^{-i\mathcal{E}_0(x_0-y_0)}. \tag{4.23}$$

In the following, we extend our considerations by including in the quark propagator the contributions due to the excited quark states and neglect the part due to the antiquark states, i.e.

$$iG_\psi(x,y) = \theta(x_0-y_0)\sum_\alpha u_\alpha(\vec{x})\bar{u}_\alpha(\vec{y})e^{-i\mathcal{E}_\alpha(x_0-y_0)}. \tag{4.24}$$

Energetically, two low-lying excited quark states will be included into Eq. (4.24). The first excitation concerns the p-states, which in the nonrelativistic notation are the $1p_{1/2}$ and the $1p_{3/2}$. The second excited states contain the $1d_{3/2}$, $1d_{5/2}$ and $2s_{1/2}$, which are degenerate in energy. The general form of the wave functions is shown in Appendix B.

For the meson fields, we adopt the free Feynman propagator

$$\begin{aligned} i\Delta_{ij}(x-y) &= \langle 0|T\left[\Phi_i(x)\Phi_j(y)\right]|0\rangle \\ &= \delta_{ij}\int \frac{d^4k}{(2\pi)^4 i}\frac{\exp[-ik(x-y)]}{M_\Phi^2-k^2-i\epsilon}. \end{aligned} \tag{4.25}$$

To evaluate the matrix element between baryon states, we have to project the quark operators onto the baryonic level. The baryonic wave function $|B\rangle$ is constructed by the product of the SU(6) spin-flavor and the $\mathrm{SU(3)_c}$ color wave function. For one-body operators the projection is

$$\chi^\dagger_{f'}\chi^\dagger_{s'}I^{f'f}J^{s's}\chi_f\chi_s \overset{Projection}{\longrightarrow} \langle B'|\sum_{i=1}^{3}(IJ)^{(i)}|B\rangle, \tag{4.26}$$

where I and J are operators which act in flavor and spin spaces, respectively. Analogously, for two-body operators, we have

$$\begin{aligned} &\chi^\dagger_{f'}\chi^\dagger_{s'}I_1^{f'f}J_1^{s's}\chi_f\chi_s\otimes\chi^\dagger_{k'}\chi^\dagger_{\sigma'}I_2^{k'k}J^{\sigma'\sigma}\chi_k\chi_\sigma \\ &\qquad\qquad \overset{Projection}{\longrightarrow} \langle B'|\sum_{i\neq j}^{3}(I_1J_1)^{(i)}\otimes(I_2J_2)^{(j)}|B\rangle. \end{aligned} \tag{4.27}$$

4.4 Renormalization

For the first application, we apply our technique to calculate the mass shift of the nucleon due to the presence of the quark-meson interaction. Applying the Gell–Mann and Low theorem [94] and the technique developed in [95, 96], the mass shift of the nucleon can be calculated from

$$\Delta m_N = {}^N\langle\phi_0|\sum_{n=1}^{\infty}\frac{i^n}{n!}\int i\delta(t_1)d^4x_1\ldots d^4x_nT\left[\mathcal{L}_I(x_1)\ldots\mathcal{L}_I(x_n)\right]|\phi_0\rangle_c^N. \tag{4.28}$$

At one-loop, with an order of accuracy $o(1/F^2)$, the diagrams that contribute to this mass shift are shown in Fig. 4.1. The so-called "meson cloud" (MC) diagram of Fig. 4.1(a) describes the emission and reabsorption of the meson on the same quark, whereas the "meson exchange" (EX) diagram of Fig. 4.1(b) connects two quark lines. As discussed above, the MC and EX diagrams are examples of one- and two-body operators, respectively.

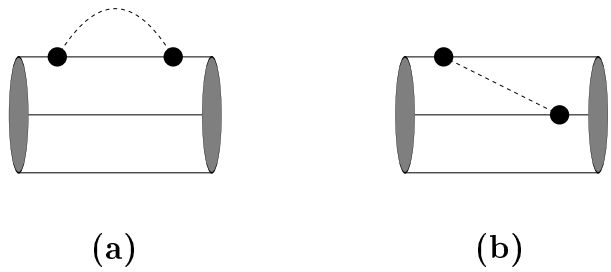

Figure 4.1: *Diagrams contributing to the mass shift of the nucleon: meson cloud (a) and meson exchange diagram (b).*

For simplicity, we will first discuss the case where the quark propagator is truncated to the contribution from the ground state quark wave function u_0 as in Eq. (4.23). By using $\mathcal{L}_I(x)$ from Eq. (4.21), applying Wick's theorem and the projection technique to Eq. (4.28), the MC diagram contribution can be written as

$$\Delta m_N^{MC} = \sum_{\Phi=\pi,K,\eta} d_N^{\Phi;MC} \Pi(M_\Phi^2), \tag{4.29}$$

where

$$d_N^{\pi;MC} = \frac{81}{400}, \;\; d_N^{K;MC} = \frac{54}{400}, \;\; d_N^{\eta;MC} = \frac{9}{400}\,. \tag{4.30}$$

The self-energy operators $\Pi(M_\Phi^2)$, which depend on the meson mass M_Φ^2 are defined by

$$\Pi(M_\Phi^2) = -\left(\frac{g_A}{\pi F}\right)^2 \int_0^\infty \frac{dp\, p^4}{w_\Phi^2(p^2)}\, F_{\pi NN}^2(p^2), \tag{4.31}$$

for a meson with a three-momentum $\vec{p}$ and an energy $w_\Phi(p^2) = \sqrt{M_\Phi^2 + p^2}$, where $p = |\vec{p}|$. In Eq. (4.31), $F_{\pi NN}(p^2)$ is the πNN form factor normalized to unity at

zero recoil

$$F_{\pi NN}(p^2) = \exp\left(-\frac{p^2R^2}{4}\right)\left\{1+\frac{p^2R^2}{8}\left(1-\frac{5}{3g_A}\right)\right\}. \tag{4.32}$$

The EX diagram contribution to the nucleon mass shift is

$$\Delta m_N^{EX} = \sum_{\Phi=\pi,K,\eta} d_N^{\Phi;EX}\Pi(M_\Phi^2), \tag{4.33}$$

with

$$d_N^{\pi;EX} = \frac{90}{400},\ \ d_N^{K;EX} = 0,\ \ d_N^{\eta;EX} = -\frac{6}{400}\,. \tag{4.34}$$

Therefore, the nucleon mass shift due to the presence of the Goldstone bosons is

$$\begin{aligned}\Delta m_N^{str} &= \Delta M_N^{MC} + \Delta M_N^{Ex} \\ &= \sum_{\Phi=\pi,K,\eta} d_N^{\Phi}\Pi(M_\Phi^2),\end{aligned} \tag{4.35}$$

where $d_N^{\Phi} = d_N^{\Phi;MC} + d_N^{\Phi;EX}$ and

$$d_N^{\pi} = \frac{171}{400},\ \ d_N^{K} = \frac{6}{19}d_N^{\pi},\ \ d_N^{\eta;MC} = \frac{1}{57}d_N^{\pi}\,. \tag{4.36}$$

There is another source for the nucleon mass shift due to the finite current mass of the u and d quarks. Originally, in the Dirac equation of Eq. (4.14), we exclude the presence of the finite mass of the quark. Including now the mass term for $i = u$, d, s quarks the Dirac equation becomes

$$\left[-i\gamma^0\vec{\gamma}\cdot\vec{\nabla} + \gamma^0 m_i + \gamma^0 S(r) + V(r) - \mathcal{E}_\alpha(m_i)\right] u_\alpha(\vec{x};m_i) = 0. \tag{4.37}$$

The eigen energies $\mathcal{E}_\alpha(m_i)$ and the quark wave functions $u_\alpha(\vec{x};m_i)$ now depend on m_i. As a consequence of this modification and when we treat m_i perturbatively we can write the single quark energy as

$$\mathcal{E}_\alpha(m_i) = \mathcal{E}_\alpha + \delta\mathcal{E}_\alpha(m_i), \tag{4.38}$$

and the wave function is changed to

$$u_\alpha(\vec{x}; m_i) = u_\alpha(\vec{x}) + \delta u_\alpha(\vec{x}; m_i). \tag{4.39}$$

As will become clear later, the one-loop calculation as of Fig. 4.1(a) is of the order $o(1/F^2)$, which is the order of accuracy we are working in, including the excited quark states in the quark propagator with the term $\delta u_\alpha(\vec{x}; m_i)$ of Eq. (4.39) will lead to higher order contributions. Therefore, in the one-loop diagrams and in the diagrams which are of the order $o(1/F^2)$, it is enough to only use $u_\alpha(\vec{x})$ in the calculation of the matrix element. However, the redefinition of Eq. (4.39) is important for the tree-level diagram with no meson fields present. In such a diagram only the ground state quark wave function u_0 contributes and both terms on the right-hand-side of Eq. (4.39) with $\alpha = 0$ will give rise to the leading-order (LO) and next-to-leading-order (NLO) contributions, respectively.

For the ground state energy $\mathcal{E}_0(\hat{m})$ of Eq. (4.38) one can explicitly write

$$\mathcal{E}_0(\hat{m}) = \mathcal{E}_0 + \gamma\hat{m} + o(\hat{m}), \tag{4.40}$$

where the relativistic reduction factor γ is

$$\gamma = \frac{1 - \frac{3}{2}\rho^2}{1 + \frac{3}{2}\rho^2} = \frac{9}{10} g_A - \frac{1}{2}. \tag{4.41}$$

Therefore, for the renormalized nucleon mass, one obtains

$$\begin{aligned} m_N^r &= m_N^{core} + \Delta m_N^{str} \\ &= 3\,(\mathcal{E}_0 + \gamma\hat{m}) + \sum_{\Phi=\pi,K,\eta} d_N^\Phi \Pi(M_\Phi^2). \end{aligned} \tag{4.42}$$

On the other hand, in terms of the renormalized quark mass $\hat{m}^r$, one obtains

$$m_N^r = 3\,(\mathcal{E}_0 + \gamma\hat{m}^r) + \sum_{\Phi=\pi,K,\eta} d_N^{\Phi;EX} \Pi(M_\Phi^2), \tag{4.43}$$

where the effect due to the MC diagram is included in the renormalization of the quark mass

$$\hat{m}^r = \hat{m} + \frac{1}{3\gamma} \sum_{\Phi=\pi,K,\eta} d_N^{\Phi;MC} \Pi(M_\Phi^2). \tag{4.44}$$

As mentioned earlier, in the perturbative picture, the renormalized quark energy up to a linear term in $\hat{m}^r$ is

$$\begin{aligned} \mathcal{E}_0^r(\hat{m}^r) &= \mathcal{E}_0 + \delta\mathcal{E}_0^r(\hat{m}^r) \\ &= \mathcal{E}_0 + \gamma\hat{m}^r. \end{aligned} \tag{4.45}$$

Renormalization of the quark wave function

The renormalized quark masses at order of accuracy $o(1/F^2, \hat{m})$ are shown in Eq. (4.44). We can use this renormalized quark masses to obtain the renormalized quark field ψ^r of Eq. (4.13). Restricting to positive energy states in the expansion of the renormalized quark fields we have

$$\psi_i^r(x; m_i^r) = \sum_\alpha b_\alpha u_\alpha^r(\vec{x}; m_i^r) \exp\left(-i\mathcal{E}_\alpha^r(m_i^r)t\right). \tag{4.46}$$

The renormalized quark wave function $u_\alpha^r(\vec{x}; m_i^r)$ and energy of the quark field are obtained from the Dirac equation of Eq. (4.37) with the modification $m_i \to m_i^r$

$$\left[-i\gamma^0\vec{\gamma}\cdot\vec{\nabla} + \gamma^0 m_i^r + \gamma^0 S(r) + V(r) - \mathcal{E}_\alpha(m_i^r)\right] u_\alpha(\vec{x}; m_i^r) = 0. \tag{4.47}$$

The solutions are

$$u_0^r(\vec{x}; m_i^r) = N(m_i^r) \exp\left[-c(m_i^r)\frac{\vec{x}^2}{2R^2}\right] \begin{pmatrix} 1 \\ i\frac{\rho(m_i^r)}{R}\vec{\sigma}\cdot\vec{x} \end{pmatrix} \chi_s\chi_f\chi_c, \tag{4.48}$$

with the normalization

$$\int d^3 u_0^{\dagger r}(x; m_i^r) u_0^r(x; m_i^r) \equiv 1. \tag{4.49}$$

Note, that $N(m_i^r)$, $c(m_i^r)$ and $\rho(m_i^r)$ are normalized as

$$N(0) = N, \;\; c(0) = 1, \;\; \rho(0) = \rho \tag{4.50}$$

as indicated in Eq. (4.17) for the case $m_i^r = 0$. As stated in Ref. [30], the product $\rho(m_i^r)c(m_i^r)$ is independent of m_i^r and we have the constraint

$$\rho(m_i^r)c(m_i^r) = \rho(0)c(0) = \rho. \tag{4.51}$$

The renormalized quark energy after treating m_i^r as a small perturbation is written in general form as

$$\mathcal{E}_0^r(m_i^r) = \mathcal{E}_0 + \gamma m_i^r, \tag{4.52}$$

where Eq. (4.45) is the special case for $\hat{m}^r = m_u^r = m_d^r$. For the ground state wave function $u_0^r(\vec{x}; m_i^r)$, we have

$$u_0^r(\vec{x}; m_i^r) = u_0(\vec{x}) + \delta u_0(\vec{x}; m_i^r), \tag{4.53}$$

where

$$\delta u_0^r(\vec{x}; m_i^r) = \frac{m_i^r}{2} \frac{\rho R}{1 + \frac{3}{2}\rho^2} \left(\frac{\frac{1}{2} + \frac{21}{4}\rho^2}{1 + \frac{3}{2}\rho^2} - \frac{\vec{x}^2}{R^2} + \gamma^0 \right) u_0(\vec{x}). \tag{4.54}$$

Renormalization of the effective Lagrangian

To set the stage for the renormalization of the effective Lagrangian, we first introduce the electromagnetic interaction to the effective Lagrangian. This will be used for renormalizing the charge of the nucleon. In a standard procedure, the electromagnetic interaction of the quark and the meson with an electromagnetic field A_μ is introduced through the minimal substitution,

$$\partial_\mu \psi \;\rightarrow\; D_\mu \psi = \partial_\mu \psi + ieQA_\mu, \tag{4.55}$$

$$\partial_\mu \Phi_i \;\rightarrow\; D_\mu \Phi_i = \partial_\mu \Phi_i + e \left[f_{3ij} + \frac{f_{8ij}}{\sqrt{3}} \right] A_\mu \Phi_j, \tag{4.56}$$

where $Q = \mathrm{diag}\{2/3, -1/3, -1/3\}$ is the quark charge matrix and f_{ijk} are the totally antisymmetric structure constants of the group SU(3). The resulting electromagnetic interaction Lagrangian is

$$\begin{aligned} \mathcal{L}_{I,em} \;=\; & -e\bar{\psi}(x)\gamma^\mu Q\psi(x)A_\mu(x) - e\sum_{i,j=1}^{8} \left[f_{3ij} + \frac{f_{8ij}}{\sqrt{3}} \right] \Phi_i(x)\partial^\mu \Phi_j(x) A_\mu(x) \\ & + \frac{e^2}{2} \sum_{i=1,2,4,5} \Phi_i^2(x) A_\mu^2(x). \end{aligned} \tag{4.57}$$

In order to renormalize the effective Lagrangian we replace the quark field $\psi(x)$ by the renormalized quark field $\psi^r(x)$. We also add a set of appropriate counterterms with the purpose that the renormalized mass and charge of the nucleon can be directly calculated from the part of the Lagrangian which only contains the effective potential. In other words, we construct the free dynamical nucleon Lagrangian from the renormalized quark field that is already taken into account by the diagram of Fig. 4.1. Applying this to the effective Lagrangian of Eq. (4.12) and

including the electromagnetic interaction of Eq. (4.57), the renormalized effective Lagrangian is

$$\mathcal{L}^r_{\rm eff}(x) = \mathcal{L}^r_\psi + \mathcal{L}_\Phi + \mathcal{L}_{ph} + \mathcal{L}^r_{int}, \tag{4.58}$$

where $\mathcal{L}^r_\psi$, $\mathcal{L}_\Phi$, $\mathcal{L}_{ph}$ and $\mathcal{L}_{int}$ are the terms corresponding to the quark fields confined by the effective potential, the free meson, the free photon and the interaction parts, respectively. The Lagrangian $\mathcal{L}^r_\psi$ is

$$\mathcal{L}^r_\psi = \mathcal{L}^r_{\bar\psi\psi} + \mathcal{L}^r_{(\bar\psi\psi)^2}, \tag{4.59}$$

where

$$\mathcal{L}^r_{\bar\psi\psi} = \bar\psi^r(x)\left[i\partial\!\!\!/ - \mathcal{M}^r - S(r) - \gamma^0 V(r)\right]\psi^r(x), \tag{4.60}$$

$$\begin{aligned}\mathcal{L}^r_{(\bar\psi\psi)^2} &= c_\pi \sum_{i=1}^{3}\left[\bar\psi^r(x) i\gamma^5\lambda_i\psi^r(x)\right]^2 + c_K\sum_{i=4}^{7}\left[\bar\psi^r(x) i\gamma^5\lambda_i\psi^r(x)\right]^2 \\ &\quad + c_\eta\left[\bar\psi^r(x) i\gamma^5\lambda_8\psi^r(x)\right]^2.\end{aligned} \tag{4.61}$$

$\mathcal{L}^r_{\bar\psi\psi}$ contains the meson cloud contribution of Fig. 4.1(a) through the renormalized quark mass $\mathcal{M}^r = \mathcal{M} - \delta\mathcal{M}$. The meson exchange diagram of Fig. 4.1(b) is described by $\mathcal{L}^r_{(\bar\psi\psi)^2}$. The parameters c_π, c_K and c_η can be deduced from Eq. (4.34) and Eq. (4.43) to be

$$c_\Phi = -\frac{9}{200}\frac{(2\pi R^2)^{3/2}}{1-\gamma^2}\Pi(M^2_\Phi). \tag{4.62}$$

The free meson Lagrangian $\mathcal{L}_\Phi$ is

$$\mathcal{L}_\Phi = \frac{1}{2}[\partial_\mu\Phi_i(x)]^2 - \frac{B}{2}\mathrm{Tr}\left[\hat\Phi^2(x)\mathcal{M}\right], \tag{4.63}$$

which can be written in the standard form as

$$\mathcal{L}_\Phi = \frac{1}{2}[\partial_\mu\Phi_i(x)]^2 - \frac{1}{2}\delta_{ij}M^2_{ij}\Phi_i(x)\Phi_j(x). \tag{4.64}$$

The diagonal meson mass matrix M^2_{ij} has the components

$$\begin{aligned} M^2_{11} = M^2_{22} = M^2_{33} &= M^2_\pi, \\ M^2_{44} = M^2_{55} = M^2_{66} = M^2_{77} &= M^2_K, \\ M^2_{88} &= M^2_\eta. \end{aligned} \tag{4.65}$$

For the free photon Lagrangian $\mathcal{L}_{ph}$ one has the usual familiar term

$$\mathcal{L}_{ph} = -\frac{1}{4}F_{\mu\nu}(x)F^{\mu\nu}(x), \tag{4.66}$$

with the field tensor

$$F_{\mu\nu}(x) = \partial_\mu A_\nu(x) - \partial_\nu A_\mu(x). \tag{4.67}$$

The interaction Lagrangian is composed of both the strong and electromagnetic interaction parts as

$$\mathcal{L}^r_{int} = \mathcal{L}^r_{int,str} + \mathcal{L}^r_{int,em}, \tag{4.68}$$

where

$$\mathcal{L}^r_{int,str} = \mathcal{L}^r_{I,str} + \delta\mathcal{L}_{str}, \tag{4.69}$$

$$\mathcal{L}^r_{int,em} = \mathcal{L}^r_{I,em} + \delta\mathcal{L}_{em}. \tag{4.70}$$

The Lagrangian $\mathcal{L}^r_{I,str}$ is the one of Eq. (4.21) but now with the renormalized quark field $\psi^r(x)$

$$\mathcal{L}^r_{I,str}(x) = -\bar{\psi}^r(x)i\gamma^5\frac{\hat{\Phi}(x)}{F}S(r)\psi^r(x), \tag{4.71}$$

and the same for $\mathcal{L}^r_{I,em}$ of Eq. (4.57)

$$\begin{aligned}\mathcal{L}^r_{I,em} &= -e\bar{\psi}^r(x)\gamma^\mu Q\psi^r(x)A_\mu(x) - e\sum_{i,j=1}^{8}\left[f_{3ij} + \frac{f_{8ij}}{\sqrt{3}}\right]\Phi_i(x)\partial^\mu\Phi_j(x)A_\mu(x) \\ &\quad + \frac{e^2}{2}\sum_{i=1,2,4,5}\Phi_i^2(x)A_\mu^2(x).\end{aligned} \tag{4.72}$$

The set of counterterms $\delta\mathcal{L}_{str}$ and $\delta\mathcal{L}_{em}$ is

$$\delta\mathcal{L}_{str} = \delta\mathcal{L}_{1,str} + \delta\mathcal{L}_{2,str} + \delta\mathcal{L}_{3,str} \tag{4.73}$$

with

$$\begin{aligned}
\delta\mathcal{L}_{1,str} &= \bar{\psi}^r(x)(Z-1)\left[i\partial\!\!\!/ - \mathcal{M}^r - S(r) - \gamma^0 V(r)\right]\psi^r(x), && (4.74)\\
\delta\mathcal{L}_{2,str} &= -\bar{\psi}^r(x)\delta\mathcal{M}\psi^r(x), && (4.75)\\
\delta\mathcal{L}_{3,str} &= -c_\pi \sum_{i=1}^{3}\left[\bar{\psi}^r(x)i\gamma^5\lambda_i\psi^r(x)\right]^2 - c_K\sum_{i=4}^{7}\left[\bar{\psi}^r(x)i\gamma^5\lambda_i\psi^r(x)\right]^2 \\
&\quad -c_\eta\left[\bar{\psi}^r(x)i\gamma^5\lambda_8\psi^r(x)\right]^2, && (4.76)
\end{aligned}$$

and

$$\delta\mathcal{L}_{em} = -eA_\mu(x)\bar{\psi}^r(x)(Z-1)\gamma^\mu Q\psi^r(x). \tag{4.77}$$

Renormalization of the nucleon mass

We will reconsider the renormalization of the nucleon mass by using the renormalized effective Lagrangian. By constructing of the renormalized effective Lagrangian, the renormalized mass of the nucleon is defined by the expectation value of the Hamiltonian, $\mathcal{H}^r_\psi(x)$, which can be obtained from $\mathcal{L}^r_\psi(x)$ of Eq. (4.59). Averaging over the unperturbed state $|\phi_0\rangle$ which is projected on the respective nucleon states we have

$$m^r_N \equiv {}^N\langle\phi_0|\int \delta(t)d^4x\,\mathcal{H}^r_\psi(x)|\phi_0\rangle^N. \tag{4.78}$$

Following this definition, the shift of the nucleon mass due to the inclusion of the strong interaction Lagrangian $\mathcal{L}^r_{int,str}$ of Eq. (4.69) evaluated at one loop vanish, i.e.

$$\begin{aligned}
\Delta m^r_N &= {}^N\langle\phi_0|\sum_{n=1}^{2}\frac{i^n}{n!}\int i\delta(t_1)d^4x_1\ldots d^4x_n \mathrm{T}\left[\mathcal{L}^r_{int,str}(x_1)\ldots\mathcal{L}^r_{int,str}(x_n)\right]|\phi_0\rangle^N_c \\
&= {}^N\langle\phi_0| -\frac{i}{2}\int \delta(t_1)d^4x_1d^4x_2\mathrm{T}\left[\mathcal{L}^r_{I,str}(x_1)\mathcal{L}^r_{I,str}(x_2)\right]|\phi_0\rangle^N_c \\
&\quad -{}^N\langle\phi_0|\int\delta(t)d^4x\sum_{i=1}^{3}\delta\mathcal{L}_{i,str}(x)|\phi_0\rangle^N \\
&\equiv 0. && (4.79)
\end{aligned}$$

Note, that due to the equation of motion Eq. (4.47) which results in

$$ {}^{N}\langle\phi_0| \int \delta(t) d^4x \, \delta\mathcal{L}_{1,str}(x) |\phi_0\rangle^N \equiv 0, \tag{4.80} $$

and because of the role of $\delta\mathcal{L}_{2,str}(x)$ and $\delta\mathcal{L}_{3,str}(x)$ which compensate the contributions of Fig. 4.1, which is

$$ \begin{aligned} 0 \;\equiv\; & {}^{N}\langle\phi_0| - \frac{i}{2} \int \delta(t_1) d^4x_1 d^4x_2 \mathrm{T} \left[\mathcal{L}^r_{I,str}(x_1) \mathcal{L}^r_{I,str}(x_2) \right] |\phi_0\rangle^N_c \\ & - {}^{N}\langle\phi_0| \int \delta(t) d^4x \left[\delta\mathcal{L}_{2,str}(x) + \delta\mathcal{L}_{3,str}(x) \right] |\phi_0\rangle^N, \end{aligned} \tag{4.81} $$

Eq. (4.79) is justified. The resulting mass renormalization of the nucleon is the same as in Eq. (4.42).

Renormalization of the nucleon charge

In order to properly renormalize the nucleon charge we first explicitly express the electromagnetic currents involved. The electromagnetic field can couple to both quarks and charged pseudoscalar mesons with the corresponding currents. In addition, there exists a current arising from the counterterms. The total electromagnetic current is, therefore,

$$ j^\mu_r = j^\mu_{\psi^r} + j^\mu_\Phi + \delta j^\mu_{\psi^r}. \tag{4.82} $$

The renormalized electromagnetic quark current is

$$ j^\mu_{\psi^r} = \bar{\psi}^r \gamma^\mu Q \psi^r = \frac{2}{3} \bar{u}^r \gamma^\mu u^r - \frac{1}{3} \bar{d}^r \gamma^\mu d^r - \frac{1}{3} \bar{s}^r \gamma^\mu s^r, \tag{4.83} $$

whereas the part concerning the charged pseudoscalar mesons is

$$ \begin{aligned} j^\mu_\Phi &= \left[f_{3ij} + \frac{f_{8ij}}{\sqrt{3}} \right] \Phi_i \partial^\mu \Phi_j \\ &= \left[\pi^- i\partial^\mu \pi^+ - \pi^+ i\partial^\mu \pi^- + K^- i\partial^\mu K^+ - K^+ i\partial^\mu K^- \right]. \end{aligned} \tag{4.84} $$

The counterterms contribute to the current as

$$ \begin{aligned} \delta j^\mu_{\psi^r} &= \bar{\psi}^r \left(Z - 1 \right) \gamma^\mu Q \psi^r \\ &= \left(\hat{Z} - 1 \right) \left[\frac{2}{3} \bar{u}^r \gamma^\mu u^r - \frac{1}{3} \bar{d}^r \gamma^\mu d^r \right] - \frac{1}{3} \left(Z_s - 1 \right) \bar{s}^r \gamma^\mu s^r. \end{aligned} \tag{4.85} $$

The renormalized nucleon charge at one loop is then defined as

$$\begin{aligned} Q_N^r &= {}^N\langle\phi_0| \sum_{n=0}^{2} \frac{i^n}{n!} \int \delta(t) d^4x d^4x_1 \ldots d^4x_n \\ &\quad \times \mathrm{T}\left[\mathcal{L}_{int,str}^r(x_1) \ldots \mathcal{L}_{int,str}^r(x_n) j_r^0(x)\right] |\phi_0\rangle^N . \end{aligned} \tag{4.86}$$

The resulting renormalized charge

$$Q_N^r \equiv Q_N = \begin{cases} 1 & \text{for } N = p \text{ (proton)} \\ 0 & \text{for } N = n \text{ (neutron)} \end{cases} \tag{4.87}$$

takes, due to charge conservation, the expected values, where Q_N, by construction of our renormalized Lagrangian, is the part which arises solely from the $3q$-core, i.e.

$$Q_N = {}^N\langle\phi_0| \int \delta(t) d^4x j_{\psi^r}^0(x) |\phi_0\rangle^N . \tag{4.88}$$

In other words, the contributions of the currents j_Φ^μ and $\delta j_{\psi^r}^\mu$ cancel each other, when renormalizing the nucleon charge. Hence by introducing appropriate counterterms the number of diagrams to be calculated is reduced. The corresponding Feynman diagrams resulting from Eq. (4.86) are shown in Fig. 4.2. In Appendix C, we also indicate the explicit expressions of the set of diagrams of Fig. 4.2. As a consequence the renormalization constant $Z = \mathrm{diag}\left(\hat{Z}, \hat{Z}, Z_s\right)$, set up in flavor space, can be obtained from charge conservation with the result

$$\begin{aligned} \hat{Z} &= 1 - \frac{27}{400} \left(\frac{g_A}{\pi F}\right)^2 \int_0^\infty dp p^4 F_{\pi NN}^2(p^2) \left[\frac{1}{w_\pi^3(p^2)} + \frac{2}{3w_K^3(p^2)} + \frac{1}{9w_\eta^3(p^2)}\right], \\ Z_s &= 1 - \frac{27}{400} \left(\frac{g_A}{\pi F}\right)^2 \int_0^\infty dp p^4 F_{\pi NN}^2(p^2) \left[\frac{4}{3w_K^3(p^2)} + \frac{4}{9w_\eta^3(p^2)}\right]. \end{aligned} \tag{4.89}$$

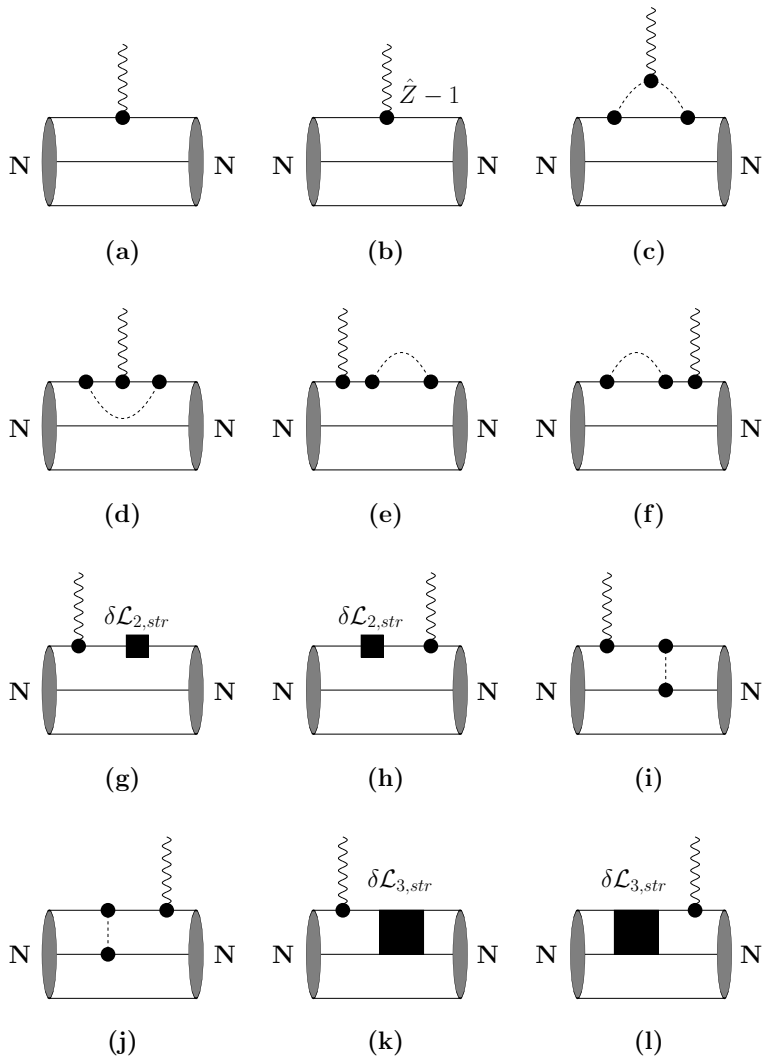

Figure 4.2: *Diagrams contributing to the nucleon charge: triangle diagram (a), triangle counterterm diagram (b), meson cloud diagram (c), vertex correction diagram (d), self-energy diagrams (e) and (f), self-energy counterterm diagrams (g) and (h), exchange current diagrams (i) and (j), and exchange current counterterm diagrams (k) and (l).*

4.5 Physical applications

The PCQM has been applied to a variety of observables related to the nucleon. Here, we present two selected applications concerning the electromagnetic properties of the nucleon and of the full baryon octet. The first application are the

electromagnetic form factors of the baryon octet. The second application refers to the electromagnetic $N - \Delta$ transition.

4.5.1 Electromagnetic form factors of the baryon octet

In Ref. [34] the PCQM has been applied to the calculation of the electromagnetic form factors of the baryon octet. The diagrams that contribute to the matrix element of the electromagnetic transition between the baryon states "B" and "B'" are shown in Fig. 4.3. For the charge form factors these coincide with the diagrams (a)-(d) of Fig. 4.2, where in addition diagrams (e)-(l) cancel each other as mentioned previously. The so-called "meson-in-flight" diagram of Fig. 4.3(e), which characterizes the two-body quark interaction, has to be included for the case of the magnetic form factors. This diagram does not contribute to the charge form factors.

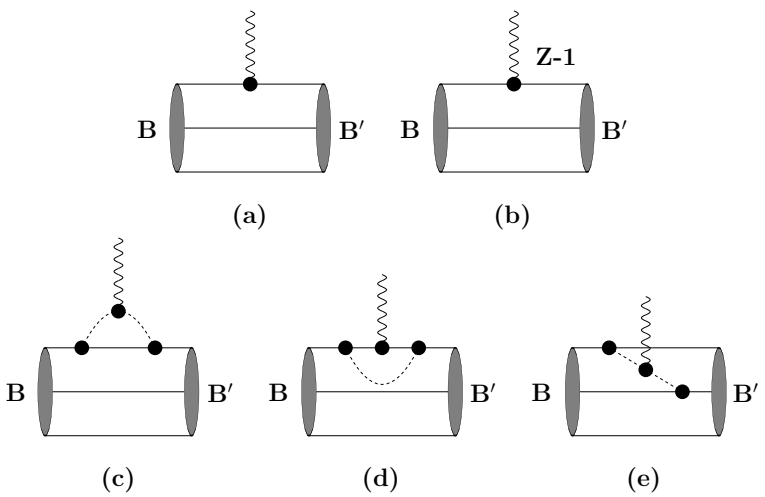

Figure 4.3: *Diagrams contributing to the charge and magnetic form factors of the baryon octet: three-quark diagram (a), three-quark counterterm diagram (b), meson cloud diagram (c), vertex correction diagram (d) and meson-in-flight diagram (e).*

In the framework of the PCQM and in the Breit frame, the Sachs form factors of the baryon octet evaluated at one loop are defined by

$$\begin{aligned}
\chi^\dagger_{s'}\chi_s G^B_E(Q^2) &= \langle\phi_0|\sum_{n=0}^{2}\frac{i^n}{n!}\int\delta(t)d^4xd^4x_1\ldots d^4x_n e^{-iq\cdot x} \\
&\quad\times\mathrm{T}\left[\mathcal{L}^r_{int,str}(x_1)\ldots\mathcal{L}^r_{int,str}(x_n)j^0_r(x)\right]|\phi_0\rangle^B_c, \qquad (4.90)\\
\chi^\dagger_{s'}\frac{i\vec{\sigma}_B\times\vec{q}}{m_B+m_{B'}}\chi_s G^B_M(Q^2) &= \langle\phi_0|\sum_{n=0}^{2}\frac{i^n}{n!}\int\delta(t)d^4xd^4x_1\ldots d^4x_n e^{-iq\cdot x} \\
&\quad\times\mathrm{T}\left[\mathcal{L}^r_{int,str}(x_1)\ldots\mathcal{L}^r_{int,str}(x_n)\vec{j}_r(x)\right]|\phi_0\rangle^B_c, \qquad (4.91)
\end{aligned}$$

where $j^\mu_r(x)$ is the electromagnetic current of Eq. (4.82), $\mathcal{L}^r_{int,str}(x)$ denotes the strong interaction Lagrangian between quarks and mesons of Eq. (4.69). χ_s and $\chi^\dagger_{s'}$ are the baryon spin wave functions in the initial and final states, $\vec{\sigma}_B$ is the baryon spin operator. In the Breit frame, the photon carries the four-momentum $q^\mu = (0,\vec{q})$. The masses of the initial and final baryon states involved in the transitions are denoted by m_B and $m_{B'}$. The normalization of the Sachs form factors at zero recoil ($Q^2 = 0$) is such that

$$G^B_E(0) = Q_B, \quad G^B_M(0) = \mu_B, \qquad (4.92)$$

where Q_B and μ_B are charge and magnetic moment of a state in the baryon octet, respectively. The charge and magnetic radii of the respective baryons follow from the definitions

$$\langle r^2_{E,M}\rangle^B = -\frac{6}{G^B_{E,M}(0)}\frac{d}{dQ^2}G^B_{E,M}(Q^2)\bigg|_{Q^2=0}. \qquad (4.93)$$

For a neutral baryon, the charge radius is just defined as

$$\langle r^2_E\rangle^B = -6\frac{d}{dQ^2}G^B_E(Q^2)\bigg|_{Q^2=0}. \qquad (4.94)$$

The numerical results for the magnetic moments, charge and magnetic radii of the baryon octet are presented in Table 4.1, Table 4.2 and Table 4.3, respectively. The contributions from the leading-order (LO) three-quark core, the next-to-leading order (NLO) three-quark core, the counterterm (CT) of the three-quark core and from the meson loops corresponding to the diagrams of Fig. 4.3 are presented separately. Here, the NLO contribution is resulting from the use of the renormalized

quark field of Eq. (4.54). The range of the results is due to the variation of the size parameter R in the region 0.55 - 0.65 fm.

As evident from Table 4.1, the main contribution to the magnetic moments of the baryon octet can be traced to the LO three-quark core diagram. Meson cloud corrections are significant for the magnetic moments up to $20-40\%$ except for the Ξ^-, where the contribution is only 3%. Hence, meson-cloud corrections generate a significant shift of the baryon magnetic moments compared to the valence quark results. Our results for the magnetic moments are in good agreement with the experimental data.

For the squared charge radii, listed in Table 4.2, the mesonic contributions are of the order of $20-40\%$, except for Ξ^- where they contribute less than 1%. For neutral baryons the LO three-quark contribution to the charge radii vanishes in the isospin limit, whereas the NLO three-quark and the CT results might contribute. A special case is the neutron in which a contribution to the charge radius only arises from the mesonic cloud. The truncation of the quark propagator to the ground state (GS) results in a small contribution to the charge radius compared to the experimental value as can be seen from Table 4.2. At this point we also consider the case, where excited states (ES) are included in the quark propagator. In Table 4.2 the results for the neutron charge radius for the case of the GS quark propagator and after including the low-lying excited states are denoted by $\langle r_E^2\rangle_{GS}^n$ and $\langle r_E^2\rangle_{ES}^n$, respectively. The total result is simply the sum of both contributions– see Table 4.2. The inclusion of the low-lying excited states in the quark propagator leads to an increase of the value of the neutron charge radius in accord with the experimental data. Therefore, for quantities where the three-quark contribution vanishes, a proper treatment of the quark propagator including the excited states becomes rather important. A similar feature will be encountered in the next section, where in the case of electromagnetic $N-\Delta$ transitions excited state contributions in the quark propagator are relevant to reach the empirical values. Similarly, meson cloud contributions play an important role to understand the measured values of the magnetic radii of the nucleon. For completeness we indicate our results for this observable for the full baryon octet in Table 4.3, although experimental results are only available partially, that is for the nucleon.

	3q [LO]	3q [NLO+CT]	Meson loops [MC+VC+MF]	Total	Exp [98]
μ_p	1.80 ± 0.15	0.01 ± 0.03	0.79 ±0.12	2.60 ± 0.03	2.793
μ_n	-1.20 ± 0.10	-0.01 ± 0.02	-0.77 ± 0.12	-1.98 ± 0.02	-1.913
μ_{Σ^+}	2.28 ± 0.19	-0.04 ± 0.04	0.51 ± 0.11	2.75 ± 0.09	2.458 ± 0.010
μ_{Σ^0}	0.76 ± 0.06	-0.05 ± 0.02	0.34 ± 0.07	1.05 ± 0.01	—
μ_{Σ^-}	-0.76 ± 0.06	-0.06 ± 0.01	-0.26 ± 0.02	-1.08 ± 0.05	-1.160 ± 0.025
μ_Λ	-0.71 ± 0.06	0.15 ± 0.04	-0.33 ± 0.09	-0.89 ± 0.03	-0.613 ± 0.004
μ_{Ξ^0}	-1.69 ± 0.14	0.23 ± 0.09	-0.28 ± 0.11	-1.74 ± 0.03	-1.250 ± 0.014
μ_{Ξ^-}	-0.85 ± 0.07	0.23 ± 0.06	-0.05 ± 0.07	-0.68 ± 0.01	-0.651± 0.003
$\lvert\mu_{\Sigma^0\Lambda}\rvert$	1.28 ± 0.11	0.01 ± 0.02	0.61 ± 0.09	1.89 ± 0.01	1.61 ± 0.08

Table 4.1: *Results for the magnetic moments μ_B of the baryon octet (in units of the nucleon magneton μ_N).*

	3q [LO]	3q [NLO+CT]	Meson loops [MC+VC]	Total	Exp
$\langle r_E^2\rangle^p$	0.60 ± 0.10	0.004±0.004	0.12±0.01	0.72 ± 0.09	0.76±0.02 [98]
$\langle r_E^2\rangle^n_{\rm GS}$	0	0	-0.043 ± 0.004	-0.043 ± 0.004	
$\langle r_E^2\rangle^n_{\rm ES}$	0	0	-0.068 ± 0.013	-0.068 ± 0.013	
$\langle r_E^2\rangle^n_{\rm Full}$	0	0	-0.111± 0.014	-0.111 ± 0.014	-0.116±0.002 [98]
$\langle r_E^2\rangle^{\Sigma^+}$	0.60 ± 0.10	0.07±0.004	0.14 ± 0.004	0.81 ± 0.10	—
$\langle r_E^2\rangle^{\Sigma^0}$	0	0.038±0.010	0.012 ± 0.010	0.050 ± 0.010	—
$\langle r_E^2\rangle^{\Sigma^-}$	0.60 ± 0.10	-0.04±0.01	0.15 ± 0.03	0.71± 0.07	0.61 ± 0.21 [100]
$\langle r_E^2\rangle^{\Lambda}$	0	0.038±0.010	0.012 ± 0.010	0.050 ± 0.010	—
$\langle r_E^2\rangle^{\Xi^0}$	0	0.07±0.02	0.07±0.02	0.14 ± 0.02	—
$\langle r_E^2\rangle^{\Xi^-}$	0.60 ± 0.10	-0.08 ± 0.03	0.10 ± 0.03	0.62 ± 0.07	—
$\langle r_E^2\rangle^{\Sigma^0\Lambda}$	0	0	0	0	—

Table 4.2: *Results for the charge radii squared $\langle r_E^2\rangle^B$ of the baryon octet (in units of* fm^2*).*

	3q [LO]	3q [NLO+CT]	Meson loops [MC+VC+MF]	Total	Exp
$\langle r_M^2 \rangle^p$	0.37±0.09	0.03±0.001	0.34±0.02	0.74± 0.07	0.74±0.10 [101]
$\langle r_M^2 \rangle^n$	0.33±0.08	0.03±0.002	0.43±0.01	0.79± 0.07	0.76±0.02 [71]
$\langle r_M^2 \rangle^{\Sigma^+}$	0.45±0.10	0.02±0.006	0.17±0.02	0.64± 0.08	—
$\langle r_M^2 \rangle^{\Sigma^0}$	0.39±0.10	-0.02±0.01	0.32±0.03	0.69± 0.07	—
$\langle r_M^2 \rangle^{\Sigma^-}$	0.38±0.08	0.09±0.01	0.31±0.01	0.78± 0.07	—
$\langle r_M^2 \rangle^{\Lambda}$	0.44±0.12	-0.14±0.06	0.35±0.07	0.65± 0.05	—
$\langle r_M^2 \rangle^{\Xi^0}$	0.52±0.12	-0.01±0.04	0.03±0.05	0.54± 0.06	—
$\langle r_M^2 \rangle^{\Xi^-}$	0.67±0.17	-0.31±0.12	-0.04±0.13	0.32± 0.04	—
$\langle r_M^2 \rangle^{\Sigma^0\Lambda}$	0.36±0.09	0.03±0.001	0.36±0.02	0.75± 0.07	—

Table 4.3: *Results for the magnetic radii squared* $\langle r_M^2 \rangle^B$ *of the baryon octet (in units of* fm^2*).*

Finally, the Q^2-dependence of the charge and magnetic Sachs form factors of the baryon octet are shown in Figs. 4.4 to 4.8. Due to the lack of full covariance in the model, the form factors can be expected to be reasonable up to $Q^2 < \vec{p}^2 = 0.4\ \mathrm{GeV}^2$ where $\vec{p}$ is the typical three-momentum transfer, which defines the region where relativistic effects $\leq 10\%$ or where the following inequality $\vec{p}^2/(4m_N^2) < 0.1$ is fulfilled. We choose to present the results separately for charged and neutral baryons. In Fig. 4.4 the charge form factors for the charged baryons $B = p$, Σ^+, Σ^- and Ξ^- are presented for the size parameter $R = 0.6\,\mathrm{fm}$ in comparison to the dipole fit $G_D(Q^2) = [1 + (Q^2/0.71\,\mathrm{GeV}^2)]^{-2}$. The charge form factor of the neutron with the quark propagator restricted to the GS contribution is separately shown in Fig. 4.5. Comparison of $G_E^n(Q^2)$ to the charge form factors of the other neutral baryons are presented in Fig. 4.6. The magnetic form factors of the charged and the neutral baryons (normalized to one at zero-recoil) in comparison to the dipole fit $G_D(Q^2)$ are given in Fig. 4.7 and Fig. 4.8.

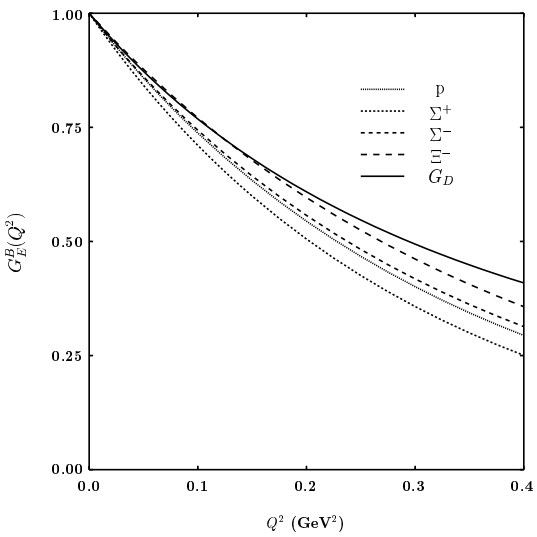

Figure 4.4: *The charge form factors $G_E^B(Q^2)$ for $B = p$, Σ^+, Σ^- and Ξ^- for a size parameter $R = 0.6$ fm compared to the dipole fit $G_D(Q^2)$. For Σ^- and Ξ^-, the absolute value of $G_E^B(Q^2)$ is shown.*

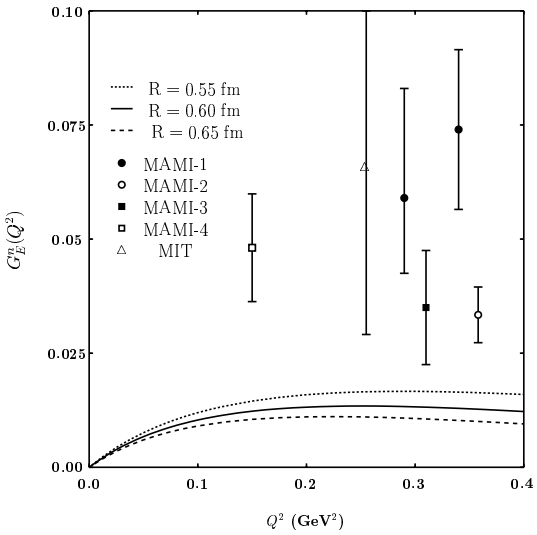

Figure 4.5: *Results for the neutron charge form factor $G_E^n(Q^2)$ for different values of $R = 0.55$, 0.6, and 0.65 fm. Here the theoretical result is based on the quark propagator truncated to the ground state (GS). Experimental data are taken from [84] (MAMI-1), [90] (MAMI-2), [102] (MAMI-3), [83] (MAMI-4), and [81] (MIT).*

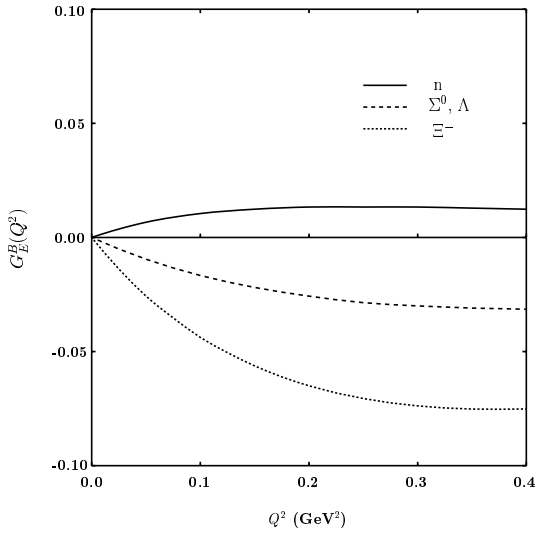

Figure 4.6: *The charge form factors* $G_E^B(Q^2)$ *for* $B = n$, Σ^0, Λ *and* Ξ^0 *for* $R = 0.6$ fm.

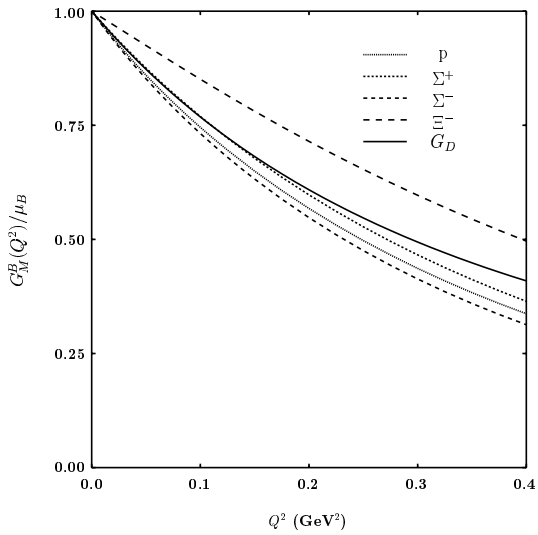

Figure 4.7: *The normalized magnetic form factors* $G_M^B(Q^2)/\mu_B$ *for* $B = p$, Σ^+, Σ^- *and* Ξ^- *at* $R = 0.6$ fm *in comparison to the dipole fit* $G_D(Q^2)$.

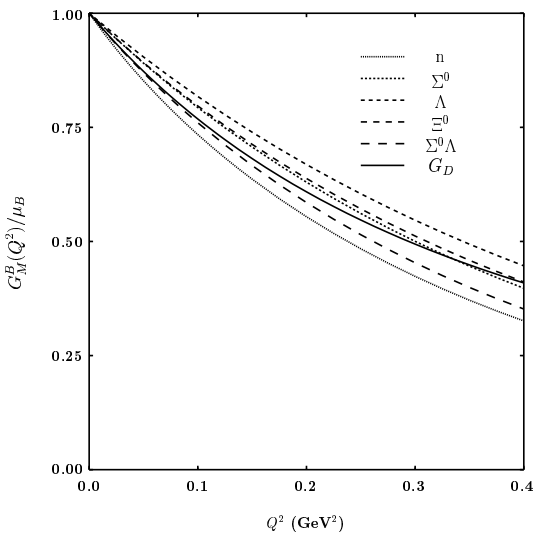

Figure 4.8: *The normalized magnetic form factors* $G_M^B(Q^2)/\mu_B$ *for* $B = n$, Σ^0, Λ *and* Ξ^0 *at* $R = 0.6$ fm *in comparison to the dipole fit* $G_D(Q^2)$.

4.5.2 Electromagnetic $N - \Delta$ transition

The electromagnetic $N-\Delta$ transition has been studied in Ref. [33] in the framework of the PCQM. The relevant observables which characterize this process are the transverse helicity amplitudes, which are defined as

$$A_M = -\frac{e}{\sqrt{2\omega_\gamma}} \left\langle \Delta, s_z' = M | \vec{j} \cdot \vec{\epsilon} | N, s_z = M - 1 \right\rangle, \tag{4.95}$$

where $M = 1/2, 3/2$. In the Δ rest-frame the photon with polarization vector $\vec{\epsilon}$ has an energy $\omega_\gamma \equiv P^* = \left(M_\Delta^2 - M_N^2\right)/2M_\Delta$. The electromagnetic current operator is denoted by $\vec{j}$. The masses M_Δ and M_N are the physical masses of the $\Delta(1232)$ resonance and the nucleon, respectively. With these helicity amplitudes other observables, such as the decay rate can be obtained by

$$\Gamma(\Delta^+ \to p\gamma) = \frac{(P^*)^2}{2\pi} \left(\frac{M_p}{M_\Delta}\right) \{|A_{1/2}|^2 + |A_{3/2}|^2\}. \tag{4.96}$$

The experimental values for the helicity amplitudes $A_{1/2}$ and $A_{3/2}$ at the real-photon point and for the branching ratio $\mathrm{BR}(\Delta^+ \to p\gamma) = \Gamma(\Delta^+ \to p\gamma)/\Gamma_{\mathrm{total}}(\Delta^+)$

are reported as [43]

$$\begin{aligned} A_{1/2}(Q^2=0) &= -135 \pm 6 \times 10^{-3}\ \mathrm{GeV}^{-1/2}, \\ A_{3/2}(Q^2=0) &= -250 \pm 8 \times 10^{-3}\ \mathrm{GeV}^{-1/2}, \\ \mathrm{BR}(\Delta^+ \to p\gamma) &= (0.52 - 0.60)\%. \end{aligned} \tag{4.97}$$

Alternatively, the transverse helicity amplitudes $A_{1/2}$ and $A_{3/2}$ can be expressed in terms of electromagnetic production multipoles, that is, the magnetic dipole $M1$ and the electric quadrupole $E2$ moments. The two sets of amplitudes are related by

$$A_{1/2} = -\frac{1}{2}(M1 + 3E2), \qquad A_{3/2} = -\frac{\sqrt{3}}{2}(M1 - E2). \tag{4.98}$$

A nonvanishing ratio $E2/M1$ indicates the possibility of an intrinsic deformation of the nucleon [112, 113, 114] or, alternatively, a sizable contribution from meson exchange currents [106, 107] with the latest experimental value [43] of

$$\frac{E2}{M1} = -0.025 \pm 0.005. \tag{4.99}$$

Previously, the transverse helicity amplitudes for the electromagnetic $N - \Delta$ transition have been studied in various approaches, such as in the constituent quark model [103, 104, 105] and in extensions where two-body currents based on gluon exchange are included [106, 107]. A long-standing problem in the description of these helicity amplitudes is that the valence quark contributions alone can explain only about two thirds of the experimental values. Relativistic corrections seemingly do not contribute too much in order to reach agreement with data. In the context of the cloudy bag model [108, 109, 110] the situation is improved, where the pion cloud gives a significant increase in the values for the helicity amplitudes. The important role of the meson cloud in the context of the $N - \Delta$ helicity amplitudes was also indicated in other models, e.g. the relativistic potential quark model of Ref. [111].

In the PCQM the $N - \Delta$ transverse helicity amplitudes evaluated at one loop can be obtained from

$$
\begin{aligned}
A_{1/2}(Q^2) &= -\frac{e}{\sqrt{2\,\omega_\gamma}}\langle\Delta^+,1/2| - \frac{1}{2}\int \delta(t)\,d^4x\,d^4x_1\,d^4x_2 \\
&\quad \times e^{-iq\cdot x}\,\mathrm{T}\left[\mathcal{L}^r_{int,str}(x_1)\mathcal{L}^r_{int,str}(x_2)\,\vec{j}_r(x)\cdot\vec{\epsilon}\right]|p,-1/2\rangle_c\ , \\
A_{3/2}(Q^2) &= -\frac{e}{\sqrt{2\,\omega_\gamma}}\langle\Delta^+,3/2| - \frac{1}{2}\int \delta(t)\,d^4x\,d^4x_1\,d^4x_2 \\
&\quad \times e^{-iq\cdot x}\,\mathrm{T}\left[\mathcal{L}^r_{int,str}(x_1)\mathcal{L}^r_{int,str}(x_2)\,\vec{j}_r(x)\cdot\vec{\epsilon}\right]|p,1/2\rangle_c\ , \qquad (4.100)
\end{aligned}
$$

where $\vec{\epsilon}$ is the polarization vector of the photon. The diagrams that contribute to $A_{1/2}(Q^2)$ and $A_{3/2}(Q^2)$ are the same as in Fig. 4.3 where $B = p$ and $B' = \Delta^+$. The explicit expressions for $A_{1/2}(Q^2)$ and $A_{3/2}(Q^2)$ resulting from each diagram are reported in Appendix D. Our results for $A_{1/2}(Q^2)$ and $A_{3/2}(Q^2)$ at the real photon point with $Q^2 = 0$ are given in Table 4.4. As can be seen from Table 4.4, meson corrections are essential to reach the empirical value for both amplitudes. Pion contributions play the dominant role in the meson corrections, as evident from Table 4.5. There we list the individual contributions of the octet mesons to the sizable terms generated by the meson-cloud and vertex-correction diagrams. The suppression of K and η loops can be traced to the large meson masses occurring in the denominators, that is meson propagators. The relative contribution of K and η mesons, with respect to π, is between 8% and 10% in the amplitude, as can be naively expected from the ratio of meson masses $(m_\pi/m_{K,\eta})^2$, which is also about 8%. Again, in Table 4.4 we indicate our results for the two variables of the quark propagator (GS and ES) occurring in the loop diagrams. For the GS version, although sizable corrections are generated, the theoretical results fall short to fully explain the experimental data. Only when including the low-lying excited states in the quark propagator (ES quark propagator) the results are improved at the level of 15%, nearly in full accord with data.

Comparison of our results to other model calculations are presented in Table 4.6. Note, that our results for $A_{1/2}(Q^2 = 0)$ and $A_{3/2}(Q^2 = 0)$ follow the relation $A_{3/2} = \sqrt{3}A_{1/2}$ as in the naive SU_6 quark model. Recently, in the framework of large-N_c QCD [115] it was shown that the ratio $A_{3/2}/A_{1/2}$ is mostly saturated by the naive SU_6 value. Deviations from this standard result are due to higher order corrections with $A_{3/2}/A_{1/2} = \sqrt{3}+O(1/N_c^2)$. In the PCQM we evaluate the helicity amplitudes at one loop or, equivalently, to the order of accuracy $o(1/F^2, \hat{m}, m_s)$, where $F \sim \sqrt{N_c}$. Therefore, to get a non-trivial deviation from the SU_6 result the formalism has to be extended up to two loops or up to order $O(1/F^4) \sim O(1/N_c^2)$.

	$A_{1/2}(Q^2=0)$	$A_{3/2}(Q^2=0)$
GS quark propagator		
3q-core		
-LO	-69.7 ± 5.9	-120.7 ± 10.2
-NLO	-8.6 ± 1.2	-14.9 ± 2.1
Counter-term	8.2 ± 1.1	14.2 ± 1.9
Meson-cloud	-16.7 ± 2.6	-28.9 ± 4.5
Vertex-correction	-0.7 ± 0.1	-1.2 ± 0.1
Meson-in-flight	-23.0 ± 3.4	-39.8 ± 5.9
Total(GS)	-110.5 ± 0.3	-191.3 ± 0.5
ES quark propagator		
NLO	-10.3 ± 1.1	-17.8 ± 1.9
Counter-term	4.9 ± 0.6	8.5 ± 1.0
Meson-cloud	-13.5 ± 2.5	-23.4 ± 4.3
Vertex-correction	-0.7 ± 0.1	-1.2 ± 0.1
Total(ES)	-19.6 ± 3.1	-33.9 ± 5.3
Total=Total(GS)+Total(ES)	-130.1 ± 3.4	-225.2 ± 5.8
Experiment [43]	-135 ± 6	-250 ± 8

Table 4.4: *Contributions of the individual diagrams to the transverse helicity amplitudes for $Q^2 = 0$ (in units of 10^{-3} GeV$^{-1/2}$). Results for inclusion of ground state (GS) and excited states (ES) in the quark propagator are indicated separately.*

	$A_{1/2}(\pi)$	$A_{1/2}(K)$	$A_{1/2}(\eta)$	Total
GS quark propagators				
MC	-15.3	-1.4	-	-16.7
VC	-0.73	-	0.06	-0.67
ES quark propagators				
MC	-12.4	-1.1	-	-13.5
VC	-0.80	-	0.08	-0.72

Table 4.5: *Absolute contributions of π, K and η to $A_{1/2}(Q^2 = 0)$ for the meson-cloud (MC) and vertex-correction (VC) diagrams in units of 10^{-3} GeV$^{-1/2}$.*

The result for the Q^2 dependence of helicity amplitude $A_{1/2}(Q^2)$, when truncating the quark propagator to the ground state, is indicated in Fig. 4.9. We also list the individual contributions of the different diagrams which add up coherently. The leading order three-quark diagram dominates the prediction for $A_{1/2}$,

	$A_{1/2}(Q^2=0)$	$A_{3/2}(Q^2=0)$
NRQM [106]	-90.9	-181.9
Cloudy bag model [110]	-128	-222
Relativistic quark potential model [111]	-147	-277
PCQM	-130.1 ± 3.4	-225.2 ± 5.8
Experiment [43]	-135 ± 6	-250 ± 8

Table 4.6: *Total result for the helicity amplitudes $A_{1/2}(Q^2=0)$ and $A_{3/2}(Q^2=0)$ in comparison to other theoretical models (in units of 10^{-3} GeV$^{-1/2}$). The cloudy bag model results are taken for the values of a typical bag radius of $R = 0.8$ fm.*

whereas meson cloud corrections add about 30% to the total result. Here, both the meson-in-flight and the meson-cloud diagrams give the largest contribution. The effect on $A_{1/2}$ by including the intermediate excited quark states with quantum numbers $1p_{1/2}$, $1p_{3/2}$, $1d_{3/2}$, $1d_{5/2}$ and $2s_{1/2}$, that is, excitations up to $2\hbar\omega$, in the propagator is given in Fig. 4.10. Although higher lying state contributions are suppressed relative to the ground-state one, they still have a noticeable effect on $A_{1/2}$ for $Q^2 < 0.5$ GeV^2 at the order of 15%. The results for both $A_{1/2}(Q^2)$ and $A_{3/2}(Q^2) = \sqrt{3}A_{1/2}(Q^2)$ are shown in Fig. 4.11.

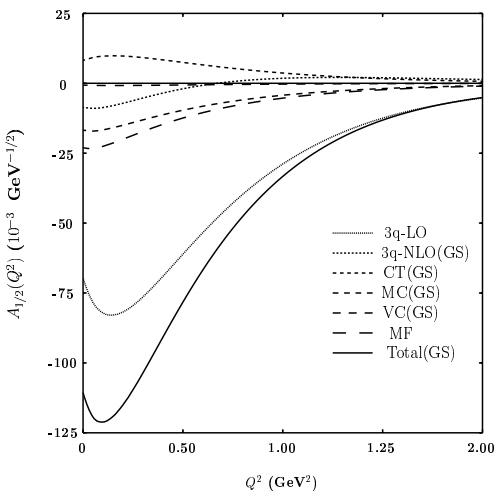

Figure 4.9: *Q^2 dependence of the transverse helicity amplitude $A_{1/2}(Q^2)$ for the case where the quark propagator is truncated to the ground state (GS) contribution. Legend: [3q-LO], 3q-diagram (leading order); [3q-NLO], 3q-diagram (next-to-leading order); [CT (GS)], counterterm; [MC (GS)], meson-cloud diagram; [VC (GS)], vertex-correction diagram; [MF], meson-in-flight diagram; and [Total (GS)], total result.*

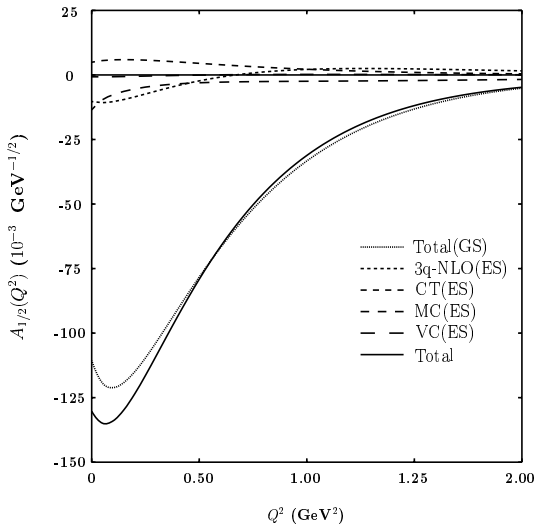

Figure 4.10: *Same as Fig. 4.9 but now for the case where excited quark states (ES) are included in the loop diagrams. The total GS result is also shown here for comparison.*

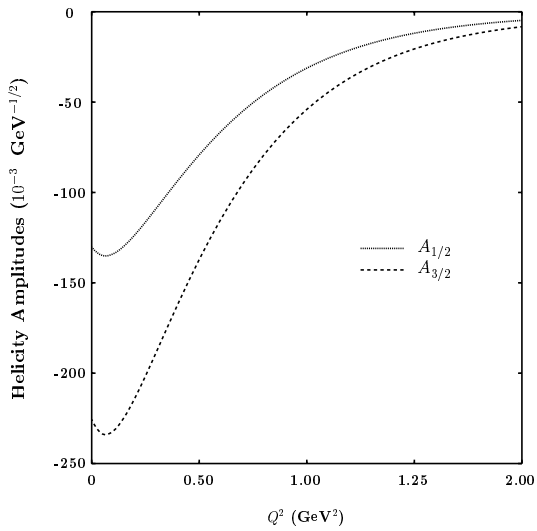

Figure 4.11: *Total results for the transverse helicity amplitudes $A_{1/2}(Q^2)$ and $A_{3/2}(Q^2) = \sqrt{3}\, A_{1/2}(Q^2)$.*

To complete our set of predictions we also indicate the results for the radiative transition $\Delta^+ \to p\gamma$. For the decay width, as based on Eq. (4.96), we obtain $\Gamma(\Delta^+ \to p\gamma) = 0.55 \pm 0.03$ MeV. Using the experimental value $\Gamma_{\text{total}}(\Delta^+) =$

111.2 MeV for the total decay width, we deduce the branching ratio

$$\mathrm{BR}(\Delta^+ \to p\gamma) = (0.47 - 0.52)\% \,. \tag{4.101}$$

In similar fashion we set for the partial decay branching ratios of helicity 1/2 and 3/2

$$\mathrm{BR}_{1/2} = (0.12 - 0.13)\% \quad \text{and} \quad \mathrm{BR}_{3/2} = (0.35 - 0.39)\% \,. \tag{4.102}$$

These results are in good agreement with the experimental data [43] : $\mathrm{BR}(\Delta^+ \to p\gamma) = (0.52 - 0.60)\%$, $\mathrm{BR}_{1/2} = (0.11 - 0.13)\%$ and $\mathrm{BR}_{3/2} = (0.41 - 0.47)\%$.

4.6 Summary

In this chapter we presented the perturbative chiral quark model (PCQM) and its applications to the electromagnetic form factors of the baryon octet and the electromagnetic $N - \Delta$ transitions. The PCQM is developed from the relativistic quark model suggested in [26, 28] which can be considered as a further development of chiral quark models with a perturbative treatment of the pion cloud [24, 25, 26, 28]. Compared to the previous similar models of Refs. [24, 25] our current approach contains several new features: i) generalization of the phenomenological confining potential; ii) SU(3) extension of chiral symmetry to include the K and η-meson cloud contributions; iii) consistent formulation of perturbation theory both on the quark and baryon level by use of renormalization techniques and by allowing to account for excited quark states in the meson loop diagrams; iv) fulfillment of the constraints imposed by chiral symmetry (low-energy theorems), including the current quark mass expansion of the matrix elements; v) possible consistency with chiral perturbation theory as for example in the chiral expansion of the nucleon mass.

The PCQM is based on an effective chiral Lagrangian describing quarks as relativistic fermions moving in a self-consistent field (static potential). The model potential defines unperturbed wave functions of quarks which are subsequently used in the calculation of baryon properties. Baryons in the PCQM are described as bound states of valence quarks surrounded by a cloud of Goldstone bosons (π, K, η) as required by chiral symmetry. Interaction of quarks with Goldstone bosons is introduced on the basis of the nonlinear σ-model [99]. When considering mesons fields as small fluctuations we restrict ourselves to the linear form of the meson-quark interaction. With the derived interaction Lagrangian we do our perturbation theory in the expansion parameter $1/F$ (where F is the pion leptonic decay constant in the chiral limit). We also treat the mass term of the current quarks as a small perturbation. Dressing the baryon three-quark core by a cloud

of Goldstone mesons corresponds to the inclusion of the sea-quark contribution. All calculations are performed at one loop or at order of accuracy $o(1/F^2, \hat{m}, m_s)$. The chiral limit with $\hat{m}, m_s \to 0$ is well defined. The PCQM has been applied to the study of the neutron electric dipole form factor [116], the nucleon polarizabilities [37], the mass spectrum of the J(P) = 1/2- and 3/2- pentaquark antidecuplets [117], the ground-state baryon masses [118], the axial form factor of the nucleon [36], the meson nucleon sigma terms [29, 35], the electromagnetic nucleon Delta transition [33], the electromagnetic form factors of the baryon [30, 34], the strange nucleon form factors [32], the electromagnetic couplings of the ChPT Lagrangian [119] and πN scattering including electromagnetic corrections [31]. Meson effects contribute significantly to the physical observables and improve the values arising from the three-quark core alone. The simplification of the calculational technique by restricting to the ground state quark propagator in the loop calculations was shown to result in a satisfactory phenomenology of a variety of baryon observables. However, the importance of including the low-lying excited quark states in the propagator is also reflected in the improvement of observables, where the meson cloud dominates. This concerns the neutron charge radius and the transverse helicity amplitudes of the electromagnetic $N - \Delta$ transition. The model, as it stands right now, has several simplifications: confinement is modelled by a non-covariant, local potential and meson corrections are evaluated up to one loop. Despite these restrictions, the PCQM works phenomenologically rather well in working out the role of valence quark degrees of freedom and the meson cloud. In the following we consider a further development of this approach, both in formulating a manifestly covariant description of valence quarks bound in the baryon and in a consistent inclusion of higher order chiral corrections.

Chapter 5

Lorentz covariant chiral quark model

In this chapter we present a further development of the perturbative chiral quark model (PCQM) as was discussed in Chapter 4. This involves a manifest Lorentz covariant formulation as opposed to the original non-covariant PCQM. Furthermore, we intend to include higher order chiral corrections in a consistent fashion. The corresponding chiral quark Lagrangian thereby stays in close analogy to the one of Chiral Perturbation Theory (ChPT). The basic idea is still the same, that is, the quark operators will be dressed by the Goldstone bosons as dictated by the chiral symmetry and these quark operators are projected on the baryonic level for calculating baryon matrix elements. In the following we will present the relevant Lagrangians for the dressing of the quark operators and the technique for calculating the electromagnetic nucleon matrix elements. The extension to study the properties of the baryon octet is straightforward. Finally, the physical applications of our approach will be presented.

5.1 Effective Lagrangian

5.1.1 Chiral Lagrangian

In order to dress the constituent quarks by mesonic degrees of freedom, we employ the chiral quark Lagrangian $\mathcal{L}_{qU}$ motivated from the chiral Lagrangians of ChPT. This Lagrangian consists of the two main pieces $\mathcal{L}_q$ and $\mathcal{L}_U$

$$\mathcal{L}_{qU} = \mathcal{L}_q + \mathcal{L}_U, \tag{5.1}$$

where

$$\begin{aligned}\mathcal{L}_q &= \mathcal{L}_q^{(1)} + \mathcal{L}_q^{(2)} + \mathcal{L}_q^{(3)} + \mathcal{L}_q^{(4)} + \dots\,, \\ \mathcal{L}_U &= \mathcal{L}_U^{(2)} + \dots\,. \end{aligned} \tag{5.2}$$

$\mathcal{L}_U$ is the Lagrangian composed of the mesonic degrees of freedom, whereas $\mathcal{L}_q$ refers to the quark degrees of freedom also containing the interaction with the mesonic degrees of freedom. Note that $\mathcal{L}_{qU}$ in general contains an infinite string of terms. In the practical calculation, we restrict to some specific order of accuracy. The superscript (i) attached to $\mathcal{L}_{q(U)}^{(i)}$ denotes the low energy dimension of the Lagrangian. For a fourth-order $O(p^4)$ calculation the explicit form of these terms relevant for the calculation of the baryonic properties are

$$\mathcal{L}_U^{(2)} = \frac{F^2}{4}\langle u_\mu u^\mu + \chi_+\rangle, \tag{5.3}$$

$$\mathcal{L}_q^{(1)} = \bar{q}\left[i\not{D} - m + \frac{1}{2}\, g \not{u}\, \gamma^5\right] q, \tag{5.4}$$

$$\begin{aligned}\mathcal{L}_q^{(2)} &= c_1\,\langle\chi_+\rangle\,\bar{q}q \;-\; \frac{c_2}{4m^2}\,\langle u_\mu u_\nu\rangle\,(\bar{q}\,D^\mu\,D^\nu\,q \;+\; \text{h.c.}\,) \\ &\quad + \frac{c_3}{2}\,\langle u_\mu\,u^\mu\rangle\bar{q}q + \frac{c_4}{4}\,\bar{q}\,i\,\sigma^{\mu\nu}\,[u_\mu, u_\nu]\,q \;+\; \frac{c_6}{8m}\,\bar{q}\,\sigma^{\mu\nu}\,F^+_{\mu\nu}\,q \\ &\quad -\bar{q}\mathcal{M}q + c_5\bar{q}\hat{\chi}_+q \;+\; \dots, \end{aligned} \tag{5.5}$$

$$\mathcal{L}_q^{(3)} = \frac{id_{10}}{2m}\,\bar{q}\,[D^\mu, F^+_{\mu\nu}]\,D^\nu\,q \;+\; \text{h.c.} \;+\dots\,, \tag{5.6}$$

$$\begin{aligned}\mathcal{L}_q^{(4)} &= -\frac{e_1}{16}\langle\chi_+\rangle^2\,\bar{q}\,q \;+\; \frac{e_2}{4}\langle\chi_+\rangle\Box(\bar{q}\,q) - \frac{e_3}{16}\langle\hat{\chi}_+^2\rangle\bar{q}q - \frac{e_4}{16}\langle\chi_+\rangle\bar{q}\hat{\chi}_+q \\ &\quad -\frac{e_5}{16}\bar{q}\hat{\chi}_+^2q + \frac{e_6}{2}\,\langle\chi_+\rangle\,\bar{q}\,\sigma^{\mu\nu}\,F^+_{\mu\nu}\,q \;+\; \frac{e_7}{4}\,\bar{q}\,\sigma^{\mu\nu}\,\{F^+_{\mu\nu}\hat{\chi}_+\}\,q \\ &\quad + \frac{e_8}{2}\,\bar{q}\,\sigma^{\mu\nu}\,\langle F^+_{\mu\nu}\hat{\chi}_+\rangle\,q \;-\; \frac{e_{10}}{2}\,\bar{q}\,[D^\alpha, [D_\alpha, F^+_{\mu\nu}]]\sigma^{\mu\nu}\,q \;+\dots, \end{aligned} \tag{5.7}$$

where $\hat{\chi}_+ = \chi_+ - \frac{1}{3}\langle\chi_+\rangle$. The symbols $\langle\ \rangle$, $[\ ]$ and $\{\ \}$ denote the trace over flavor matrices, commutator and anticommutator, respectively. The quark field is denoted by q.

The couplings m and g denote the quark mass and axial charge in the chiral limit. The low-energy coupling constants (LECs) c_i, d_i and e_i relate to the second-, third- and fourth-order and encode the contributions of heavy states. Note, that the inclusion of higher-dimensional terms in the chiral quark Lagrangian

was originally suggested in Ref. [120]. In particular, as a dimensional parameter in the higher-dimensional terms one can use the scale parameter of spontaneously broken chiral symmetry $\Lambda_\chi \simeq 4\pi F \sim 1$ GeV (F is the octet decay constant [21, 121]) instead of the constituent quark mass. This replacement is equivalent to a redefinition of the values of the low-energy constants, e.g. $c_2 \to c_2\,(m/\Lambda_\chi)^2$, $d_{10} \to d_{10}\,(m/\Lambda_\chi)$, etc.

The mesonic degrees of freedom are represented in the nonlinear realization by the SU(3) matrix U,

$$U = u^2 = \exp\left(i\frac{\phi}{F}\right), \tag{5.8}$$

containing the octet of pseudoscalar fields

$$\phi = \sum_{i=1}^{8} \phi_i \lambda_i = \sqrt{2}\begin{pmatrix} \pi^0/\sqrt{2}+\eta/\sqrt{6} & \pi^+ & K^+ \\ \pi^- & -\pi^0/\sqrt{2}+\eta/\sqrt{6} & K^0 \\ K^- & \bar{K}^0 & -2\eta/\sqrt{6} \end{pmatrix}, \tag{5.9}$$

where F is the octet decay constant [21, 121].

In the above expressions the following standard notations [11, 13, 122] are introduced

$$D_\mu = \partial_\mu + \Gamma_\mu, \;\; u_\mu = iu^\dagger \nabla_\mu U u^\dagger, \;\; \chi_\pm = u^\dagger \chi u^\dagger \pm u\chi^\dagger u, \tag{5.10}$$
$$\tag{5.11}$$

where the interaction terms of the external fields with the quarks and mesons are contained in

$$\begin{aligned} \Gamma_\mu &= \frac{1}{2}[u^\dagger, \partial_\mu u] - \frac{i}{2}u^\dagger R_\mu u - \frac{i}{2}u L_\mu u^\dagger, \\ \nabla_\mu U &= \partial_\mu U - iR_\mu U + iUL_\mu, \\ \chi &= 2B(s+ip), \;\; s = \mathcal{M} + \ldots \end{aligned} \tag{5.12}$$

Note, that s, p, v_μ and a_μ denote the external scalar, pseudoscalar, vector and axial fields with the definitions for R_μ and L_μ as

$$R_\mu = v_\mu + a_\mu, \;\; L_\mu = v_\mu - a_\mu. \tag{5.13}$$

For an electroweak interaction R_μ and L_μ are

$$R_\mu = eQA_\mu - Q\tan\theta_W Z^0_\mu + \dots , \tag{5.14}$$

$$L_\mu = eQA_\mu + \left(\frac{e}{\sin^2\theta_W}\lambda_3 - Q\right)\tan\theta_W Z^0_\mu + \frac{e}{\sin\theta_W\sqrt{2}}(W^+_\mu T_+ + \text{h.c.}) + \dots , \tag{5.15}$$

where A_μ, $W^\pm_\mu$ and Z^0_μ are the electromagnetic field, the weak charged and neutral boson fields. The quark charge matrix is denoted by $Q = \text{diag}\{2/3, -1/3, -1/3\}$ and

$$T_+ = \begin{pmatrix} 0 & V_{ud} & V_{us} \\ 0 & 0 & 0 \\ 0 & 0 & 0 \end{pmatrix} \tag{5.16}$$

is the weak matrix containing the Cabibbo-Kobayashi-Maskawa quark-mixing matrix elements V_{ij}. The tensor $F^+_{\mu\nu}$ is defined as $F^+_{\mu\nu} = u^\dagger F_{\mu\nu} Q u + u F_{\mu\nu} Q u^\dagger$, where $F_{\mu\nu} = \partial_\mu A_\nu - \partial_\nu A_\mu$ is the conventional photon field strength tensor. Here $\mathcal{M} = \text{diag}\{\hat{m}, \hat{m}, \hat{m}_s\}$ is the mass matrix of current quarks. The quark vacuum condensate parameter is denoted by

$$B = -\frac{1}{F^2}\langle 0|\bar{u}u|0\rangle = -\frac{1}{F^2}\langle 0|\bar{d}d|0\rangle . \tag{5.17}$$

To distinguish between constituent and current quark masses we attach the symbol $\hat{}$ ("hat") when referring to the current quark masses. We rely on the standard picture of chiral symmetry breaking ($B \gg F$). In the leading order of the chiral expansion the masses of pseudoscalar mesons are given by

$$M^2_\pi = 2\hat{m}B, \quad M^2_K = (\hat{m} + \hat{m}_s)B, \quad M^2_\eta = \frac{2}{3}(\hat{m} + 2\hat{m}_s)B. \tag{5.18}$$

In the numerical analysis we will use: $M_\pi = 139.57$ MeV, $M_K = 493.677$ MeV (the charged pion and kaon masses), $M_\eta = 574.75$ MeV and the canonical set of differentiated decay constants: $F_\pi = 92.4$ MeV, $F_K/F_\pi = 1.22$ and $F_\eta/F_\pi = 1.3$ [10].

The use of the physical masses and decay constants of the pseudoscalar mesons incorporates only part of the corrections due to the breaking of unitary flavor symmetry. To generate another part of $SU(3)$ symmetry-breaking corrections we add a string of terms to the Lagrangian (5.1): the current quark mass term $\bar{q}\mathcal{M}q$,

terms containing the LECs c_5, e_4, e_5, e_7 and e_8. The flavor-symmetry breaking terms containing the term $\bar{q}\mathcal{M}q$ and the LECS c_5, e_4 and e_5 allow to decouple the mass of the strange quark from the isospin-averaged mass m. The fourth-order couplings e_7 and e_8 incorporate explicit $SU(3)$ symmetry-breaking corrections in the magnetic moments of the constituent quarks and baryons. As was shown in Ref. [21] the inclusion of the $SU(3)$ symmetry-breaking terms is sufficient to obtain agreement with the experimental data for the magnetic moments of the baryon octet.

5.1.2 Inclusion of vector mesons

Following Refs. [9, 10, 20, 123], the vector mesons can be included in the chiral quark Lagrangian. The construction of the chirally invariant couplings of vector mesons to pseudoscalar mesons, photons and quarks is conveniently done in the tensor field representation of the spin-1 fields $W_{\mu\nu}$, which is an antisymmetric tensor $W_{\mu\nu} = -W_{\nu\mu}$. The explicit form is such that

$$W_{\mu\nu} = \begin{pmatrix} (\rho^0+\omega)/\sqrt{2} & \rho^+ & K^{*+} \\ \rho^- & (-\rho^0+\omega)/\sqrt{2} & K^{*0} \\ K^{*-} & \bar{K}^{*0} & -\phi \end{pmatrix}_{\mu\nu} . \tag{5.19}$$

The chirally invariant Lagrangian concerning the vector mesons is

$$\mathcal{L}_V = \mathcal{L}_V^0 + \mathcal{L}_V^{\rm int}, \tag{5.20}$$

where $\mathcal{L}_V^0$ is the free vector meson Lagrangian

$$\mathcal{L}_V^0 = -\frac{1}{2}\partial^\mu W^a_{\mu\nu}\partial_\rho W^{\rho\nu,a} + \frac{M_V^2}{4}W^a_{\mu\nu}W^{\mu\nu,a}, \tag{5.21}$$

and the interaction Lagrangian is decomposed into the terms $\mathcal{L}_V^{\rm int} = \mathcal{L}_V^{\rm int,1} + \mathcal{L}_V^{\rm int,2}$. The coupling of vector mesons to the external vector and axial-vector sources is encoded in $\mathcal{L}_V^{\rm int,1}$, whereas the vector mesons coupling to the quarks is described by $\mathcal{L}_V^{\rm int,2}$. We have

$$\begin{aligned} \mathcal{L}_V^{\rm int,1} &= \frac{F_V}{2\sqrt{2}}\langle W^{\mu\nu}F^+_{\mu\nu}\rangle + \frac{iG_V}{2\sqrt{2}}\langle W^{\mu\nu}[u_\mu,u_\nu]\rangle, \\ \mathcal{L}_V^{\rm int,2} &= \bar{q}\sigma^{\mu\nu}R_{\mu\nu}q + \bar{q}\gamma^\mu S_\mu q + \bar{q}\sigma^{\alpha\beta}U_{\mu\beta}[D_\alpha,[D^\mu,q]], \end{aligned} \tag{5.22}$$

where the definitions for $R_{\mu\nu}$, S_μ and $U_{\mu\beta}$ are

$$\begin{aligned} R_{\mu\nu} &= R_T W_{\mu\nu} + R_S \langle W_{\mu\nu} \rangle, \\ S_\mu &= S_T [D^\nu, W_{\mu\nu}] + S_S \langle [D^\nu, W_{\mu\nu}] \rangle, \\ U_{\mu\beta} &= U_T W_{\mu\beta} + U_S \langle W_{\mu\beta} \rangle. \end{aligned} \tag{5.23}$$

The effective couplings R_i, S_i and U_i can be related to the ones (g_{Vqq} and k_V) used in the canonical interaction Lagrangian of vector mesons with quarks

$$\mathcal{L}_{Vqq} = \frac{g_{Vqq}}{\sqrt{2}} \bar{q} \left(\gamma^\mu V_\mu - \frac{k_V}{2m} \sigma^{\mu\nu} \partial_\nu V_\mu \right) q, \tag{5.24}$$

where the standard nonet of vector mesons is V_μ. The matching conditions for these effective couplings are

$$\begin{aligned} R_S &= 0, \\ R_T &= -k_V g_{Vqq} \frac{M_V}{4m\sqrt{2}}, \\ U_S &= \frac{2}{m} S_S, \\ U_T &= \frac{2}{m} \left(\frac{g_{Vqq}}{M_V \sqrt{2}} + S_T \right). \end{aligned} \tag{5.25}$$

The couplings F_V and G_V can be determined by the decay widths of $\rho \to e^+e^-$ and $\rho \to \pi\pi$. Following the technique used in Refs. [20] one can write F_V and G_V in terms of the coupling g_{Vqq} and the mass of the vector meson M_V as

$$F_V = \frac{M_V}{g_{Vqq}}, \quad G_V = \frac{F_V}{2}. \tag{5.26}$$

Hence, in the vector meson sector we only deal with a single free parameter k_V.

5.2 Dressing of quark operators

With the previous considerations on the Lagrangian the total effective Lagrangian $\mathcal{L}_{\text{eff}}$ is

$$\mathcal{L}_{\text{eff}} = \mathcal{L}_{qU} + \mathcal{L}_V. \tag{5.27}$$

The Lagrangian $\mathcal{L}_{qU}$ is responsible for the dressing of quarks by a cloud of pseudoscalar mesons and heavy states, while $\mathcal{L}_V$ generates the coupling to vector mesons. To illustrate the idea of dressing quark operators by this effective Lagrangian, we consider the Fourier transform of the electromagnetic quark operator,

$$J^{\text{bare}}_{\mu,\text{em}}(q) = \int d^4x e^{-iqx} j^{\text{bare}}_{\mu,\text{em}}(x), \quad j^{\text{bare}}_{\mu,\text{em}}(x) = \bar{q}(x)\gamma_\mu Q q(x). \tag{5.28}$$

In Fig. 5.1 the Feynman diagrams generating the dressing of the quarks by $\mathcal{L}_{qU}$ up to fourth order are presented. By also taking into account the vector meson Lagrangian $\mathcal{L}_V$ additional diagrams with the coupling of vector mesons to both quarks and psedoscalar mesons occur, which are shown in Fig. 5.2.

The Fourier transform of the dressed quark operator is

$$J^{\text{dress}}_{\mu,\text{em}}(q) = \int d^4x e^{-iqx} \sum_{q=u,d,s} \bar{q}(x)\left[\gamma_\mu f^q_D(q^2) + \frac{i}{2m_q}\sigma_{\mu\nu}q^\nu f^q_P(q^2)\right]q(x), \tag{5.29}$$

where m_q is the dressed constituent quark mass. The Dirac and Pauli form factors of the quark with flavor $q = u$, d, s are f^q_D and f^q_P, respectively. The normalization of f^q_D is such that at zero recoil $f^q_D(0) \equiv e_q$, where e_q is the charge of the quark with flavor q.

Evaluation of the diagrams in Figs. 5.1 and 5.2 is based on the "infrared dimensional regularization" suggested in Ref. [13] to guarantee a straightforward connection between loop and chiral expansion in terms of quark masses and small external momenta. The discussion of the calculational technique is relegated to Appendix E. In Appendix F the explicit forms of the loop integrals are presented.

To calculate the electromagnetic form factors of the nucleon (or any baryon) we project the dressed quark operator between the nucleon (baryon) states. In the following we restrict to the case of the nucleon. The master formula is

$$\begin{aligned}
&\langle N(p')|J^{\text{dress}}_{\mu,\,\text{em}}(q)|N(p)\rangle \\
&\quad = (2\pi)^4\delta^4(p'-p-q)\bar{u}_N(p')\left\{\gamma_\mu F^N_1(q^2) + \frac{i}{2m_N}\sigma_{\mu\nu}q^\nu F^N_2(q^2)\right\}u_N(p) \\
&\quad = (2\pi)^4\delta^4(p'-p-q)\sum_{q=u,d}\left\{f^q_D(q^2)\langle N(p')|j^{\text{bare}}_{\mu,q}(0)|N(p)\rangle\right. \\
&\qquad \left. + i\frac{q^\nu}{2\bar{m}}f^q_P(q^2)\langle N(p')|j^{\text{bare}}_{\mu\nu,q}(0)|N(p)\rangle\right\},
\end{aligned} \tag{5.30}$$

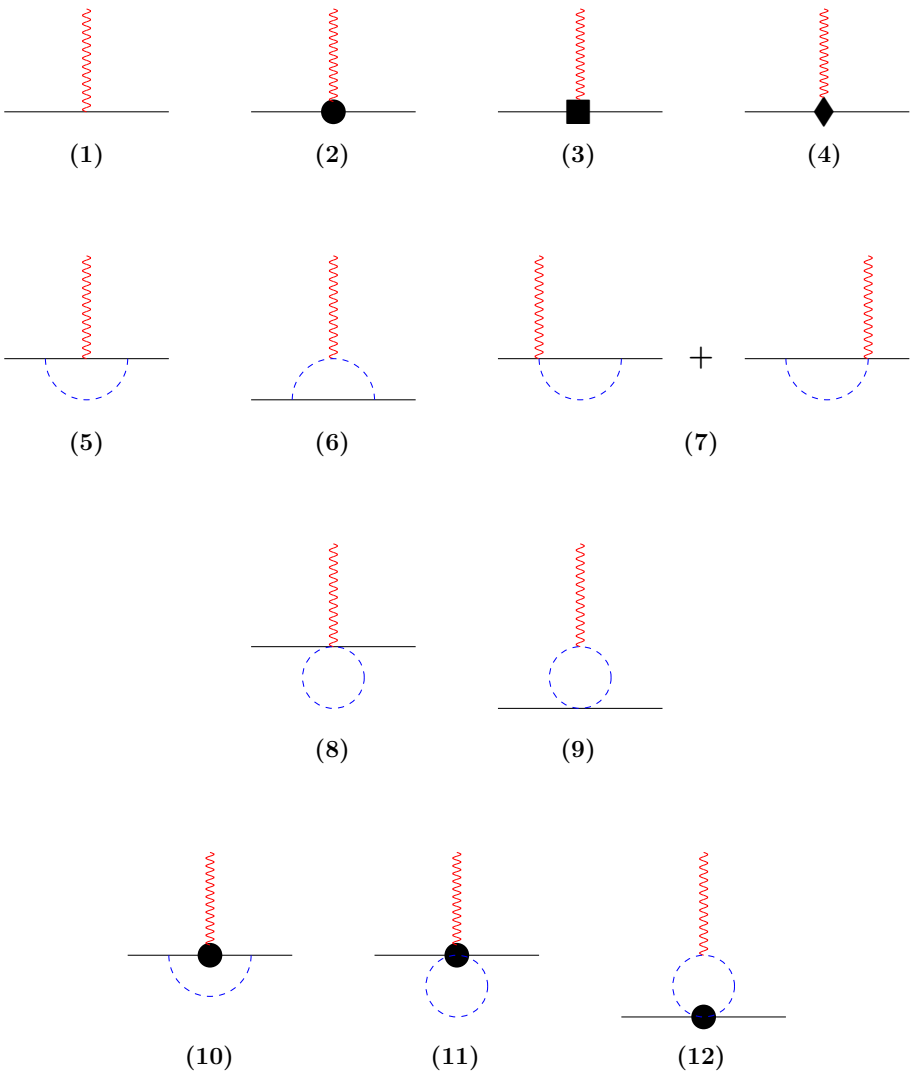

Figure 5.1: *Diagrams including pseudoscalar meson contributions to the EM quark transition operator up to fourth order. Solid, dashed and wiggly lines refer to quarks, pseudoscalar mesons and the electromagnetic field, respectively. Vertices denoted by a black filled circle, box and diamond correspond to insertions from the second, third and fourth order chiral Lagrangian.*

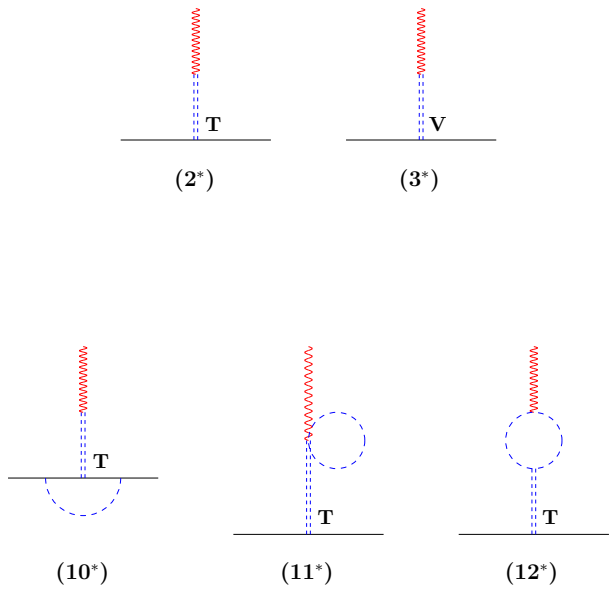

Figure 5.2: *Diagrams including vector-meson contributions to the EM quark transition operator. Double-dashed lines correspond to vector mesons. The symbols* **V** *and* **T** *refer to the vectorial and tensorial couplings of vector mesons to quarks.*

where $N(p)$ and $u_N(p)$ are the nucleon state and spinor, respectively, normalized as

$$\langle N(p')|N(p)\rangle = 2E_N(2\pi)^3\delta^3(\vec{p}-\vec{p}') \tag{5.31}$$

and

$$\bar{u}(p)u(p) = 2m_N \tag{5.32}$$

with E_N being the nucleon energy $E_N = \sqrt{m_N^2+\vec{p}^2}$. Here, $F_1^N(q^2)$ and $F_2^N(q^2)$ are the Dirac and Pauli nucleon form factors. In Eq. (5.30) we express the matrix elements of the dressed quark operator by the matrix elements of the bare operators. In our case we deal with the bare quark operators of the vector $j^{\rm bare}_{\mu,q}(0)$ and tensor $j^{\rm bare}_{\mu\nu,q}(0)$ structures defined as

$$\begin{aligned} j^{\rm bare}_{\mu,q}(0) &= \bar{q}(0)\gamma_\mu q(0), \\ j^{\rm bare}_{\mu\nu,q}(0) &= \bar{q}(0)\sigma_{\mu\nu} q(0). \end{aligned} \tag{5.33}$$

Eq. (5.30) contains our main result: we perform a model-independent factorization of the effects of hadronization and confinement contained in the matrix elements of the bare quark operators $j^{\rm bare}_{\mu,q}(0)$ and $j^{\rm bare}_{\mu\nu,q}(0)$ and the effects dictated by chiral symmetry (or chiral dynamics) which are encoded in the relativistic form factors $f^q_D(q^2)$ and $f^q_P(q^2)$. Due to this factorization the calculation of $f^q_D(q^2)$ and $f^q_P(q^2)$, on one side, and the matrix elements of $j^{\rm bare}_{\mu,q}(0)$ and $j^{\rm bare}_{\mu\nu,q}(0)$, on the other side, can be done independently. In particular, in a first step we derived a model-independent formalism based on the ChPT Lagrangian, which is formulated in terms of constituent quark degrees of freedom, for the calculation of $f^q_D(q^2)$ and $f^q_P(q^2)$. The calculation of the matrix elements of the bare quark operators can then be relegated to quark models based on specific assumptions about hadronization and confinement. The explicit forms of $f^q_D(q^2)$ and $f^q_P(q^2)$ are given in Appendix G.

5.3 Matching to ChPT

In order to calculate the matrix elements of the bare quark operators one should use a specific model with certain assumptions concerning hadronization and confinement. However, we show that additional constraints due to approximate symmetries of the system and model-independent predictions of some specific quantities can be used to relate the nucleon form factors and the quark form factors at zero recoil. Instead of using a specific quark model, we proceed with the general form deduced from Lorentz and gauge invariance of the bare matrix elements as

$$\begin{aligned}&\langle N(p')|j^{\rm bare}_{\mu,q}(0)|N(p)\rangle\\&\qquad=\bar u_N(p')\left\{\gamma_\mu F_1^{Nq}(q^2)+\frac{i}{2m_N}\sigma_{\mu\nu}q^\nu F_2^{Nq}(q^2)\right\}u_N(p),\end{aligned}\tag{5.34}$$

$$\begin{aligned}&i\frac{q^\nu}{2m_q}\langle N(p')|j^{\rm bare}_{\mu\nu,q}(0)|N(p)\rangle\\&\qquad=\bar u_N(p')\left\{\gamma_\mu G_1^{Nq}(q^2)+\frac{i}{2m_N}\sigma_{\mu\nu}q^\nu G_2^{Nq}(q^2)\right\}u_N(p).\end{aligned}\tag{5.35}$$

The Pauli and Dirac form factors $F^{Nq}_{1(2)}(q^2)$ and $G^{Nq}_{1(2)}(q^2)$ describe the distribution of quarks of flavor $q=u$, d in the nucleon.

At zero recoil, we obtain from charge conservation and isospin invariance the relations

$$
\begin{aligned}
&F_1^{pu}(0) = F_1^{nd}(0) = 2, \qquad F_1^{pd}(0) = F_1^{nu}(0) = 1,\\
&G_1^{Nq}(0) = 0,\\
&F_2^{pu}(0) = F_2^{nd}(0), \qquad F_2^{pd}(0) = F_2^{nu}(0),\\
&G_2^{pu}(0) = G_2^{nd}(0), \qquad G_2^{pd}(0) = G_2^{nu}(0).
\end{aligned}
$$

One can relate $G_2^{Nq}(0)$ to the so-called bare nucleon tensor charges $\delta_{Nq}^{\text{bare}}$ defined in Ref. [124] as

$$
\langle N(p)|j_{\mu\nu,q}^{\text{bare}}(0)|N(p)\rangle = \delta_{Nq}^{\text{bare}}\bar{u}_N(p)\sigma_{\mu\nu}u_N(p). \tag{5.36}
$$

In terms of $\delta_{Nq}^{\text{bare}}$ the relations for $G_2^{Nq}(0)$ are

$$
\begin{aligned}
G_2^{pu}(0) = G_2^{nd}(0) &= \frac{m_N}{\bar{m}}\delta_{pu}^{\text{bare}} = \frac{m_N}{\bar{m}}\delta_{nd}^{\text{bare}},\\
G_2^{pd}(0) = G_2^{nu}(0) &= \frac{m_N}{\bar{m}}\delta_{pd}^{\text{bare}} = \frac{m_N}{\bar{m}}\delta_{nu}^{\text{bare}}.
\end{aligned}
$$

Additional constraints are the so-called "chiral symmetry constraints". They are dictated by the infrared-singular structure of QCD in order to reproduce the leading nonanalytic (LNA) contributions to the magnetic moments and the charge and magnetic radii of nucleons [20, 125]

$$
\begin{aligned}
\mu_p &= -\frac{g_A^2}{8\pi}\frac{M_\pi}{F_\pi^2}\,\mathring{m}_N + \ldots,\\
\langle r^2\rangle_p^E &= -\frac{1+5g_A^2}{16\pi^2 F_\pi^2}\ln\frac{M_\pi}{\mathring{m}_N} + \ldots,\\
\langle r^2\rangle_p^M &= \frac{g_A^2}{16\pi F_\pi^2\mu_p}\frac{\mathring{m}_N}{M_\pi} + \ldots,
\end{aligned} \tag{5.37}
$$

where g_A and $\mathring{m}_N$ are the axial charge and mass of the nucleon in the chiral limit. By matching our LEC d_{10} on the quark level together with the $F_2^{Nq}(0)$ and $G_2^{Nq}(0)$ form factors to the calculation of ChPT involving the LEC d_6^{ChPT} we obtain

$$
\begin{aligned}
1 + F_2^{pu}(0) - F_2^{pd}(0) = G_2^{pu}(0) - G_2^{pd}(0) &= \left(\frac{g_A}{g}\right)^2\frac{m_N}{\bar{m}},\\
1 + F_2^{nd}(0) - F_2^{nu}(0) = G_2^{nd}(0) - G_2^{nu}(0) &= \left(\frac{g_A}{g}\right)^2\frac{m_N}{\bar{m}}
\end{aligned}
$$

and

$$\bar{d}_6^{\rm ChPT} + \frac{1+5g_A^2}{96\pi^2 F_\pi^2}\ln\frac{M_\pi}{\overset{\circ}{m}_N} \equiv \bar{d}_{10} + \frac{1+5g^2}{96\pi^2 F_\pi^2}\ln\frac{M_\pi}{\overset{\circ}{m}_N}. \tag{5.38}$$

The renormalized LECs $\bar{d}_6^{\rm ChPT}$ and $\bar{d}_{10}$ at the renormalization scale $\mu = \overset{\circ}{m}_N$ are

$$\begin{aligned} \bar{d}_6^{\rm ChPT} &= d_6^{\rm ChPT} + \frac{1+5g_A^2}{6F_\pi^2}\bar{\lambda}, \\ \bar{d}_{10} &= d_{10} + \frac{1+5g^2}{6F_\pi^2}\bar{\lambda}, \end{aligned} \tag{5.39}$$

where $\bar{\lambda} = \lambda(\overset{\circ}{m}_N)$ and

$$\lambda(\mu) = \frac{\mu^{d-4}}{(4\pi)^2}\left\{\frac{1}{d-4} - \frac{1}{2}(\ln 4\pi + \Gamma'(1) + 1)\right\}, \tag{5.40}$$

with the Euler constant $\gamma_E = -\Gamma'(1)$.

Furthermore, we apply the SU(6)-symmetry relation for the ratio of the nucleon magnetic moment and the nucleon tensor charge in the naive nonrelativistic quark model to give a further constraint on $F_2^{Nq}(0)$ and $G_2^{Nq}(0)$. The results are

$$\frac{2+F_2^{pu}(0)}{1+F_2^{pd}(0)} = \frac{2+F_2^{nd}(0)}{1+F_2^{nu}(0)} = \frac{G_2^{pu}(0)}{G_2^{pd}(0)} = \frac{G_2^{nd}(0)}{G_2^{nu}(0)} = -4. \tag{5.41}$$

Finally, by using Eq. (5.38) and Eq. (5.41) the values of $F_2^{Nq}(0)$ and $G_2^{Nq}(0)$ are

$$\begin{aligned} F_2^{pu}(0) = F_2^{nd}(0) &= \frac{4}{5}\left(\frac{g_A}{g}\right)^2\frac{m_N}{\bar{m}} - 2, \\ F_2^{pd}(0) = F_2^{nu}(0) &= -\frac{1}{5}\left(\frac{g_A}{g}\right)^2\frac{m_N}{\bar{m}} - 1, \\ G_2^{pu}(0) = G_2^{nd}(0) &= \frac{4}{5}\left(\frac{g_A}{g}\right)^2\frac{m_N}{\bar{m}}, \\ G_2^{pd}(0) = G_2^{nu}(0) &= -\frac{1}{5}\left(\frac{g_A}{g}\right)^2\frac{m_N}{\bar{m}}. \end{aligned} \tag{5.42}$$

Note that from all the constraints discussed above we automatically obtain predictions for the bare values of the nucleon magnetic moments and tensor charges

$$\mu_p^{\text{bare}} \equiv -\frac{3}{2}\mu_n^{\text{bare}} = \sum_{q=u,d} e_q[F_1^{pq}(0) + F_2^{pq}(0)] = \frac{3}{5}\left(\frac{g_A}{g}\right)^2 \frac{m_N}{\bar{m}} \tag{5.43}$$

and

$$\delta_{pu}^{\text{bare}} \equiv -4\delta_{pd}^{\text{bare}} = \frac{\bar{m}}{m_N} G_2^{pu}(0) = \frac{4}{5}\left(\frac{g_A}{g}\right)^2, \tag{5.44}$$

where $e_u = 2/3$ and $e_d = -1/3$ are the electric charges of u and d quarks, respectively.

5.4 Nucleon mass and meson-nucleon σ-terms

Two other important quantities of low-energy nucleon physics that we are going to consider are the nucleon mass and the meson-nucleon σ-terms which are constrained by the Feynman-Hellmann theorem (FHT) [126]. The FHT relates the derivative of the nucleon mass with respect to the current quark masses to the pion-nucleon sigma-term $\sigma_{\pi N}$ and to the strange quark condensate in the nucleon y_s by

$$\begin{aligned} \sigma_{\pi N}\bar{u}_N(p)u_N(p) &\doteq \hat{m}\langle N(p)|\bar{u}(0)u(0) + \bar{d}(0)d(0)|N(p)\rangle \\ &= \hat{m}\frac{\partial m_N}{\partial \hat{m}}\bar{u}_N(p)u_N(p), \end{aligned} \tag{5.45}$$

$$y_s\bar{u}_N(p)u_N(p) \doteq \langle N(p)|\bar{s}(0)s(0)|N(p)\rangle = \frac{\partial m_N}{\partial \hat{m}_s}\bar{u}_N(p)u_N(p). \tag{5.46}$$

5.4.1 Nucleon mass

In quantum field theory the nucleon mass m_N is defined as the matrix element of the trace of the energy-momentum tensor $\Theta^{\mu\nu}(x)$

$$m_N\,\bar{u}_N(p)u_N(p) \doteq \langle N(p)|\Theta^{\mu}_{\mu}(0)|N(p)\rangle\,. \tag{5.47}$$

When we restrict to one-body interactions between the quarks and neglect the contribution of the heavy quarks in the constituent quark (CQ) approach, the master formula (5.30) spells as

$$m_N \bar{u}_N(p) u_N(p) \doteq \langle N(p)|\mathcal{H}_{\rm mass}(0)|N(p)\rangle \,. \tag{5.48}$$

$\mathcal{H}_{\rm mass}(x) = \bar{q}(x) m_q q(x)$ is the part of the Hamiltonian referred to as the quark mass term where $m_q = {\rm diag}\{m_u, m_d, m_s\}$ is the matrix of constituent quark masses with $m_u = m_d = \bar{m}$ due to isospin invariance. Note, Eq.(5.48) is valid in the one-body approximation. In general, one should include in the trace of the energy-momentum tensor also two- and three-body quark operators which encode quark-quark interaction contributions to the nucleon mass. In some CQ models the nontrivial dependence of m_q (or m_N) on the current quark masses is missing. This leads to a contradiction with the low-energy behavior of the nucleon mass as a function of $\hat{m}(\hat{m}_s)$ and with the Feynman-Hellmann theorem. The use of the effective Lagrangian (5.1) constrained by Baryon ChPT enables one to perform an accurate and consistent calculation of the nucleon mass and the corresponding sigma-terms. As in the case of the electromagnetic form factors, the extension to other baryons is straightforward.

In analogy with the electromagnetic form factors we define the nucleon mass and later on the sigma-terms as expectation values of the dressed operators. First, we write down the bare quark mass term as

$$\mathcal{H}^{\rm bare}_{\rm mass}(x) = m \bar{q}(x) q(x) \tag{5.49}$$

i.e. the quark mass term at leading order of the chiral expansion (in the chiral limit). Here m is the value of the constituent quark mass in the chiral limit introduced before in the Lagrangian (5.1). The nucleon mass in the chiral limit $\overset{\circ}{m}_N$ is defined by

$$\begin{aligned} \overset{\circ}{m}_N \; \bar{u}_N(p) u_N(p) &= \langle N(p)|\mathcal{H}^{\rm bare}_{\rm mass}(0)|N(p)\rangle \\ &= m \langle N(p)|\bar{q}(0) q(0)|N(p)\rangle \,. \end{aligned} \tag{5.50}$$

The dressed quark mass term and the physical nucleon mass are given by

$$\begin{aligned} \mathcal{H}^{\rm dress}_{\rm mass}(x) &= \bar{q}(x) m_q q(x), \\ m_N \bar{u}_N(p) u_N(p) &= \langle N(p)|\mathcal{H}^{\rm dress}_{\rm mass}(0)|N(p)\rangle \\ &= \langle N(p)|\bar{q}(0) m_q q(0)|N(p)\rangle, \end{aligned} \tag{5.51}$$

where $m_q = {\rm diag}\{m_u, m_d, m_s\}$ is the matrix of the dressed (physical) constituent quark masses (in our case the constituent quark mass at one loop with inclusion

of chiral corrections) with $m_u = m_d$ due to isospin invariance. The constituent quark masses $m_q \doteq m_q(\hat{m}, \hat{m}_s)$ have a nontrivial dependence on the current quark masses $\hat{m}$ and $\hat{m}_s$ which can be accurately calculated with the use of the chiral Lagrangian (5.1). For illustration we discuss the explicit expressions for the nonstrange and strange constituent quark masses at one loop and at $O(p^4)$ with

$$m_q = m + \Sigma_q(m). \tag{5.52}$$

The quark mass operator $\Sigma_q = \mathrm{diag}\{\Sigma_u, \Sigma_d, \Sigma_s\}$, with $\Sigma_u = \Sigma_d = \bar{\Sigma}$ due to isospin invariance, is evaluated on the mass-shell $\not{p} = m$, which is ultraviolet-finite by construction. All ultraviolet divergences are removed via the renormalization of the fourth-order LECs e_1, e_3, e_4 and e_5 contributing to the Σ_q operator. Here and in the following we identify the quark mass occurring in the loop integrals with its leading order value $m_q \to m$. The operator Σ_q is described by the diagrams in Fig. 5.3 and after expansion in powers of meson masses is given by

$$\begin{aligned}
\bar{\Sigma} \;=\;& \hat{m} - \frac{3g^2}{32\pi}\left\{\frac{M_\pi^3}{F_\pi^2} + \frac{2}{3}\frac{M_K^3}{F_K^2} + \frac{M_\eta^3}{9\,F_\eta^2}\right\} - \frac{3g^2}{64\pi^2 m}\left\{\frac{M_\pi^4}{F_\pi^2} + \frac{2}{3}\frac{M_K^4}{F_K^2} + \frac{M_\eta^4}{9\,F_\eta^2}\right\} \\
& -4c_1 M^2 + \frac{3c_2}{128\pi^2}\left\{\frac{M_\pi^4}{F_\pi^2} + \frac{4}{3}\frac{M_K^4}{F_K^2} + \frac{M_\eta^4}{3\,F_\eta^2}\right\} + \frac{4}{3}c_5(M_K^2 - M_\pi^2) \\
& +\bar{e}_1 M^4 + \frac{\bar{e}_3}{6}(M_K^2 - M_\pi^2)^2 - \frac{\bar{e}_4}{3}M^2(M_K^2 - M_\pi^2) + \frac{\bar{e}_5}{36}(M_K^2 - M_\pi^2)^2
\end{aligned}$$

and

$$\begin{aligned}
\Sigma_s \;=\;& \hat{m}_s - \frac{3g^2}{32\pi}\left\{\frac{4}{3}\frac{M_K^3}{F_K^2} + \frac{4}{9}\frac{M_\eta^3}{F_\eta^2}\right\} - \frac{3g^2}{64\pi^2 m}\left\{\frac{4}{3}\frac{M_K^4}{F_K^2} + \frac{4}{9}\frac{M_\eta^4}{F_\eta^2}\right\} \\
& -4c_1 M^2 + \frac{3c_2}{128\pi^2}\left\{\frac{M_\pi^4}{F_\pi^2} + \frac{4}{3}\frac{M_K^4}{F_K^2} + \frac{M_\eta^4}{3\,F_\eta^2}\right\} - \frac{8}{3}c_5(M_K^2 - M_\pi^2) \\
& +\bar{e}_1 M^4 + \frac{\bar{e}_3}{6}(M_K^2 - M_\pi^2)^2 + \frac{2\bar{e}_4}{3}M^2(M_K^2 - M_\pi^2) + \frac{\bar{e}_5}{9}(M_K^2 - M_\pi^2)^2
\end{aligned}$$

where

$$M^2 = M_\pi^2 - M_K^2 + \frac{3}{2}M_\eta^2 = \frac{1}{2}M_\pi^2 + M_K^2\,. \tag{5.53}$$

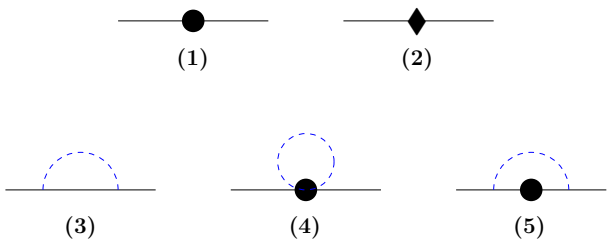

Figure 5.3: *Diagrams contributing to the mass operator of the quark at one loop. Vertices denoted by a black filled circle and diamond correspond to insertions from the second and fourth order chiral Lagrangian.*

Note, that $\bar{\Sigma}$ and Σ_s are degenerate for $\hat{m} = \hat{m}_s$ and M^2 coincides with M_π^2 at $\hat{m}_s = 0$. For simplicity the chiral logarithms are hidden in the renormalized LECs $\bar{e}_i$ with $i = 1, 3, 4, 5$:

$$\bar{e}_i = e_i^r(\mu) - \frac{\beta_{e_i}}{32\pi^2 F_\pi^2} \ln \frac{M_\pi^2}{\mu^2} = e_i - \frac{\beta_{e_i}}{F_\pi^2} \lambda_\pi, \tag{5.54}$$

where

$$\lambda_\pi = \frac{M_\pi^{d-4}}{(4\pi)^2} \left\{ \frac{1}{d-4} - \frac{1}{2}(\ln 4\pi + \Gamma'(1) + 1) \right\}. \tag{5.55}$$

The LECs e_i contain the poles at $d = 4$ which are cancelled by the divergences proportional to λ_π in the r.h.s. of Eq. (5.54). Therefore, the renormalized couplings $e_i^r(\mu)$ (or $\bar{e}_i$) are finite. The set of the β_{e_i} coefficients is given by

$$\begin{aligned}
\beta_{e_1} &= \frac{32g^2}{27m} - \frac{8}{9}(8c_1 - c_2 - 4c_3), \\
\beta_{e_3} &= \frac{52g^2}{9m} - \frac{10}{3}(8c_1 - c_2 - 4c_3) + \frac{16}{9}c_5, \\
\beta_{e_4} &= \frac{20g^2}{9m} - \frac{32}{3}c_5, \\
\beta_{e_5} &= -\frac{4g^2}{m} - \frac{16}{3}c_5.
\end{aligned} \tag{5.56}$$

Note, that the $m_s - \bar{m}$ splitting is mainly generated by the difference in the values of the strange and the nonstrange current quark masses. The chiral symmetry constraints and the matching of the nucleon mass calculated within our approach to the model-independent derivation of [13] allow to deduce certain relations between the set of our parameters and the ones in Baryon ChPT. In particular, the

coefficient connected with M_π^3/F_π^2, referred to in the literature as the "leading non-analytic coefficient" (LNAC) [9, 10, 13], is model-independent and constant due to dimensional arguments. Precisely, this coefficient is equal to $-3g_A^2/(32\pi F_\pi^2)$. The cubic term in powers of the meson mass shows up due to the infrared singularity of the diagram in Fig. 5.3(3). Using this requirement, we can relate the value of axial charge of the constituent quark in the chiral limit to the corresponding nucleon quantity

$$g_A^2 \bar{u}_N(p) u_N(p) = g^2 \langle N(p)|\bar{q}(0)q(0)|N(p)\rangle. \tag{5.57}$$

The matching condition gives a constraint for the matrix element of the bare scalar-density operator in the nucleon. A rough estimate with $g_A = 1.25$ [11], $g \sim 1$ and by taking into account the normalization of the nucleon spinors gives quite a reasonable value for the scalar condensate, $\langle N(p)|\bar{q}(0)\, q(0)|N(p)\rangle \sim (25/8)\, m_N$. Using the matching condition (5.57) we derive a final expression for the nucleon mass at one loop

$$m_N = \mathring{m}_N + \Sigma_N, \tag{5.58}$$

where

$$m_N = \left(\frac{g_A}{g}\right)^2 \bar{m}, \qquad \mathring{m}_N = \left(\frac{g_A}{g}\right)^2 m \tag{5.59}$$

and

$$\begin{aligned}
\Sigma_N \;=\; & -\frac{3g_A^2}{32\pi}\left\{\frac{M_\pi^3}{F_\pi^2} + \frac{2}{3}\frac{M_K^3}{F_K^2} + \frac{M_\eta^3}{9\,F_\eta^2}\right\} - \frac{3g_A^2}{64\pi^2 m}\left\{\frac{M_\pi^4}{F_\pi^2} + \frac{2}{3}\frac{M_K^4}{F_K^2} + \frac{M_\eta^4}{9\,F_\eta^2}\right\} \\
& + \left(\frac{g_A}{g}\right)^2 \Bigg[\hat{m} - 4c_1 M^2 + \frac{3c_2}{128\pi^2}\left\{\frac{M_\pi^4}{F_\pi^2} + \frac{4}{3}\frac{M_K^4}{F_K^2} + \frac{M_\eta^4}{3\,F_\eta^2}\right\} + \frac{4}{3}c_5(M_K^2 - M_\pi^2) \\
& + \bar{e}_1 M^4 + \frac{\bar{e}_3}{6}(M_K^2 - M_\pi^2)^2 - \frac{\bar{e}_4}{3}M^2(M_K^2 - M_\pi^2) + \frac{\bar{e}_5}{36}(M_K^2 - M_\pi^2)^2\Bigg].
\end{aligned}$$

The constituent quark mass can be removed from the expressions for nucleon observables using the matching conditions (5.59). The same is also true for other baryonic observables and where the constituent quark mass can be removed from the corresponding expressions. In the SU(2) picture (when neglecting the kaon

and η-meson loops and putting c_5 and e_5 to be equal to zero) we reproduce the result of ChPT for the nucleon mass at one loop and at order $O(p^4)$ [13]

$$\begin{aligned}
m_N &= \overset{\circ}{m}_N - 4c_1^{\rm ChPT} - \frac{3g_A^2}{32\pi}\frac{M_\pi^3}{F_\pi^2} + k_1 M_\pi^4 \ln\frac{M_\pi}{\overset{\circ}{m}_N} + k_2 M_\pi^4 + O(M_\pi^5),\\
k_1 &= -\frac{3}{32\pi^2 F_\pi^2}\left(\frac{g_A^2}{\overset{\circ}{m}_N} - 8c_1^{\rm ChPT} + c_2^{\rm ChPT} + 4c_3^{\rm ChPT}\right),\\
k_2 &= \bar{e}_1^{\rm ChPT} - \frac{3}{128\pi^2 F_\pi^2}\left(\frac{2g_A^2}{\overset{\circ}{m}_N} - c_2^{\rm ChPT}\right),\\
\bar{e}_1^{\rm ChPT} &= e_1^{\rm ChPT} - \frac{3\bar{\lambda}}{2F_\pi^2}\left(\frac{g_A^2}{\overset{\circ}{m}_N} - 8c_1^{\rm ChPT} + c_2^{\rm ChPT} + 4c_3^{\rm ChPT}\right),
\end{aligned} \tag{5.60}$$

if we fulfill the following matching conditions between the LECs of the ChPT Lagrangian and our quark-level Lagrangian

$$\begin{aligned}
&-4c_1^{\rm ChPT} M_\pi^2 = \left[\hat{m} - 4c_1 M_\pi^2\right]\left(\frac{g_A}{g}\right)^2,\\
&8c_1^{\rm ChPT} - c_2^{\rm ChPT} - 4c_3^{\rm ChPT} - \frac{g_A^2}{\overset{\circ}{m}_N} \equiv \left[8c_1 - c_2 - 4c_3 - \frac{g_A^2}{\overset{\circ}{m}_N}\right]\left(\frac{g_A}{g}\right)^2,\\
&\bar{e}_1^{\rm ChPT} - \frac{3}{64\pi^2 F_\pi^2}\left(\frac{2g_A^2}{\overset{\circ}{m}_N} - c_2^{\rm ChPT}\right)\\
&\qquad \equiv \left[\bar{e}_1^* - \frac{3}{64\pi^2 F_\pi^2}\left(\frac{2g_A^2}{\overset{\circ}{m}_N} - c_2\right)\right]\left(\frac{g_A}{g}\right)^2,
\end{aligned} \tag{5.61}$$

where $\bar{e}_1^*$ is a $SU(2)$ analogue of $\bar{e}_1$ derived in Eqs. (5.54) and (5.56) in the three-flavor picture

$$\begin{aligned}
\bar{e}_1^* &= e_1^* - \frac{\beta_{e_1^*}}{F_\pi^2}\lambda_\pi,\\
\beta_{e_1^*} &= \frac{3}{2}\left(\frac{g^2}{m} - 8c_1 + c_2 + 4c_3\right).
\end{aligned} \tag{5.62}$$

Note, that there is an additional condition on g and g_A which shows up in the calculation of the axial nucleon charge

$$g_A \bar{u}_N(p)\gamma^\mu\gamma^5\tau_3 u_N(p) = g\langle N(p)|\bar{q}(0)\gamma^\mu\gamma^5\tau_3 q(0)|N(p)\rangle. \tag{5.63}$$

Eq. (5.63) gives a constraint on the matrix element of the isovector axial current.

5.4.2 Pion-nucleon σ-terms

As an example for the sigma-terms we consider the pion-nucleon sigma-term $\sigma_{\pi N}$. In QCD (see Eq. (5.45)) this quantity is related to the expectation value of the scalar density operator. It is connected to the derivative of the part of the QCD Hamiltonian, explicitly breaking chiral symmetry, with respect to the current quark mass. This definition is consistent with the FH theorem [126]. In the context of CQ models, we should proceed with the dressed Hamiltonian $\mathcal{H}^{\rm dress}_{\rm mass}(x)$ which already showed up in the calculation of the physical nucleon mass. In particular, the dressed scalar density operators $j_i^{\rm dress}(x)$ (where $i = u, d, s$ is the flavor index), relevant for the calculation of the meson-baryon sigma-terms within our approach, are defined as the partial derivatives of $\mathcal{H}^{\rm dress}_{\rm mass}(x)$ with respect to the current quark mass $\hat{m}_i$ of i-th flavor

$$j_i^{\rm dress}(x) \doteq \frac{\partial \mathcal{H}^{\rm dress}_{\rm mass}(x)}{\partial \hat{m}_i} = \bar{q}(x)\frac{\partial m_q}{\partial \hat{m}_i}q(x) = \bar{q}(x)\frac{\partial \Sigma_q}{\partial \hat{m}_i}q(x). \tag{5.64}$$

In the case of $\sigma_{\pi N}$ we have

$$\sigma_{\pi N}\bar{u}_N(p)u_N(p) \doteq \hat{m}\langle N(p)|j_u^{\rm dress}(0) + j_d^{\rm dress}(0)|N(p)\rangle. \tag{5.65}$$

It should be clear that Eq. (5.65) is consistent with the FH theorem

$$\sigma_{\pi N}\bar{u}_N(p)u_N(p) = \hat{m}\frac{\partial}{\partial \hat{m}}\underbrace{\langle N(p)|\mathcal{H}^{\rm dress}_{\rm mass}(0)|N(p)\rangle}_{=m_N\bar{u}_N(p)u_N(p)} = \hat{m}\frac{\partial m_N}{\partial \hat{m}}\bar{u}_N(p)u_N(p). \tag{5.66}$$

Below we give the definitions of the strangeness content of the nucleon y_N, the kaon-nucleon σ_{KN} and the eta-nucleon $\sigma_{\eta N}$ sigma-terms

$$\begin{aligned}
y_N &= 2\frac{\partial m_N/\partial \hat{m}_s}{\partial m_N/\partial \hat{m}}, \\
\bar{u}_N(p)u_N(p)\sigma_{KN}^{u(d)} &= \frac{\hat{m}+\hat{m}_s}{2}\langle N(p)|j^{\rm dress}_{u(d)s;+}(0)|N(p)\rangle, \\
\bar{u}_N(p)u_N(p)\sigma_{KN}^{I=0} &= \frac{\hat{m}+\hat{m}_s}{4}\langle N(p)|j^{\rm dress}_{us;+}(0) + j^{\rm dress}_{ds;+}(0)|N(p)\rangle, \\
\bar{u}_N(p)u_N(p)\sigma_{KN}^{I=1} &= \frac{\hat{m}+\hat{m}_s}{2}\langle N(p)|j^{\rm dress}_{ud;-}(0)|N(p)\rangle, \\
\bar{u}_N(p)u_N(p)\sigma_{\eta N} &= \frac{1}{3}\langle N(p)|\hat{m}j^{\rm dress}_{ud;+}(0) + 4\hat{m}_s j^{\rm dress}_s(0)|N(p)\rangle,
\end{aligned} \tag{5.67}$$

where $j^{\rm dress}_{qq';\pm} = j^{\rm dress}_q \pm j^{\rm dress}_{q'}$ and $|N(p)\rangle$ denotes a proton state. All further details can be found in our previous papers [29, 35] and in Appendix H.

5.5 Physical applications

We will apply the covariant approach of the PCQM to some properties of nucleon. We start from the masses of the baryon octet and the meson-nucleon sigma-terms. Next, the magnetic moments of the baryon octet will be considered. We will also discuss the electromagnetic form factors of the nucleon. Finally, the coupling of vector mesons to the nucleon will be studied. Our main interest is to study nucleon properties in the small momentum transfer region where the contributions of the meson cloud is supposed to be largest.

5.5.1 Baryon masses and meson-nucleon sigma-terms

The nucleon mass and the meson-nucleon sigma-terms at one loop depend on the set of parameters: g, m, c_1, c_2, c_5, $\bar{e}_1$, $\bar{e}_3$, $\bar{e}_4$ and $\bar{e}_5$. First, we discuss a choice for g and m. Note, that these parameteres are constrained in our approach by the matching condition (5.59), $\overset{\circ}{m}_N = (g_A/g)^2 m$. In literature the value of the axial charge of the constituent quark varies approximately from 0.9 to 1 (see detailed discussion in Refs. [127]). The nucleon mass in the chiral limit was estimated in Heavy Baryon ChPT as $\overset{\circ}{m}_N = 770 \pm 110$ MeV [128] and $\overset{\circ}{m}_N = 890 \pm 180$ MeV [129]. Inserting this range of values for g and $\overset{\circ}{m}_N$ and also the experimental value for $g_A = 1.267$ [43] into Eq. (5.59) gives the following limits for the constituent quark mass in the chiral limit

$$m \simeq 500 \pm 167 \ \text{MeV}. \tag{5.68}$$

Finally, we choose

$$m = 420 \ \text{MeV} \qquad \text{and} \qquad g = 0.9. \tag{5.69}$$

Using the experimental value for the nucleon axial charge $g_A = 1.267$ [43] and Eq. (5.59) we get $\overset{\circ}{m}_N = 832.4$ MeV which is rather close to our previous estimate done in the framework of the noncovariant PCQM, $\overset{\circ}{m}_N = 828.5$ MeV [29, 35]. Here we do not pretend to a more accurate determination of m and g. However, we stress that we need a rather small value for g in the interval $0.9-1$ to justify perturbation theory. In particular, the use of $g = 0.9$ gives the shift of the nonstrange constituent quark mass equal to $\Delta m = 53$ MeV. For $g = 0.95$ and $g = 1$ we get $\Delta m = 107$ MeV and $\Delta m = 164$ MeV, respectively. On the other hand, the choice of g is constrained by the bare magnetic moments of the nucleon (see Eq. (5.83)). The use of $g = 0.9$ gives a reasonable contribution of the valence quark to the nucleon

magnetic moments (see discussion in the next section). Finally, the couplings c_1, c_2, c_5 and $\bar{e}_1$ are fixed by four conditions

$$\begin{aligned} m_N &= 938.27 \text{ MeV}, \quad \sigma_{\pi N} = 45 \text{ MeV}, \\ y_N &= 0.1, \quad m_s - \bar{m} \simeq 170 \text{ MeV}. \end{aligned} \tag{5.70}$$

The result of the fit is:

$$\begin{aligned} c_1 &= (-0.317 - 0.004\,\tilde{e}_3 + 0.020\,\tilde{e}_4 + 0.001\,\tilde{e}_5) \text{ GeV}^{-1}, \\ c_2 &= (1.093 - 1.354\,\tilde{e}_3 + 0.474\,\tilde{e}_4 - 0.338\,\tilde{e}_5) \text{ GeV}^{-1}, \\ c_5 &= (-0.316 + 0.063\,\tilde{e}_3 + 0.005\,\tilde{e}_5) \text{ GeV}^{-1}, \\ \bar{e}_1 &= (1.157 + 0.298\,\tilde{e}_3 + 0.162\,\tilde{e}_4 + 0.088\,\tilde{e}_5) \text{ GeV}^{-3}, \end{aligned} \tag{5.71}$$

where for convenience we introduce the dimensionless parameters $\tilde{e}_i = \bar{e}_i \times 1 \text{ GeV}^3$. Note, the mass difference $m_s - m_{u(d)}$ is a crucial quantity to roughly describe the splittings between the octet baryon masses. Latter quantities are proportional to $m_s - \bar{m}$. Neglecting isospin-breaking and hyperfine-splitting effects we have in our approach

$$\begin{aligned} m_\Lambda - m_N &= m_s - \bar{m} \simeq 170 \text{ MeV} \qquad (\text{data}: \ 177 \text{ MeV}), \\ m_\Sigma - m_N &= m_s - \bar{m} \simeq 170 \text{ MeV} \qquad (\text{data}: \ 251 \text{ MeV}), \\ m_\Xi - m_N &= 2[m_s - \bar{m}] \simeq 340 \text{ MeV} \qquad (\text{data}: \ 383 \text{ MeV}). \end{aligned} \tag{5.72}$$

The meson cloud corrections are important to reproduce the full empirical value of $\sigma_{\pi N}$, contributing about 2/3 to the total value (for a detailed discussion see Ref. [29, 35]). In particular, our result for $\sigma_{\pi N}$ is compiled as; the total value is $\sigma_{\pi N} = 45$ MeV, the contribution of the valence quarks is $\sigma_{\pi N}^{val} = 13.87$ MeV (30% of the total value), the contribution of the pion cloud is dominant

$$\sigma_{\pi N}^{\pi} = 26.69 \text{ MeV} \ + 0.45 \text{ MeV}\,\tilde{e}_3 - 2.58 \text{ MeV}\,\tilde{e}_4 - 0.11 \text{ MeV}\,\tilde{e}_5\,, \tag{5.73}$$

the kaon and η-meson cloud generates

$$\sigma_{\pi N}^{K+\eta} = 4.44 \text{ MeV} \ - 0.45 \text{ MeV}\,\tilde{e}_3 + 2.58 \text{ MeV}\,\tilde{e}_4 + 0.11 \text{ MeV}\,\tilde{e}_5\,. \tag{5.74}$$

The separate contributions $\sigma_{\pi N}^{\pi}$ and $\sigma_{\pi N}^{K+\eta}$ depend on the parameters $\tilde{e}_3$, $\tilde{e}_4$ and $\tilde{e}_5$, while the total contribution is independent on $\tilde{e}_i$ with $i = 3, 4, 5$. Our predictions for the kaon-nucleon σ_{KN} and eta-nucleon $\sigma_{\eta N}$ sigma-terms are; $\sigma_{KN}^{u} = 381.9$ MeV, $\sigma_{KN}^{d} = 351.8$ MeV, $\sigma_{KN}^{I=0} = 366.8$ MeV, $\sigma_{KN}^{I=1} = 15$ MeV, and $\sigma_{\eta N} = 90$ MeV.

5.5.2 Magnetic moments of the baryon octet

The magnetic moments of the nucleon can be written in terms of the Dirac and Pauli form factors as

$$\mu_N = F_1^N(0) + F_2^N(0), \tag{5.75}$$

where in our formalism $F_1^N(0)$ and $F_2^N(0)$ are of the form

$$\begin{aligned} F_1^N(0) &= \sum_{q=u,d} f_D^q(0) F_1^{Nq}(0)\,, \\ F_2^N(0) &= \sum_{q=u,d} \left[f_D^q(0) F_2^{Nq}(0) + f_P^q(0) G_2^{Nq}(0) \right], \end{aligned} \tag{5.76}$$

where $f_D^q(0) \equiv e_q$ is the quark charge due to charge conservation. It is convenient to separate the expressions for $F_1^N(0)$ and $F_2^N(0)$ into two contributions: the bare (valence-quark) and the meson cloud (sea-quark) contributions. The bare contribution is

$$\begin{aligned} F_1^{N\,\mathrm{bare}}(0) &= \sum_{q=u,d} e_q\, F_1^{Nq}(0)\,, \\ F_2^{N\,\mathrm{bare}}(0) &= \sum_{q=u,d} e_q\, F_2^{Nq}(0)\,. \end{aligned} \tag{5.77}$$

The meson cloud gives rise to

$$\begin{aligned} F_1^{N\,\mathrm{cloud}}(0) &\equiv 0\,, \\ F_2^{N\,\mathrm{cloud}}(0) &= \sum_{q=u,d} f_P^i(0) G_2^{Ni}(0)\,. \end{aligned} \tag{5.78}$$

Note, that the contribution of the meson cloud to the Dirac form factor $F_1^N(0)$ is zero due to the charge conservation of the nucleon. Therefore, the nucleon magnetic moments are given in additive form with

$$\mu_N = \mu_N^{\mathrm{bare}} + \mu_N^{\mathrm{cloud}}, \tag{5.79}$$

where

$$\mu_N^{\mathrm{bare}} = F_1^{N\,\mathrm{bare}}(0) + F_2^{N\,\mathrm{bare}}(0) \tag{5.80}$$

and

$$\mu_N^{\rm cloud} = F_1^{N\,{\rm cloud}}(0) + F_2^{N\,{\rm cloud}}(0)\,. \tag{5.81}$$

With the constraints laid out in Sec. 5.3, we derive a relation for the bare contributions to the nucleon magnetic moments [see Eq. (5.43)]

$$\mu_p^{\rm bare} \equiv -\frac{3}{2}\,\mu_n^{\rm bare} = \frac{3}{5}\left(\frac{g_A}{g}\right)^2 \frac{m_N}{\bar{m}}\,. \tag{5.82}$$

Note that Eq. (5.82) can be further simplified using the constraints of (5.59):

$$\mu_p^{\rm bare} \equiv -\frac{3}{2}\,\mu_n^{\rm bare} = \frac{3}{5}\left(\frac{g_A}{g}\right)^4. \tag{5.83}$$

As already mentioned in the previous section, the choice of g is constrained by the bare magnetic moments of the nucleon (see Eq. (5.83)). The value of $g = 0.9$ results in a reasonable contribution of the valence quarks to the nucleon magnetic moments with

$$\mu_p^{\rm bare} \equiv -\frac{3}{2}\,\mu_n^{\rm bare} = \frac{3}{5}\left(\frac{g_A}{g}\right)^4 \simeq 2.357 \tag{5.84}$$

which is about 84% (for the proton) and about 82% (for the neutron) of the experimental (total) values, where the remainder comes from the meson cloud.

The main parameters contained in the meson cloud piece that play an important role in fitting the magnetic moments are the second-order coupling c_6 and the fourth-order flavor-breaking LECs e_7, and e_8. The coupling e_6 is absorbed in c_6 after a certain redefinition. To constrain these values we need besides the experimental values for the nucleon (p and n) an additional value from the baryon octet. Therefore, we will proceed with an extension of our formalism to calculate the magnetic moments of the whole baryon octet.

In the following, for convenience, we introduce the bare Dirac (F_1^q, G_1^q) and Pauli (F_2^q, G_2^q) form factors of the quark of flavor q

$$\begin{aligned}
&\langle q(p')|\, j_{\mu,q}^{\rm bare}(0)\,|q(p)\rangle \\
&\qquad = \bar{u}_q(p')\left\{\gamma_\mu\, F_1^q(q^2) + \frac{i}{2\,m_q}\,\sigma_{\mu\nu}\,q^\nu\,F_2^q(q^2)\right\}u_q(p)\,, \\
&i\,\frac{q^\nu}{2\,m_q}\langle q(p')|\, j_{\mu\nu,q}^{\rm bare}(0)\,|q(p)\rangle \\
&\qquad = \bar{u}_q(p')\left\{\gamma_\mu\, G_1^q(q^2) + \frac{i}{2\,m_q}\,\sigma_{\mu\nu}\,q^\nu\,G_2^q(q^2)\right\}u_q(p)\,.
\end{aligned} \tag{5.85}$$

Note that the valence quark form factors (or valence quark contributions) are constrained by certain symmetries including the infrared singularities. Introducing the valence quark form factors we fulfill matching conditions between our approach and ChPT and, therefore, the structures due to chiral symmetry are not violated.

The Sachs form factors of the quark of flavor q are

$$\mathcal{F}_q^E(t) = F_q^E(t) + G_q^E(t)\,, \qquad \mathcal{F}_q^M(t) = F_q^M(t) + G_q^M(t)\,, \tag{5.86}$$

where

$$\begin{aligned} F\{G\}_q^E(t) &= F\{G\}_1^q(t) - \frac{t}{4m^2} F\{G\}_2^q(t), \\ F\{G\}_q^M(t) &= F\{G\}_1^q(t) + F\{G\}_2^q(t)\,, \quad t = -q^2, \end{aligned} \tag{5.87}$$

are the contributions to the Sachs form factors associated with the expectation values of the vector and tensor currents, respectively.

By using SU(6)-symmetry relations one can relate the Dirac and Pauli form factors describing the distribution of quarks of flavor $q = u, d, s$ in the baryon "B", that is $F_{1(2)}^{Bq}(t)$ and $G_{1(2)}^{Bq}(t)$, to $F_q^{E(M)}(t)$ and $G_q^{E(M)}(t)$ by

$$\begin{aligned} F_1^{Bq}(t) &= \frac{1}{1+\tau_B}\left\{\alpha_E^{Bq} F_q^E(t) + \alpha_M^{Bq}\,\chi^{Bq}\,F_q^M(t)\tau_B\right\}, \\ F_2^{Bq}(t) &= \frac{1}{1+\tau_B}\left\{-\alpha_E^{Bq} F_q^E(t) + \alpha_M^{Bq}\,\chi^{Bq}\,F_q^M(t)\right\}, \\ G_1^{Bq}(t) &= \frac{1}{1+\tau_B}\left\{\alpha_E^{Bq} G_q^E(t) + \alpha_M^{Bq}\,\chi^{Bq}\,G_q^M(t)\tau_B\right\}, \\ G_2^{Bq}(t) &= \frac{1}{1+\tau_B}\left\{-\alpha_E^{Bq} G_q^E(t) + \alpha_M^{Bq}\,\chi^{Bq}\,G_q^M(t)\right\}, \end{aligned} \tag{5.88}$$

where $\tau_B = t/(4m_B^2)$ and m_B is the baryon mass. In addition to the strict evaluation of SU(6) we have introduced the additional parameter χ^{Bq} for each quark of flavor q. The interpretation for adding these factors is such that to allow the quark distributions for hyperons to be different from that for the nucleons. In the case of the nucleons we set $\chi^{Bq} = 1$. The values for α_E^{Bq} and α_M^{Bq} for the baryon octet as derived from SU(6)-symmetry relations are given in Table 5.1.

	α_E^{Bu}	α_E^{Bd}	α_E^{Bd}	α_M^{Bu}	α_M^{Bd}	α_M^{Bs}
p	2	1	0	$\frac{4}{3}$	-$\frac{1}{3}$	0
n	1	2	0	-$\frac{1}{3}$	$\frac{4}{3}$	0
Λ^0	1	1	1	0	0	1
Σ^+	2	0	1	$\frac{4}{3}$	0	-$\frac{1}{3}$
Σ^-	0	2	1	0	$\frac{4}{3}$	-$\frac{1}{3}$
Ξ^-	0	1	2	0	-$\frac{1}{3}$	$\frac{4}{3}$
Ξ^0	1	0	2	-$\frac{1}{3}$	0	$\frac{4}{3}$
$\Sigma^0\Lambda^0$	0	0	0	$\frac{1}{\sqrt{3}}$	-$\frac{1}{\sqrt{3}}$	0

Table 5.1: SU(6) couplings α_E^{Bi} and α_M^{Bi}.

The quark Sachs form factors are modeled by the dipole characteristics with damping functions of an exponential form. This phenomenological form is required to reproduce in particular the deviation of the electromagnetic form factors of the nucleon from the dipole fit as evident from recent experimental measurements. We use the parameterization

$$F_q^E(t) = \frac{\rho_q^E(t)}{[1+t/\Lambda_{qE}^2]^2}\,, \qquad F_q^M(t) = \mu_q^F\,\frac{\rho_q^M(t)}{[1+t/\Lambda_{qM}^2]^2}\,,$$
$$G_q^E(t) = \gamma_q\,\rho_q^E(t)\,\frac{t/\Lambda_{qE}^2}{[1+t/\Lambda_{qE}^2]^3}\,, \quad G_q^M(t) = \mu_q^G\,\frac{\rho_q^M(t)}{[1+t/\Lambda_{qM}^2]^2}\,, \tag{5.89}$$

where $\rho_q^E(t) = \exp(-t/\lambda_{qE}^2)$ and $\rho_q^M(t) = \exp(-t/\lambda_{qM}^2)$. The parameters μ_q^F and μ_q^G are fixed by the symmetry constraints [see Eqs. (5.42) and (5.82)]

$$\mu_q^F \;=\; \mu_q^G \;=\; \mu_p^{\rm bare}\,. \tag{5.90}$$

The remaining parameters γ_q, $\Lambda_{qE(M)}$ and $\lambda_{qE(M)}$ are to be fixed later when we consider the full momentum dependence of the nucleon electromagnetic form factors. Note, that in Ref. [130] a similar parameterization of the nucleon form factors has been considered. In Ref. [131] the damping functions $\rho(t)$ have been parameterized with constant values.

The magnetic moment of the octet baryon "B" can be written in complete analogy to the nucleon case as

$$\mu_B \;=\; \mu_B^{\rm bare} \;+\; \mu_B^{\rm cloud} \tag{5.91}$$

where

$$\begin{aligned}
\mu_B^{\text{bare}} &= \sum_{q=u,d,s} e_q \left(F_1^{Bq}(0) + F_2^{Bq}(0) \right) , \\
\mu_B^{\text{cloud}} &= \sum_{q=u,d,s} f_P^q(0) G_2^{Bq}(0) \, . \qquad (5.92)
\end{aligned}$$

At $t = 0$, the parameters c_6, $\bar{e}_6$, $\bar{e}_7$, $\bar{e}_8$, c_2, and k_V contained in $f_P^q(0)$ will contribute, where the renormalized LECs $\bar{e}_6$, $\bar{e}_7$, $\bar{e}_8$ are given in Appendix G. The parameter $\bar{e}_6$ can be absorbed in the coupling c_6 via

$$c_6 \to \tilde{c}_6 = c_6 - 16 m M^2 \bar{e}_6 \, . \qquad (5.93)$$

Finally, the form factor $f_P^q(0)$ depends on the parameters $\tilde{c}_6$, $\bar{e}_7$, $\bar{e}_8$, c_2 and k_V. Three of them ($\tilde{c}_6$, $\bar{e}_7$, $\bar{e}_8$) can now be fixed using the experimental values for the magnetic moments of the nucleons and of a hyperon in the baryon octet. We choose the Λ^0-hyperon with $\mu_{\Lambda^0} = -0.613 \pm 0.004$ (in units of the nuclear magneton). In our analysis of the magnetic moments of the octet baryons we present two cases. First, we restrict to the SU(6) case by setting all values $\chi^{Bi} = 1$. Secondly, we allow the χ^{Bi} to be additional parameters. From now on we will name these two cases shortly as "Set I" and "Set II", respectively.

A variation in the value of the axial charge g of the constituent quark will also give rise to different contributions of the bare and the meson cloud parts to the total values of the magnetic moments. However, the total magnetic moments are the same in any case. As was discussed in the previous section, for the axial charge we choose $g = 0.9$. In case of Set I we then obtain for c_6, $\bar{e}_7$, and $\bar{e}_8$

$$\begin{aligned}
\tilde{c}_6 &= 0.859 - 0.106\, \tilde{c}_2 - 1.254\, k_V \, , \\
\bar{e}_7 &= (-0.656 + 0.073\, \tilde{c}_2 + 0.607\, k_V) \ \text{GeV}^{-3} \, , \qquad (5.94) \\
\bar{e}_8 &= (0.033 - 0.008\, \tilde{c}_2 - 0.141\, k_V) \ \text{GeV}^{-3} \, ,
\end{aligned}$$

where $\tilde{c}_2 = c_2(1+k_V)$. The resulting values for the magnetic moments of the baryon octet for this case (Set I) are shown in Table 5.2, where reasonable agreement with data is obtained. Meson cloud contributions to the total values of the magnetic moments are about $5 - 30\%$ depending on the baryon.

	Set I			Set II			Exp.
	3q	Meson Cloud	Total	3q	Meson Cloud	Total	
μ_p	2.357	0.436	2.793	2.357	0.436	2.793	2.793
μ_n	-1.571	-0.342	-1.913	-1.571	-0.342	-1.913	-1.913
μ_{Λ^0}	-0.786	0.173	-0.613	-0.518	-0.095	-0.613	-0.613 ± 0.004
μ_{Σ^+}	2.357	0.317	2.674	2.085	0.373	2.458	2.458 ± 0.010
μ_{Σ^0}	0.786	0.005	0.791	0.570	0.073	0.643	-
μ_{Σ^-}	-0.786	-0.306	-1.092	-0.935	-0.225	-1.160	-1.160 ± 0.025
μ_{Ξ^0}	-1.571	0.136	-1.435	-1.058	-0.192	-1.250	-1.250 ± 0.014
μ_{Ξ^-}	-0.7855	0.2921	-0.4934	-0.5580	-0.0927	-0.6507	-0.6507 ± 0.003
$\lvert\mu_{\Sigma^0\Lambda^0}\rvert$	1.36	0.27	1.63	1.34	0.27	1.61	1.61 ± 0.08

Table 5.2: *Magnetic moments of the baryon octet (in units of the nucleon magneton μ_N).*

For the case of Set II we start from the SU(6) result with the additional breaking parameter $\chi^{\Lambda s}$ for $\mu^{\rm bare}_{\Lambda^0}$ which can be written in terms of $\mu^{\rm bare}_p$ as $\mu^{\rm bare}_{\Lambda^0} = -\mu^{\rm bare}_p \chi^{\Lambda s}/3$. Then we have

$$\chi^{\Lambda s} = -3\frac{\mu^{\rm bare}_{\Lambda^0}}{\mu^{\rm bare}_p} \approx -3\frac{\mu_{\Lambda^0}}{\mu_p}, \tag{5.95}$$

where we further assume that the contributions from the meson cloud part to the total magnetic moments both of Λ^0 and of p are of the same order. With the experimental values for μ_{Λ^0} and μ_p we get $\chi^{\Lambda s} = 0.66$. By fitting μ_p, μ_n, and μ_{Λ^0}, with $\chi^{\Lambda s} = 0.66$ as an additional input, we obtain

$$\begin{aligned} \tilde{c}_6 &= 0.834 - 0.106\,\tilde{c}_2 - 1.254\,k_V\,, \\ \bar{e}_7 &= (-0.832 + 0.073\,\tilde{c}_2 + 0.607\,k_V)\ \ \mathrm{GeV}^{-3}\,, \\ \bar{e}_8 &= (0.051 - 0.008\,\tilde{c}_2 - 0.141\,k_V)\ \ \mathrm{GeV}^{-3}\,, \end{aligned} \tag{5.96}$$

where the constants contained in these parameters are slightly different from Set I. With appropriate values for the remaining χ^{Bq}, the central values of the experimental results of the other magnetic moments in the baryon octet can be fully reproduced. For the set of χ^{Bq} we get

$$\begin{aligned} \chi^{\Sigma u} &= \chi^{\Sigma d} = 0.963, \quad \chi^{\Sigma s} = 0.259, \\ \chi^{\Xi u} &= \chi^{\Xi d} = 0.633, \quad \chi^{\Xi s} = 0.694, \\ \chi^{\Sigma\Lambda u} &= \chi^{\Sigma\Lambda d} = 0.988. \end{aligned} \tag{5.97}$$

relying on isospin symmetry. The isotriplet Σ^+, Σ^0, and Σ^- shares the same set of $\chi^{\Sigma q}$ for the quark of flavor q, while Ξ^0 and Ξ^- contains the same set of $\chi^{\Xi q}$. The

parameters $\chi^{\Sigma\Lambda u}$ and $\chi^{\Sigma\Lambda d}$ are directly related to the $\Sigma - \Lambda$ magnetic transition moment. For completeness, our corresponding results for the magnetic moments are also listed in Table 5.2. In the following we will use the last set of values for $\tilde{c}_6$, $\bar{e}_7$, and $\bar{e}_8$, when considering the electromagnetic nucleon form factors.

5.5.3 Nucleon electromagnetic form factors

Using the parameters from the analysis of the magnetic moments and the masses of the baryon octet, further supplied by the ones from the meson-nucleon sigma-terms, we now can consider the full electromagnetic form factors of the nucleon. We recall that the Dirac and Pauli form factors for the nucleons are

$$\begin{aligned} F_1^N(t) &= \sum_{q=u,d} \left[f_D^q(t) F_1^{Nq}(t) + f_P^q(t) G_1^{Nq}(t) \right], \\ F_2^N(t) &= \sum_{q=u,d} \left[f_D^q(t) F_2^{Nq}(t) + f_P^q(t) G_2^{Nq}(t) \right], \end{aligned} \tag{5.98}$$

where $F_{1(2)}^{Nq}(t)$ and $G_{1(2)}^{Nq}(t)$ refer to the bare constituent quark structure, while $f_D^q(t)$ and $f_P^q(t)$ contain the chiral dynamics due to the dressing of the quark operators. For clarity we recall the forms of $F_{1(2)}^{Nq}(t)$ and $G_{1(2)}^{Nq}(t)$ of Eq. (5.88) with

$$\begin{aligned} F_1^{Nq}(t) &= \frac{1}{1+\tau_N} \left\{ \alpha_E^{Nq} F_q^E + \alpha_M^{Nq} F_i^M \tau_N \right\}, \\ F_2^{Nq}(t) &= \frac{1}{1+\tau_N} \left\{ -\alpha_E^{Nq} F_q^E + \alpha_M^{Nq} F_q^M \right\}, \\ G_1^{Nq}(t) &= \frac{1}{1+\tau_N} \left\{ \alpha_E^{Nq} G_q^E + \alpha_M^{Nq} G_q^M \tau_N \right\}, \\ G_2^{Nq}(t) &= \frac{1}{1+\tau_N} \left\{ -\alpha_E^{Nq} G_q^E + \alpha_M^{Nq} G_q^M \right\}, \end{aligned} \tag{5.99}$$

where α_E^{Nq} and α_M^{Nq} are the SU(6) spin-flavor couplings ($\alpha_E^{pu} = \alpha_E^{nd} = 2$, $\alpha_E^{pd} = \alpha_E^{nu} = 1$, $\alpha_M^{pu} = \alpha_M^{nd} = 4/3$, $\alpha_M^{pd} = \alpha_M^{nu} = -1/3$); $t = -q^2$ is the Euclidean momentum squared and $\tau_N = t/(4m_N^2)$. The Dirac and Pauli form factors $f_{D(P)}^q(t)$ of the quark of flavor i are shown explicitly in Appendix G. Again, Eq. (5.99) can be separated into a bare part and a meson cloud part as

$$\begin{aligned} F_1^{N\,\mathrm{bare}}(t) &= \sum_{q=u,d} e_q \, F_1^{Nq}(t), \\ F_2^{N\,\mathrm{bare}}(t) &= \sum_{q=u,d} e_q \, F_2^{Nq}(t), \end{aligned} \tag{5.100}$$

and the meson cloud contribution is

$$\begin{aligned} F_1^{N\,\mathrm{cloud}}(t) &= \sum_{q=u,d} [(f_D^q(t) - e_q) F_1^{Nq}(t) + f_P^q(t) G_1^{Nq}(t)], \\ F_2^{N\,\mathrm{cloud}}(t) &= \sum_{q=u,d} [(f_D^q(t) - e_q) F_2^{Nq}(t) + f_P^q(t) G_2^{Nq}(t)]. \end{aligned} \tag{5.101}$$

where e_q are the electric quark charges.

In the following we try to achieve a reasonable description of the electromagnetic form factors of the nucleon by an appropriate set of parameters contained in $F_1^N(t)$ and $F_2^N(t)$. In general both the bare and the meson cloud parts will contribute to the form factors. The bare part should well describe the form factors up to high Q^2 whereas the meson cloud part should play a role only for small Q^2. Our strategy is that we first fit the bare part of all the form factors to the experimental data from $Q^2 \sim 0.5$ GeV^2 to high Q^2. After that we reconsider the low Q^2 region by taking into account the meson cloud effect. At this point we do not pretend to an accurate analysis (or prediction) of the nucleon form factors at large Q^2. This is a task more appropriate for perturbative QCD (pQCD) which is the most convenient theoretical tool in this momentum region (for recent progress see e.g. Refs. [132, 133]). In particular, in Ref. [133] the following large Q^2-behavior for the ratio of the nucleon Pauli F_2 and Dirac F_1 form factors has been derived using pQCD:

$$\frac{F_2}{F_1} \propto \frac{\ln^2(Q^2/\Lambda^2)}{Q^2}\,, \tag{5.102}$$

where Λ is a soft scale related to the size of the nucleon. Our main idea is to use a physically reasonable parameterization of the nucleon form factors (valence quark contribution) which fits the data at intermediate and high Q^2 scale, while the derived constraints at zero recoil [see Sec. II] are also satisfied. Then on top of the valence (or bare) form factors we place the meson cloud contribution which is relevant only at small Q^2 and calculated consistently using effective chiral Lagrangian (5.1). Finally we might conclude on the role of the meson cloud in the infrared domain.

Due to the finite size of the source of the meson fields, meson loops are expected to be strongly suppressed for large Q^2. To mimic the effect of additional regularisation of the integral, which leads to a restriction of the meson cloud contribution in the low Q^2 region, we introduce the cutoff function $f_{cut}(t)$. The modification is such that

$$F_{1(2)}^{N\,\mathrm{cloud}}(t) \;\rightarrow\; f_{cut}(t)\, F_{1(2)}^{N\,\mathrm{cloud}}(t)\,. \tag{5.103}$$

The specific form of $f_{cut}(t)$ should not modify $F_{1(2)}^{N\,\mathrm{cloud}}(t)$ in the low Q^2 region, but should diminish its contribution beyond a certain Q^2. This function $f_{cut}(t)$ should have zero (or almost zero) slope at the point $Q^2 = 0$ GeV^2 to ensure that it will not artificially contribute to the slope of the form factors. First the step function seems to be an appropriate choice for $f_{cut}(t)$ but its sharp boundary affects the continuity of the form factors, and hence one must be careful. To avoid the problems associated with a sharp boundary we choose a smeared-out version for $f_{cut}(t)$ with

$$f_{cut}(t) = \frac{1 + \exp(-A/B)}{1 + \exp[(t - A)/B]}\,, \tag{5.104}$$

where the parameter A characterizes the cut-off and B the smearing of the function.

In our fitting procedure we use the experimental data (Refs. [1, 2, 3, 47, 48, 49, 50, 51, 55, 57, 58, 60, 62, 69, 70, 71, 72, 73, 74, 75, 79, 80, 81, 82, 83, 84, 85, 88, 91, 93, 135, 136, 137, 138, 139]) on the ratios of the electromagnetic Sachs form factors of nucleons to the corresponding dipole form factors and on the neutron charge form factors. For the axial charge of the constituent quark $g = 0.9$ we first fit the contribution of the bare part, where the parameters are contained in the ansatz of Eq. (5.89). Our parameter results for the fit of the bare part are (in units of GeV)

$$\begin{aligned} \lambda_{uE} = 2.0043,\ \ \lambda_{dE} &= 0.9996,\ \ \lambda_{uM} = 7.3367,\ \ \lambda_{dM} = 2.2954, \\ \Lambda_{uE} = 0.8616,\ \ \Lambda_{dE} &= 0.9234,\ \ \Lambda_{uM} = 0.9278,\ \ \Lambda_{dM} = 1.0722. \end{aligned} \tag{5.105}$$

Note that the parameters γ_u and γ_d entering in Eq. (5.89) cannot be fixed by considering only the bare part since they also occur in $F_1^{N\,\mathrm{cloud}}(t)$ and $F_2^{N\,\mathrm{cloud}}(t)$. The complete fit to the full data on the electromagnetic form factors of the nucleon fixes the remaining low-energy constants in the effective Lagrangian as

$$\begin{aligned} \gamma_u &= 1.081, \quad \gamma_d = 2.596, \\ c_2 &= 2.502\ \mathrm{GeV}^{-1}, \quad c_4 = 1.693\ \mathrm{GeV}^{-1}, \quad \bar{d}_{10} = 1.110\ \mathrm{GeV}^{-2}, \\ \bar{e}_7 &= -0.650\ \mathrm{GeV}^{-3}, \quad \bar{e}_8 = 0.030\ \mathrm{GeV}^{-3}, \quad \bar{e}_{10} = 0.039\ \mathrm{GeV}^{-3}, \end{aligned} \tag{5.106}$$

where in the current manuscript we put $k_V = 0$ for simplicity. The couplings $\bar{d}_{10}$, $\bar{e}_7$, $\bar{e}_8$ and $\bar{e}_{10}$ are defined in Appendix G. With the choice $A = (0.4 - 0.5)$ GeV^2 and $B = 0.025$ GeV^2 in $f_{cut}(t)$ the meson cloud contributions are suitably suppressed for values larger than $t \sim 0.5\,\mathrm{GeV}^2$. Note, that from the analysis of the nucleon mass and meson-nucleon sigma-terms we get the following constraint on the parameter $c_2 = (1.093 - 1.354\,\tilde{e}_3 + 0.474\,\tilde{e}_4 - 0.338\,\tilde{e}_5)$ GeV^{-1}. The best description of the electromagnetic properties of the nucleon is obtained

at the value of $c_2 = 2.502$ GeV^{-1} fixed from the data on the electromagnetic form factors. It means that we obtain the following constraint on the LECs $\tilde{e}_3$, $\tilde{e}_4$ and $\tilde{e}_5$: $1.354\,\tilde{e}_3 - 0.474\,\tilde{e}_4 + 0.338\,\tilde{e}_5 = -1.409$.

Results for the measured ratio of the electromagnetic form factors of the nucleon to the dipole form factor $G_D(t) = (1 + t/0.71 \text{ GeV}^2)^{-2}$ are presented in Figs. 5.4, 5.5 and 5.6. In Fig. 5.7 we present our result for the ratio of charge to magnetic form factor of the proton. For completeness, the electromagnetic form factors of the nucleon are also shown in Fig. 5.8, where the meson cloud contributions are shown explicitly in comparison to the dipole form factor. The role of $f_{cut}(t)$, which restricts the meson cloud contribution to the low Q^2 region, is indicated in Fig. 5.9. Although the bare constituent quark contribution is fully parameterized, a consistent explanation of the form factors can only be achieved, when meson cloud corrections are included. We stress that the bare constituent quark Sachs form factors and hence the magnetic form factors at zero recoil ($t = 0$) are determined by the general constraints discussed in Sec. 5.3. At this point the specific form of the quark form factors of Eq. (5.89), leading to a satisfactory description in particular beyond $t \sim 0.5\,\text{GeV}^2$, is not required. The results concerning the charge and magnetic radii of nucleons are

$$\begin{aligned} r_E^p &= 0.881 \text{ fm}, \ \langle r^2 \rangle_E^n = -0.1177 \text{ fm}^2, \\ r_M^p &= 0.869 \text{ fm}, \ r_M^n = 0.847 \text{ fm}. \end{aligned} \tag{5.107}$$

The experimental values reported in Ref. [43] for the charge radii of nucleons are $r_E^p = 0.875 \pm 0.007$ fm and $\langle r^2 \rangle_E^n = -0.1161 \pm 0.0022$ fm^2. For the magnetic radii, the analysis of Refs. [71, 134] gives $r_M^p = 0.855 \pm 0.035$ fm and $r_M^n = 0.873 \pm 0.011$ fm, respectively.

For further illustration we follow Ref. [130] to deduce the radial dependence of the charge and magnetization densities of nucleons. The charge and magnetization densities of nucleons in the rest frame are

$$\rho_E^N(r) = \frac{2}{\pi} \int_0^\infty dk\, k^2\, j_0(k\,r) \tilde{\rho}_E^N(k)\,, \qquad \rho_M^N(r) = \frac{2}{\pi} \int_0^\infty dk\, k^2\, j_0(k\,r) \tilde{\rho}_M^N(k), \tag{5.108}$$

where $k^2 = t/(1+\tau_N)$ and $j_0(kr)$ is the Bessel function. The intrinsic form factors $\tilde{\rho}_E^N(k)$ and $\tilde{\rho}_M^N(k)$ are

$$\tilde{\rho}_E^N(k) = G_E^N(Q^2)(1+\tau_N)^{\lambda^E}, \quad \tilde{\rho}_M^N(k) = \frac{G_M^N(Q^2)}{\mu_N}(1+\tau_N)^{\lambda^M}. \tag{5.109}$$

Restricting to the discrete values $\lambda^E = 0, 1, 2$, where the full range is discussed in Ref. [130], the results for the charge and magnetization densities of the nucleon

are shown in Figs. 5.10 and 5.11. The separated meson cloud contributions to the charge and magnetization densities of the nucleon are presented in Figs. 5.12 and 5.13, respectively.

In Ref. [131] the electromagnetic form factors of the nucleons are represented by the phenomenological ansatz

$$G_N(Q^2) = G_s(Q^2) + a_b \cdot Q^2\, G_b(Q^2), \tag{5.110}$$

where the "smooth" part $G_s(Q^2)$ and the structured or "bump" part $G_b(Q^2)$ are parameterized as

$$\begin{aligned} G_s(Q^2) &= \frac{a_{10}}{(1+Q^2/a_{11})^2} + \frac{a_{20}}{(1+Q^2/a_{21})^2}, \\ G_b(Q^2) &= e^{-\frac{1}{2}\left(\frac{Q-Q_b}{\sigma_b}\right)^2} + e^{-\frac{1}{2}\left(\frac{Q+Q_b}{\sigma_b}\right)^2}. \end{aligned} \tag{5.111}$$

The parameters a_{10}, a_{11}, a_{20}, a_{21}, a_b, Q_b, and σ_b are obtained by a fit to experimental data and the values are reported in Table 2 of Ref. [131]. The meson cloud part of our evaluation cannot be directly compared or matched to $G_b(Q^2)$, since meson corrections contribute to the magnetic form factors even at $Q^2 = 0$, which is not the case in the treatment of Ref. [131]. However, charge conservation restricts the meson cloud not to contribute to the charge form factors at zero recoil. Therefore, we can compare our results for the charge form factors to the phenomenological ones of Ref. [131]. Fig. 5.4 shows such a comparison for the case of the charge form factor of the proton. Based on the phenomenological ansatz of Ref. [131] our result can be reproduced by readjusting the parameters of Eq. (5.111) as compiled in Table 5.3, which are not so much different from the original analysis of Ref. [131].

	Ref. [131]	Present result
a_{10}	1.041	1.053
a_{11}	0.765	0.768
a_{20}	-0.041	-0.053
a_{21}	6.2	4.7
a_b	-0.23	-0.38
Q_b	0.07	0.14
σ_b	0.21	0.20

Table 5.3: *Comparison of the parameters of the original phenomenological ansatz in Ref. [131] to an equivalent set, which is obtained by fitting to our results for the charge form factor of the proton.*

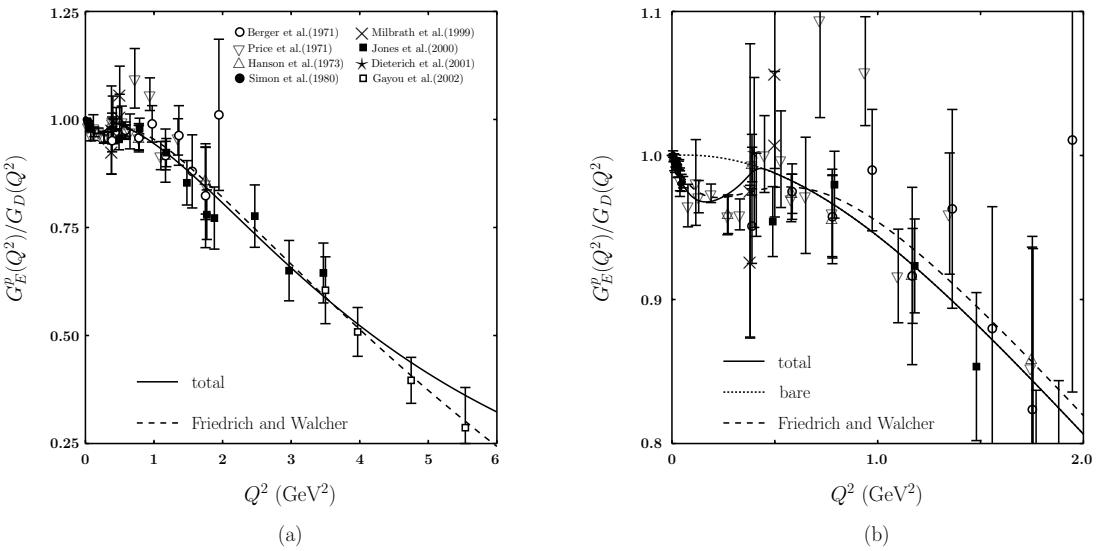

Figure 5.4: *Ratio $G_E^p(Q^2)/G_D(Q^2)$: (a) Overall range, (b) Up to $Q^2 =$ 2 GeV^2, the solid line is the total contribution, the dotted line is the bare contribution and the dashed line is the result reported in Ref. [131]. Experimental data are taken from Refs. [1, 2, 50, 58, 60, 62, 135, 136].*

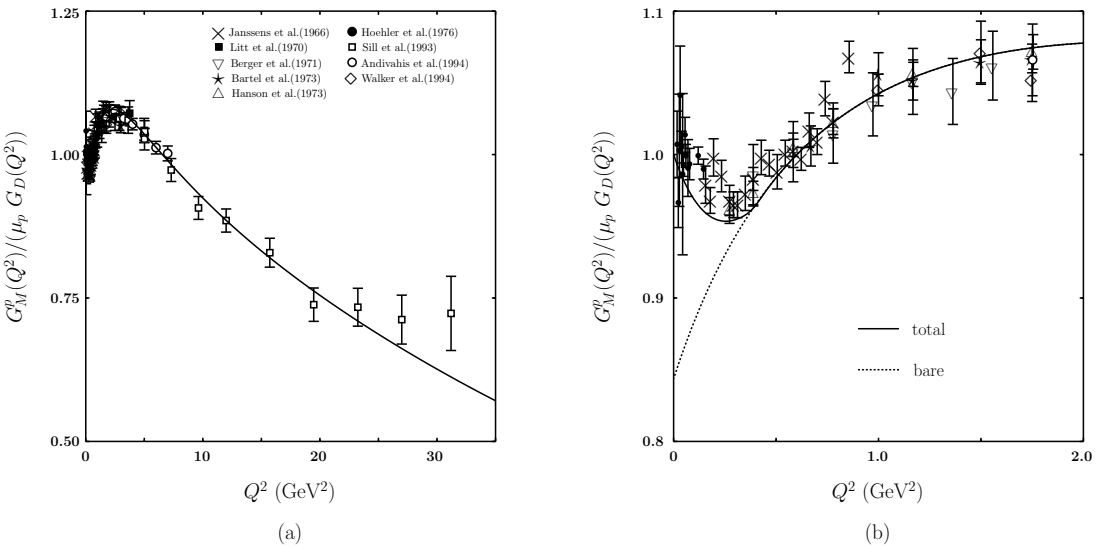

Figure 5.5: *Ratio $G_M^p(Q^2)/(\mu_p\, G_D(Q^2))$: (a) Overall range, (b) Up to $Q^2 = 2$ GeV^2, the solid line is the total contribution and the dotted line is the bare contribution. Experimental data are taken from Refs. [47, 48, 49, 51, 55, 57, 58, 136, 137].*

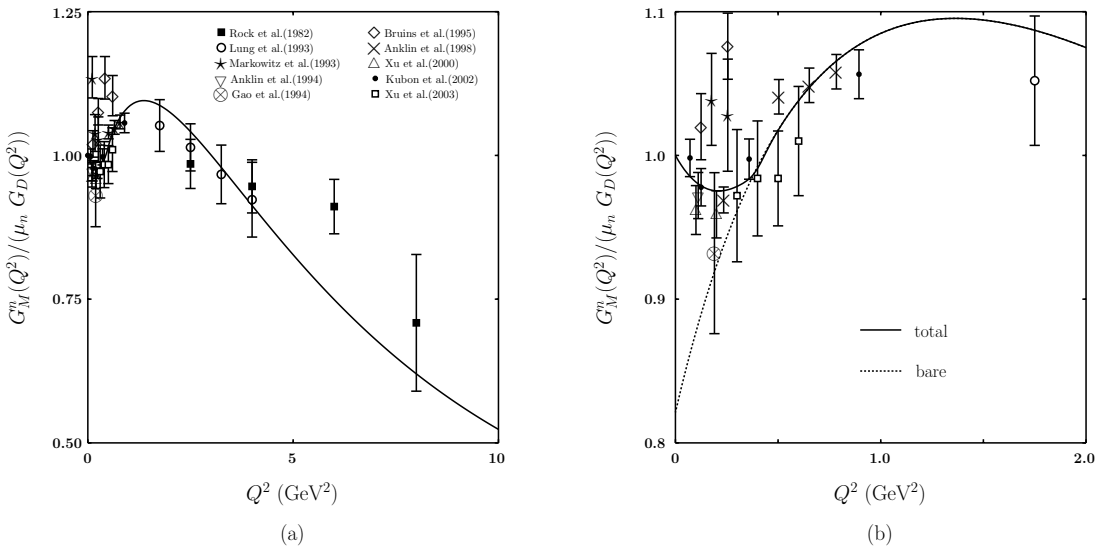

Figure 5.6: *Ratio $G_M^n(Q^2)/(\mu_n\, G_D(Q^2))$: (a) Overall range, (b) Up to $Q^2 = 2$ GeV^2, the solid line is the total contribution and the dotted line is the bare contribution. Experimental data are taken from Refs. [69, 70, 71, 72, 73, 74, 75, 79, 80, 138].*

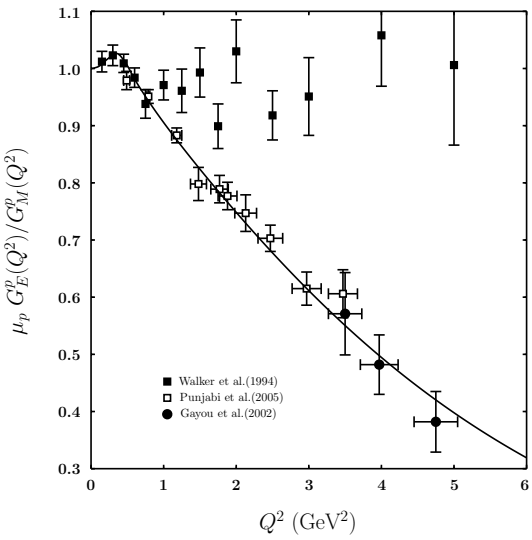

Figure 5.7: *Ratio $\mu_p G_E^p(Q^2)/G_M^p(Q^2)$ in comparison to the experimental data. Experimental data are taken from Refs. [2, 3, 48].*

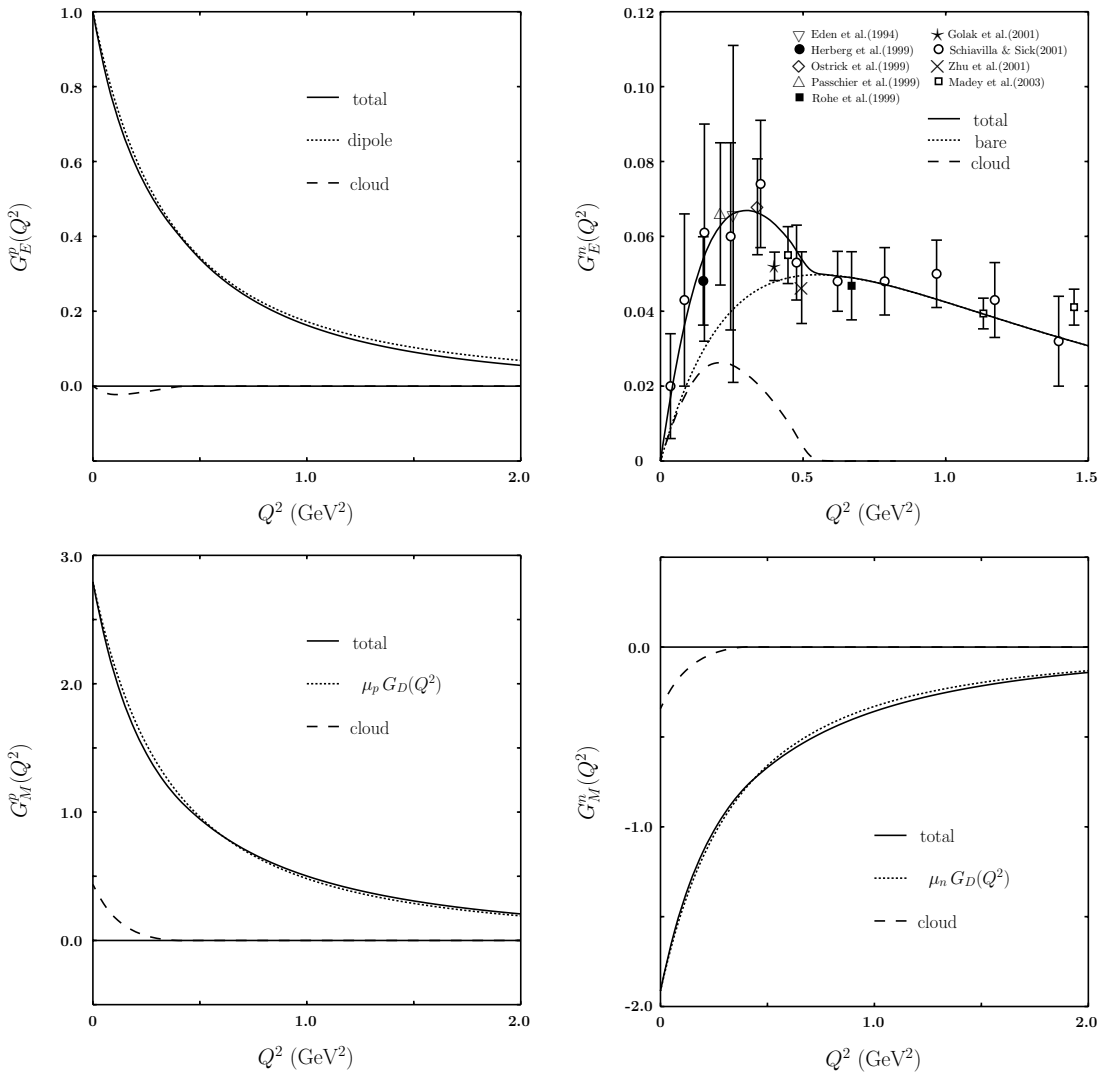

Figure 5.8: *The charge and magnetic form factors of the nucleon and the contribution due to the meson cloud. The corresponding dipole fit for $G_E^p(Q^2)$, $G_M^p(Q^2)$ and $G_M^n(Q^2)$ are also presented. Experimental data for $G_E^n(Q^2)$ are taken from Refs. [81, 82, 83, 84, 85, 88, 91, 93, 139].*

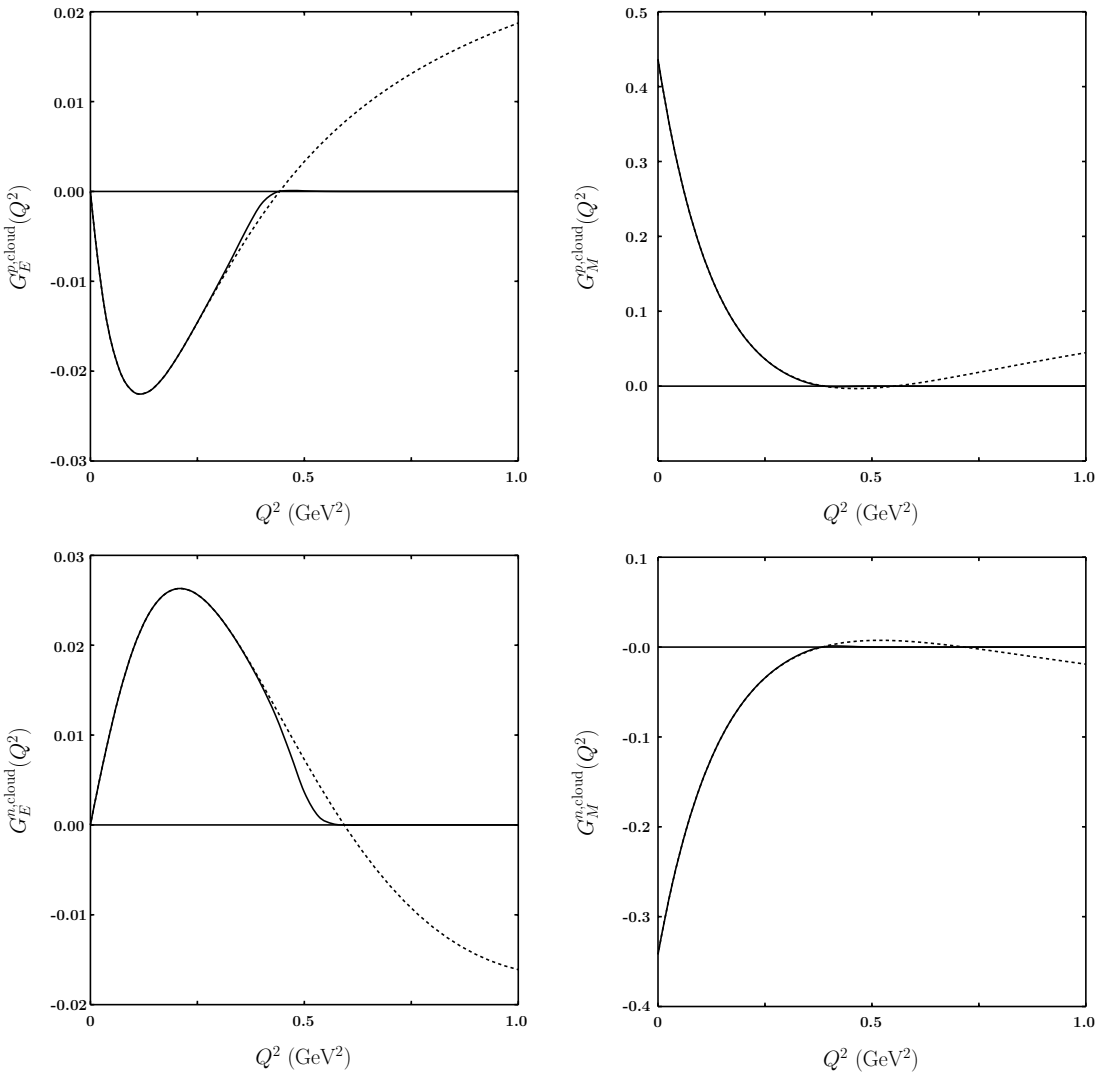

Figure 5.9: *The meson cloud contribution to the nucleon charge and magnetic form factors with the cutoff function $f_{cut}(Q^2)$ (solid line) and without $f_{cut}(Q^2)$ (dotted line).*

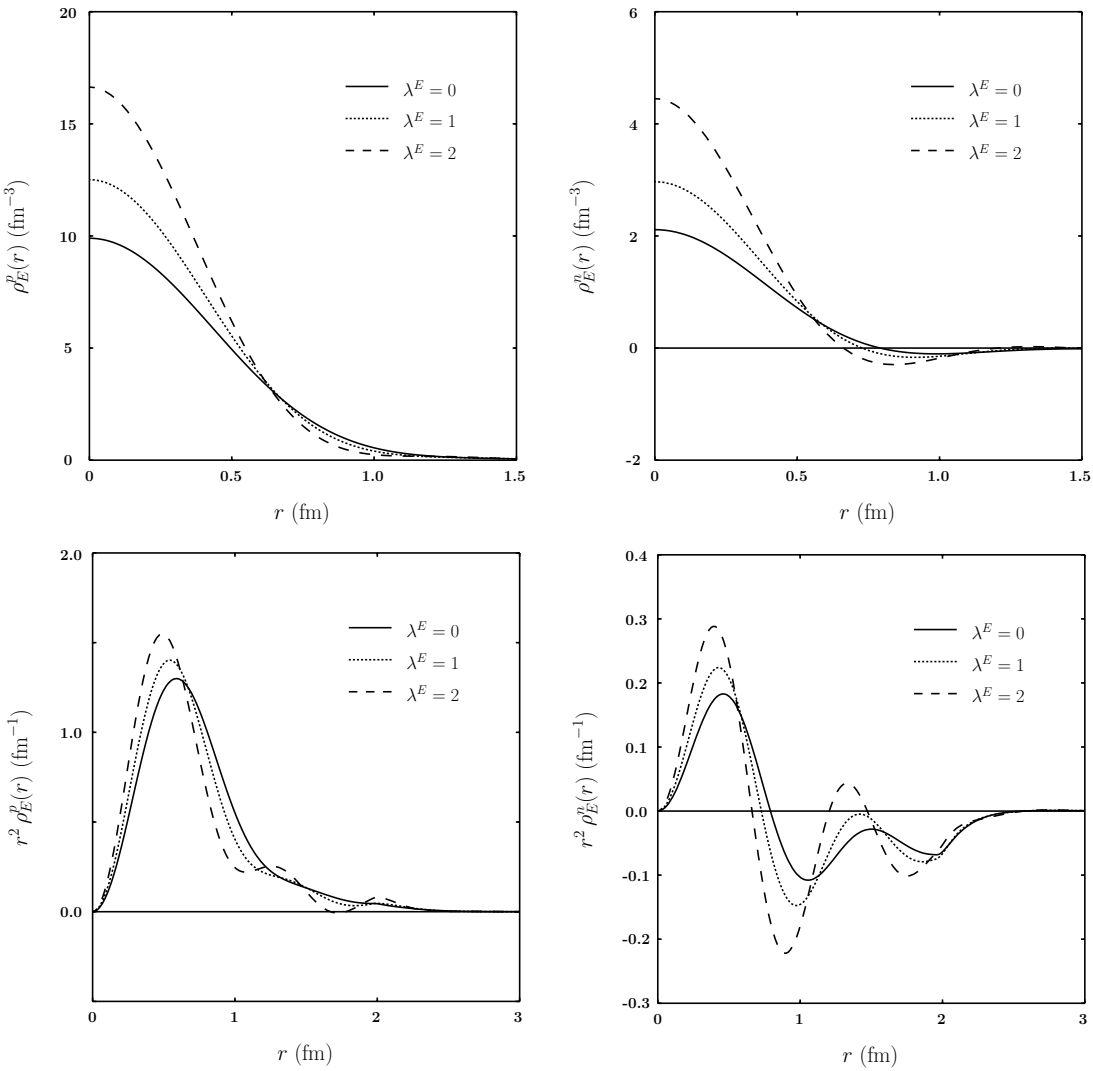

Figure 5.10: *Variation of the charge density of the nucleon* $\rho_E^N(r)$ *and* $r^2\,\rho_E^N(r)$ *with* λ^E*:* $\lambda^E = 0$ *(solid line),* $\lambda^E = 1$ *(dotted line), and* $\lambda^E = 2$ *(dashed line).*

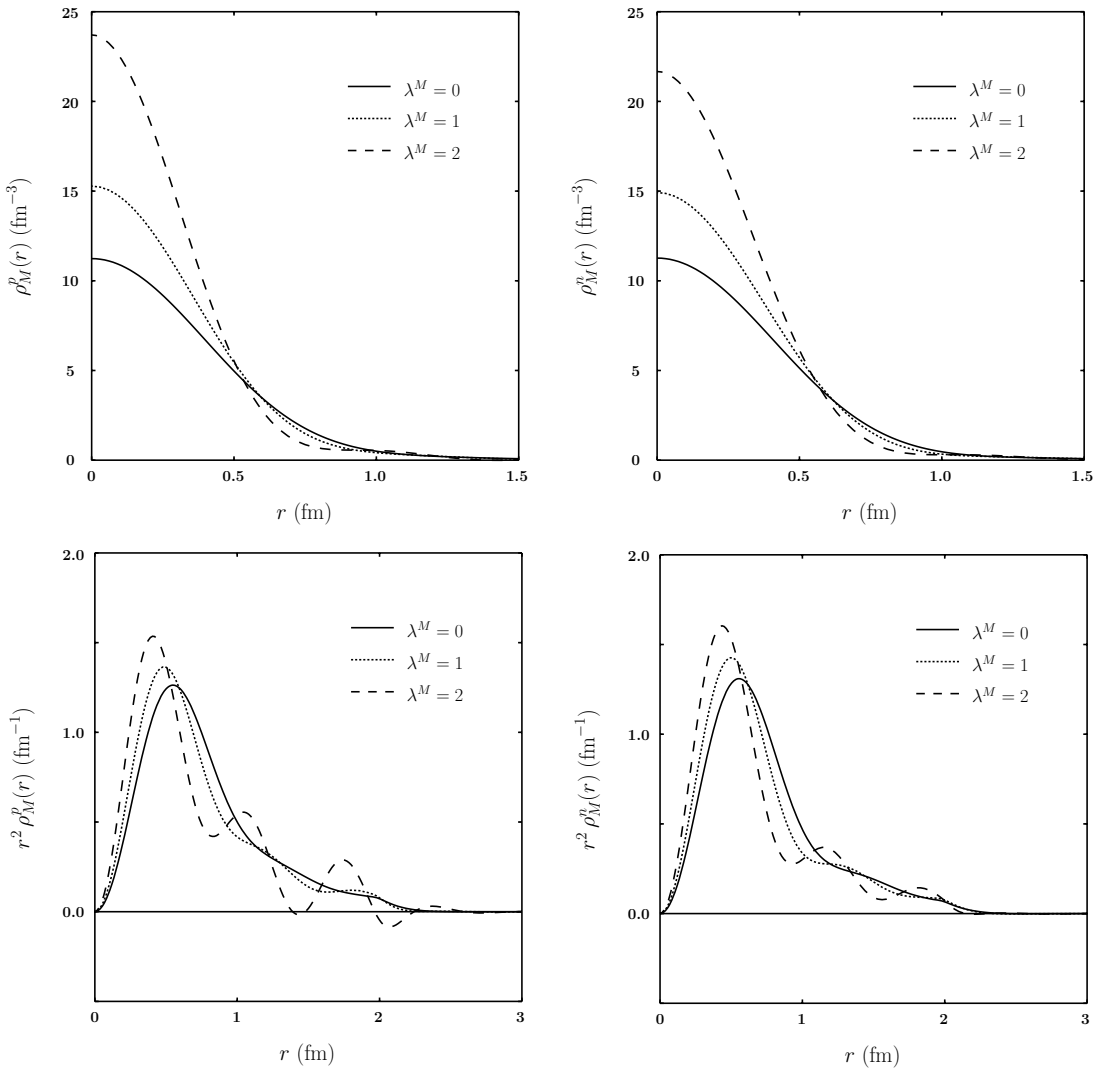

Figure 5.11: *Variation of the magnetization density of the nucleon* $\rho_M^N(r)$ *and* $r^2\,\rho_M^N(r)$ *with* λ^M*:* $\lambda^M = 0$ *(solid line),* $\lambda^M = 1$ *(dotted line), and* $\lambda^M = 2$ *(dashed line).*

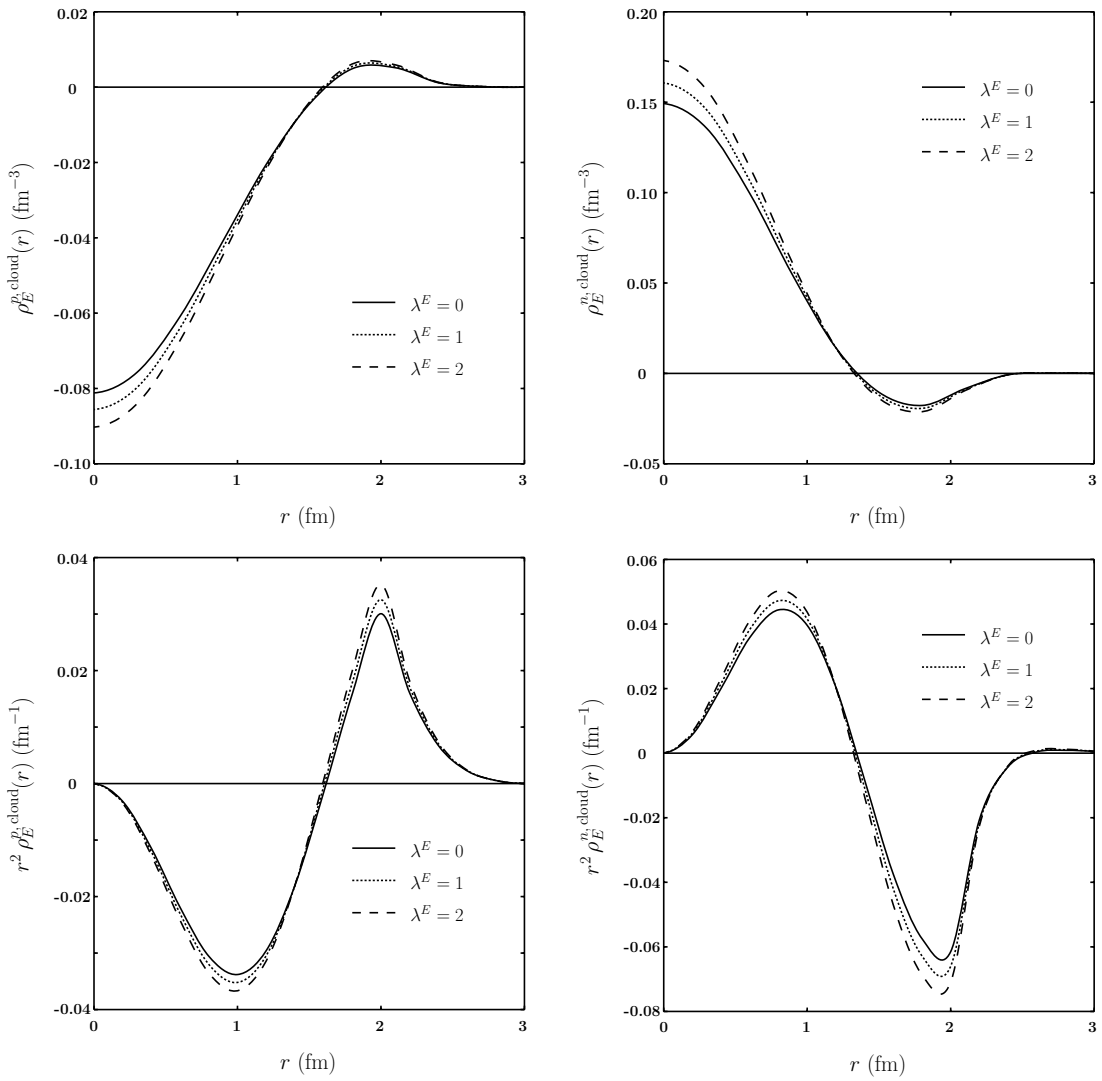

Figure 5.12: *Variation of the charge density of meson cloud contribution to the nucleon* $\rho_E^{N,\mathrm{cloud}}(r)$ *and* $r^2\,\rho_E^{N,\mathrm{cloud}}(r)$ *with* λ^E*:* $\lambda^E = 0$ *(solid line),* $\lambda^E = 1$ *(dotted line), and* $\lambda^E = 2$ *(dashed line).*

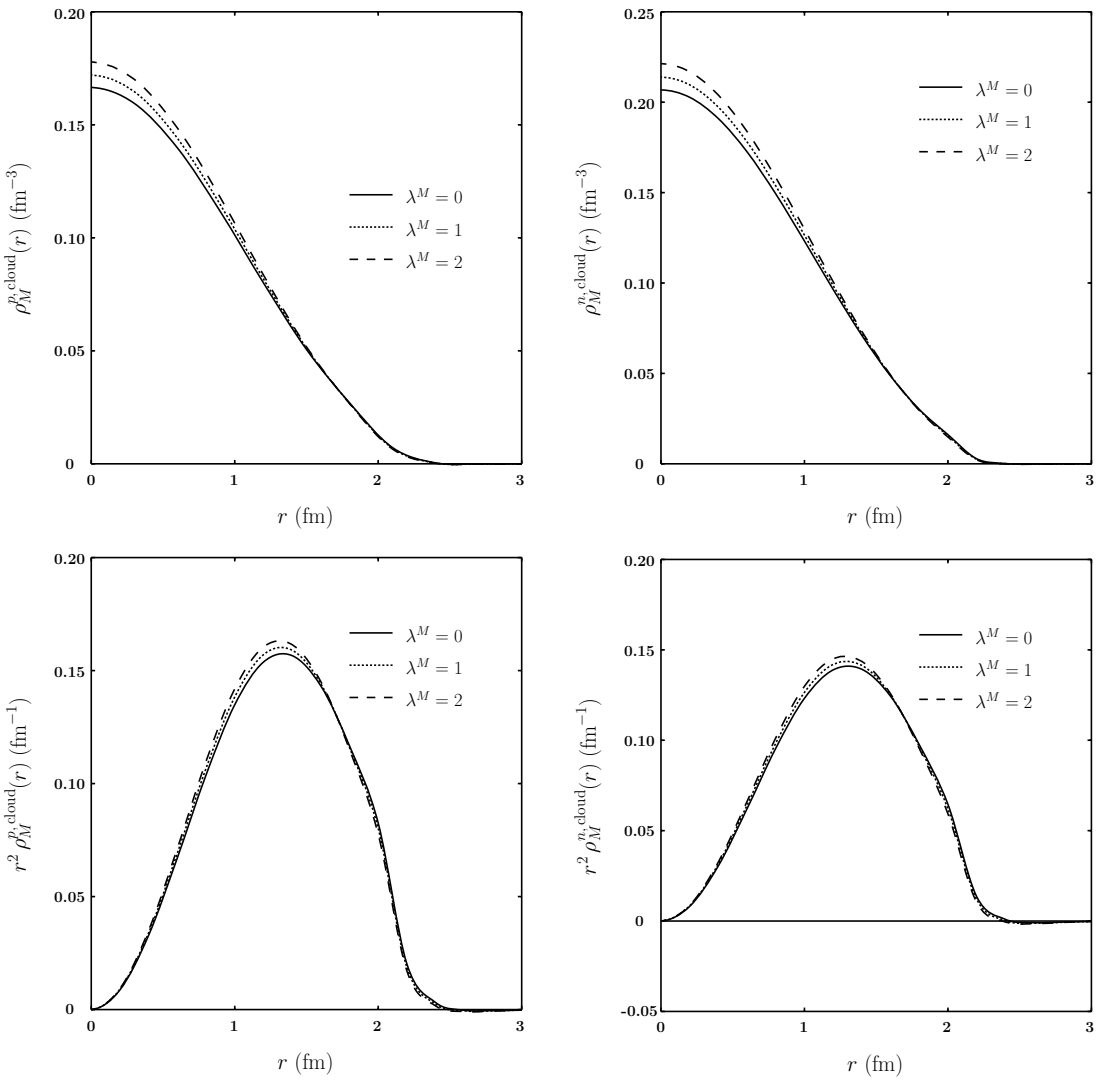

Figure 5.13: *Variation of the magnetization density of meson cloud contribution to the nucleon* $\rho_M^{N,\mathrm{cloud}}(r)$ *and* $r^2\,\rho_M^{N,\mathrm{cloud}}(r)$ *with* λ^M*:* $\lambda^M = 0$ *(solid line),* $\lambda^M = 1$ *(dotted line), and* $\lambda^M = 2$ *(dashed line).*

5.5.4 Strong vector meson-nucleon form factors

Finally, we calculate the strong vector meson-nucleon form factors ρNN and ωNN at one loop. We follow the strategy already developed for the electromagnetic nucleon form factors. The corresponding bare operator is derived from the tree-level Lagrangian (5.24):

$$\begin{aligned} J^{\rm bare}_{\mu,V}(q) &= \int d^4x\, e^{-iqx}\, j^{\rm bare}_{\mu,V}(x)\,, \\ j^{\rm bare}_{\mu,V}(x) &= g_{Vqq}\,\bar{q}\left(\gamma_\mu + \frac{k_V}{2m_q}\,\sigma_{\mu\nu}\,\overleftrightarrow{\partial}^\nu\right)\frac{\lambda_V}{2}\,q\,, \end{aligned} \tag{5.112}$$

where $\bar{q}\;\overleftrightarrow{\partial}^\nu\;q = \bar{q}\,(\overleftarrow{\partial}^\nu + \overrightarrow{\partial}^\nu)\,q$ and λ_V is the corresponding flavor matrix: $\lambda_\rho = \mathrm{diag}\{1,-1,0\}$ for the ρ^0 and $\lambda_\omega = \mathrm{diag}\{1,1,0\}$ for the ω meson. The diagrams contributing to these quantities are displayed in Fig. 5.14: tree-level diagrams (Figs. 5.14(1) and 5.14(2)) and one-loop diagrams due to the dressing by a cloud of pseudoscalar mesons (Figs. 5.14(3) and 5.14(4)).

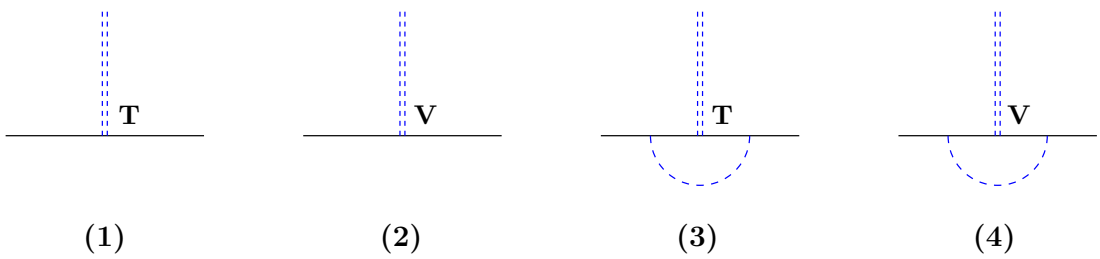

Figure 5.14: *Diagrams contributing to the quark operator describing the stong interaction of vector mesons with quarks. The symbols* **V** *and* **T** *refer to the vectorial and tensorial couplings of vector mesons to quarks.*

The Fourier transform of the dressed vector-meson-quark transition operator has the following form

$$J^{\rm dress}_{\mu,V}(q) = \frac{1}{2}\int d^4x e^{-iqx}\bar{q}(x)\left[\gamma_\mu f_{V_D}(q^2) + \frac{i}{2m_q}\sigma_{\mu\nu}q^\nu f_{V_P}(q^2)\right]q(x) \tag{5.113}$$

where f_{V_D} and f_{V_P} are the matrices of the Dirac and Pauli form factors describing the coupling of u, d and s quarks to the ρ and ω vector mesons. These form factors

are given in terms of the Euclidean values of momentum squared $t = -q^2$ with:

$$
\begin{aligned}
f_{V_D}(t) &= \sum_{i=u,d,s} f^i_{V_D}(t)\,, \qquad f_{V_P}(t) = \sum_{i=u,d,s} f^i_{V_P}(t)\,,\\
f^u_{\rho_D}(t) &= -f^d_{\rho_D}(t) = g_{Vqq}\left\{1 - \epsilon^\pi_5(t) + \frac{1}{3}\epsilon^\eta_5(t)\right\},\\
f^u_{\omega_D}(t) &= f^d_{\omega_D}(t) = g_{Vqq}\left\{1 + 3\epsilon^\pi_5(t) + \frac{1}{3}\epsilon^\eta_5(t)\right\},\\
f^s_{\rho_D}(t) &= 0\,, \qquad f^s_{\omega_D}(t) = g_{Vqq}\left\{-4\ \epsilon^K_5(t)\right\},\\
f^u_{\rho_P}(t) &= -f^d_{\rho_P}(t) = k_V\, g_{Vqq}\left\{1 - m^\pi_{10}(t) + \frac{1}{3}m^\eta_{10}(t)\right\},\\
f^u_{\omega_P}(t) &= f^d_{\omega_P}(t) = k_V\, g_{Vqq}\left\{1 + 3m^\pi_{10}(t) + \frac{1}{3}m^\eta_{10}(t)\right\},\\
f^s_{\rho_P}(t) &= 0\,, \qquad f^s_{\omega_P}(t) = k_V\, g_{Vqq}\left\{-4\ m^K_{10}(t)\right\},
\end{aligned}
\tag{5.114}
$$

where $\lambda_\phi = \mathrm{diag}\{0,0,1\}$. Here $\epsilon^P_5(t)$ and $m^P_5(t)$ are the meson-cloud contributions given in Appendix G.

To project the dressed quark operator (5.113) onto the nucleon we proceed in analogy to the electromagnetic operator

$$
\begin{aligned}
&\langle\ N(p')|\, J^{\rm dress}_{\mu,V}(q)\,|N(p)\rangle\\
&= (2\pi)^4\,\delta^4(p'-p-q)\,\bar{u}_N(p')\,\frac{1}{2}\left\{\gamma_\mu\, G_{VNN}(q^2)\ +\ \frac{i}{2\,m_N}\,\sigma_{\mu\nu}q^\nu\, F_{VNN}(q^2)\right\}u_N(p)\\
&= (2\pi)^4\,\delta^4(p'-p-q)\,\frac{1}{2}\left\{f^{ij}_{V_D}(q^2)\,\langle N(p')|\, j^{\rm bare}_{\mu,ij}(0)\,|N(p)\rangle\right.\\
&\quad \left. +i\,\frac{q^\nu}{2\,m_q}\, f^{ij}_{V_P}(q^2)\,\langle N(p')|\, j^{\rm bare}_{\mu\nu,ij}(0)\,|N(p)\rangle\right\},
\end{aligned}
\tag{5.115}
$$

where the bare matrix elements $\langle N(p')|\, j^{\rm bare}_{\mu\nu,ij}(0)\,|N(p)\rangle$ are defined in Eq. (5.33). Here $G_{VNN}(q^2)$ and $F_{VNN}(q^2)$ are the vectorial and tensorial couplings of vector mesons to nucleons. We can express the strong ρNN and ωNN form factors through the bare electromagnetic nucleon form factors. After a simple algebra we arrive at:

$$
\begin{aligned}
G_{\rho NN}(t) &= g_{Vqq}\,[\,F_1^{p-}(t)\,f^u_{\rho_D}(t) \,+\, G_1^{p-}(t)\,f^u_{\rho_P}(t)\,]\,,\\
G_{\omega NN}(t) &= g_{Vqq}\,[\,F_1^{p+}(t)\,f^u_{\omega_D}(t) \,+\, G_1^{p+}(t)\,f^u_{\omega_P}(t)\,]\,,\\
F_{\rho NN}(t) &= g_{Vqq}\,[\,F_2^{p-}(t)\,f^u_{\rho_D}(t) \,+\, G_2^{p-}(t)\,f^u_{\rho_P}(t)\,]\,,\\
F_{\omega NN}(t) &= g_{Vqq}\,[\,F_2^{p+}(t)\,f^u_{\omega_D}(t) \,+\, G_2^{p+}(t)\,f^u_{\omega_P}(t)\,]\,,
\end{aligned}
\tag{5.116}
$$

where $t = -q^2$ and $H_I^{p\pm} = H_I^{pu} \pm H_I^{pd}$ with $H = F$ or G and $I = 1$ or 2.

Finally, we present the expressions for the values of the vector-meson nucleon form factors at zero recoil or the coupling constants G_{VNN} and F_{VNN} which originate from the nucleon-level Lagrangian (for details on the nucleon-level Lagrangian see Ref. [20]):

$$
\begin{aligned}
\mathcal{L}_{VNN} \;=\; & \frac{1}{2}\,\bar{N}\Bigg\{\left(\gamma^\mu\,G_{\rho NN} \,-\, \frac{F_{\rho NN}}{2\,m_N}\,\sigma^{\mu\nu}\,\partial_\nu\right)\vec{\rho}_\mu\,\vec{\tau}\\
& + \left(\gamma^\mu\,G_{\omega NN} \,-\, \frac{F_{\omega NN}}{2\,m_N}\,\sigma^{\mu\nu}\,\partial_\nu\right)\omega_\mu\Bigg\}N\,.
\end{aligned}
\tag{5.117}
$$

After a simple algebra we arrive at:

$$
\begin{aligned}
& G_{\rho NN} = g_{Vqq}\,,\\
& \frac{F_{\rho NN}}{G_{\rho NN}} \;=\; \mu_p^{\rm bare} \,-\, \mu_n^{\rm bare} \,-\, 1 \,+\, k_V\,\frac{m_N}{m_q}\,(\,\delta_{pu}^{\rm bare} \,-\, \delta_{pd}^{\rm bare}\,)\,[1+\delta_\rho]\,,\\
& G_{\omega NN} \;=\; 3\,g_{Vqq}\,,\\
& \frac{F_{\omega NN}}{G_{\omega NN}} \;=\; \mu_p^{\rm bare} \,+\, \mu_n^{\rm bare} \,-\, 1 \,+\, k_V\,\frac{m_N}{m_q}\,(\,\delta_{pu}^{\rm bare} \,+\, \delta_{pd}^{\rm bare}\,)\,[1+\delta_\omega]\,,
\end{aligned}
\tag{5.118}
$$

where

$$
\delta_\rho \;=\; -m_{10}^\pi(0) + \frac{1}{3}m_{10}^\eta(0)\,, \qquad \delta_\omega \;=\; 3m_{10}^\pi(0) + \frac{1}{3}m_{10}^\eta(0)
\tag{5.119}
$$

are the corresponding one-loop corrections. For $k_V \equiv 0$ these equations reduce to the well-known SU(3) relations, relating the matrix elements of the vector current with different flavor content [141]. Using the actual expressions for the bare

magnetic moments and the tensor charges of the nucleons we finally obtain for the ratios of the tensor and vector couplings:

$$\begin{aligned}
\frac{F_{\rho NN}}{G_{\rho NN}} &= \left(\frac{g_A}{g}\right)^4 \left(1 + k_V\,[1+\delta_\rho]\right) - 1\,, \\
\frac{F_{\omega NN}}{G_{\omega NN}} &= \frac{1}{5}\left(\frac{g_A}{g}\right)^4 \left(1 + 3\,k_V\,[1+\delta_\omega]\right) - 1\,.
\end{aligned} \tag{5.120}$$

Note, that numerically the one-loop corrections to the tree-level results for the strong vector-meson nucleon form factors $F_{\rho NN}$ and $F_{\omega NN}$ are rather small: $\delta_\rho = 0.005$ and $\delta_\omega = 0.011$.

5.6 Summary

We developed a manifestly Lorentz covariant chiral quark model for the study of baryons as bound states of constituent quarks. The approach is based on the effective chiral Lagrangian motivated from the Baryon ChPT involving constituent quarks and the chiral fields as effective degrees of freedom. This Lagrangian is used in the calculation of the dressed transition operators which are relevant for the interaction of quarks with external fields in the presence of a virtual meson cloud. Then the dressed operators are used in the calculation of baryon matrix elements.

Our main result is as follows: we perform a model-independent factorization of the effects of hadronization and confinement contained in the matrix elements of the bare quark operators and the effects dictated by chiral symmetry which are encoded in the corresponding relativistic form factors [see e.g. Eq. (5.30)]. Due to this factorization the calculation of chiral effects and the effects of hadronization and confinement can be done independently. All low-energy theorems are reproduced in our approach due to the chiral invariance of the effective Lagrangian. The evaluated meson-cloud corrections are in agreement with the infrared-singular structure of the corresponding nucleon matrix elements [20, 125]. In particular, we reproduce the leading nonanalytic (LNA) contributions to the nucleon mass, to the pion-nucleon sigma-term, to the magnetic moments and to the charge radii of the nucleons. The LNA contributions to the nucleon mass and magnetic moment are proportional to the M_P^3 and M_P, respectively, where M_P is the pseudoscalar meson mass. The nucleon radii are divergent in the chiral limit. Using model-independent constraints on the bare constituent quark distributions in the octet baryons, we work out model predictions for the magnetic moments. Based on a full parameterization of the bare constituent quark distributions in the nucleon, we give results for the full momentum dependence of the electromagnetic form factors

of the nucleon and indicate the role of the meson cloud contributions. Presently, the calculation of the matrix elements of the bare quark operators is, besides the model independent constraints, based on parameterizations. The direct calculation of these matrix elements should be performed in quark models based on specific assumptions about hadronization and confinement.

As the further applications of this approach we intend to study other interesting aspects such as magnetic moments of heavy baryons, $N \to \Delta + \gamma$ transitions, strangeness and electric dipole form factors of nucleons.

Chapter 6

Summary

In this work we have studied low-energy properties of baryons based on the so-called perturbative chiral quark model (PCQM). In this model baryons are viewed as a composite system of three valence quarks and in addition are surrounded by a cloud of Goldstone bosons (π, K, η) as imposed by chiral symmetry requirements. The confinement of valence quarks is in a first step simply modelled by a static potential leading to a violation of covariance, thereby restricting the model to the description of low-energy quantities. The meson cloud and the quark masses are treated perturbatively and all the calculations are done up to one loop or at the order of accuracy $o(1/F^2, \hat{m}, m_s)$ where F is the pion decay constant in the chiral limit, $\hat{m} = m_u = m_d$ and m_s are the u, d and s current quark masses. The model contains only one parameter, that is R, which can be related to the size of the charge distribution of the proton in the leading order (LO) calculation. We first further simplify the loop calculation technique by restricting the quark propagator to its ground state configuration. This amounts in a hadronic language to a restriction to N and Δ intermediate states in the loop diagrams. In a next step we also include the low-lying intermediate excited quark states in the quark propagator. Up to excitations of $2\hbar\omega$, these states contain the quantum numbers, $1p_{1/2}$, $1p_{3/2}$, $1d_{3/2}$, $1d_{5/2}$ and $2s_{1/2}$.

In a first application of the PCQM we study the electromagnetic form factors of the baryon octet. When restricting to the ground state quark propagator alone, reasonable results for the magnetic moments, the charge and magnetic radii of the baryon octet compared to the experimental data are obtained. A special case is the charge radius of the neutron which has zero contribution from the three-quark core and purely arises from meson loops. Without the intermediate excited quark states, the charge radius of the neutron is rather small when compared to the experimental result. However, when excited quark states are included, the value increases and is close to the experimental point. Although the ground state contribution dominates the observables, excited quark states are shown to have

considerable influence, when the leading contribution is suppressed.

In a second application of the PCQM we study the electromagnetic $N - \Delta$ transitions. The transversal helicity amplitudes, $A_{1/2}$ and $A_{3/2}$, for these transitions are the convenient and relevant quantities to be compared to the experiment. A long- standing problem for the case of the helicity amplitudes in quark model descriptions is that the valence-quark contribution gives rise to only about two thirds of the experimental results. As was already pointed out in the context of the cloudy bag model a significant contribution is generated by the pion cloud possibly resulting in agreement with data. In the PCQM we found the same role of the meson cloud contribution as in the cloudy bag model. The meson cloud contributes up to 30% of the total values, where the pions are dominant. In addition, the excited quark states are also important and contribute at the level of 15%. Another interesting quantity which indicates a possible intrinsic deformation of the nucleon is the $E2/M1$ ratio. The experimental result for $E2/M1$ is rather small, roughly 2.5%. In the PCQM we cannot reproduce this $E2/M1$ ratio in the one-loop calculation. As for example shown in large N_c considerations, the ratio is generated by higher-order effects which show up when two-loop calculations are considered.

Although the PCQM works with specific assumptions introduced for simplicity, such as noncovariant treatment of confinement and restriction to a one-loop evaluation, the model gives overall reasonable results for the study of low-energy baryonic properties. As for the improvement of the model, we considered a further step, both to formulate a manifestly Lorentz covariant approach and to consistently include higher order chiral corrections.

Starting point for the Lorentz covariant approach is first the concept of dressing the quark operators by the chiral fields. The underlying Lagrangian is motivated by the one of Chiral Perturbation Theory (ChPT), where here the fundamental fermionic degrees of freedom are the bare valence quarks. The chiral Lagrangian contains a set of low energy constants (LECs) which are parameters encoding short-distance effects and contributions due to heavy particle states. The vector mesons as additional degrees of freedom are included in our study as well. In a next step, the dressed quark operators are projected on the baryonic level in order to obtain hadronic matrix elements. For the case of the electromagnetic current operator we obtain the important result, that the parts concerning the meson cloud and the bare three-quark core factorize in the matrix element. Both parts can be separately calculated. The meson cloud part involves the chiral dynamics which arises from the chiral Lagrangian and can be calculated to the order of accuracy desired. The bare three-quark core part in turn can be relegated to a quark model with specific assumptions concerning confinement and hadronization, hence modelling the bare valence quark structure. At this stage the factorization scheme can be viewed as a well-defined method to include chiral dynamics in a valence quark model.

In a first attempt, instead of working in a specific scheme for the bare valence quark structure, we resort to a parameterization of the quark form factors in the electromagnetic sector. The symmetries of the system such as charge conservation, isospin invariance, SU(6)-symmetry relations can be utilized together with chiral symmetry constraints to restrict the bare quark form factors at zero recoil. This automatically leads to a prediction for the values for the bare magnetic moments of the nucleon. Further studies involving the baryon masses, their chiral expansion and their relation to the pion-nucleon σ-terms can be used as another tool to pin down the relations among the LECs. Using these relations of the LECs the magnetic moments of the baryon octet can be well explained with meson cloud contributions up to 30% of the total values. With part of the LECs constrained by observables in the low-energy sector, we can further study the full Q^2-dependence of the electromagnetic nucleon form factors.

Recent polarization transfer measurements reveal a remarkable feature of the electromagnetic form factors of the nucleon. In particular, the linear decline of the ratio of charge to magnetic proton form factor with increasing Q^2 indicates that the proton charge form factor falls off relative to the conventional dipole form factor. In addition, at low Q^2 up to about 0.5 GeV^2 all nucleon form factors show subtle structures relative to the corresponding dipole parameterization. These structures are possibly interpreted to arise from meson cloud effects.

In our framework we investigate the electromagnetic form factors of the nucleon starting from the bare valence quark contribution. The values for all the bare quark form factors at zero recoil are fixed by the previous considerations involving the symmetries of the system, the matching to the chiral expansions of baryon masses, sigma-terms and the magnetic moments. Due to the finite meson sizes the meson cloud contribution should be significant for small Q^2 only. We therefore use the data on the form factors beyond $Q^2 \sim 0.5$ GeV^2 to model the bare contribution, which in addition is fixed at $Q^2 = 0$. On top of the bare form factors at low Q^2, we therefore adjust the remaining LECs to reproduce the experimental data. Our results for the electromagnetic form factors display a significant role of the meson cloud at low Q^2, which is necessary to reproduce the detailed structure of these observables.

In a final application concerning the explicit vector meson degrees of freedom, we site expressions for the values of the vector-meson nucleon coupling constants G_{VNN} and F_{VNN} which originate from the chiral Lagrangian formulated on the quark level.

At this point it should mentioned that the current work can be extended and improved in several directions. Up to now the dressed quark operators are restricted to the one-body approximation, that is in a straight forward extension of the present formalism two-body operator can and will be included. Furthermore, the bare valence quark form factors should be calculated in a specific quark model with rigorous assumptions concerning confinement and hadronization. Recently

we have calculated particular baryonic properties, such as the helicity amplitudes for the $N - \Delta$ transitions and the electromagnetic form factors of the nucleon, in a relativistic three-quark model with a non-local quark-hadron interaction Lagrangian. Due to the complexity of the loop calculations, all the observables based on this model were first evaluated in the valence quark approximation, but with reasonable results. A further inclusion of the dressed quark operators, as presented in this work, is currently studied. To finally summarize, we presented a novel approach in the field of chiral quark models, which allows both to work in a covariant framework and to include chiral corrections even of higher orders. At the same time the model is consistent with the low-energy chiral structure set by ChPT. As at least partially, phenomenologically demonstrated, the Q^2-range of applicability goes far beyond the one set by ChPT. Thus the covariant chiral quark model presented here sets the stage for a wide range of applications which should be studied in future.

Appendix A

Basic notions of the SU(3) group

The group SU(3) is the set of all unitary, unimodular and 3×3 matrices U i.e.

$$U^\dagger U = 1, \quad \det(U) = 1. \tag{A.1}$$

Elements of SU(3) can be obtained from the exponential representation with the eight real parameters $\theta = (\theta_1, \ldots, \theta_8)$

$$U[\theta] = \exp\left(-i \sum_{a=1}^{8} \theta_a \frac{\lambda_a}{2}\right), \tag{A.2}$$

where λ_a are the Gell-Mann matrices with the explicit forms

$$\begin{aligned}
\lambda_1 &= \begin{pmatrix} 0 & 1 & 0 \\ 1 & 0 & 0 \\ 0 & 0 & 0 \end{pmatrix}, \ \lambda_2 = \begin{pmatrix} 0 & -i & 0 \\ i & 0 & 0 \\ 0 & 0 & 0 \end{pmatrix}, \ \lambda_3 = \begin{pmatrix} 1 & 0 & 0 \\ 0 & -1 & 0 \\ 0 & 0 & 0 \end{pmatrix}, \\
\lambda_4 &= \begin{pmatrix} 0 & 0 & 1 \\ 0 & 0 & 0 \\ 1 & 0 & 0 \end{pmatrix}, \ \lambda_5 = \begin{pmatrix} 0 & 0 & -i \\ 0 & 0 & 0 \\ i & 0 & 0 \end{pmatrix}, \ \lambda_6 = \begin{pmatrix} 0 & 0 & 0 \\ 0 & 0 & 1 \\ 0 & 1 & 0 \end{pmatrix}, \\
\lambda_7 &= \begin{pmatrix} 0 & 0 & 0 \\ 0 & 0 & -i \\ 0 & i & 0 \end{pmatrix}, \ \lambda_8 = \sqrt{\frac{1}{3}} \begin{pmatrix} 1 & 0 & 0 \\ 0 & 1 & 0 \\ 0 & 0 & -2 \end{pmatrix}.
\end{aligned} \tag{A.3}$$

Note that λ_a can be obtained from Eq. (A.2) by

$$\lambda_a = 2i \frac{\partial U[\theta]}{\partial \theta_a}\bigg|_{\theta=(0,\ldots,0)}. \tag{A.4}$$

These Gell-Mann matrices also satisfy

$$\lambda_a = \lambda_a^\dagger, \qquad \mathrm{Tr}(\lambda_a \lambda_b) = 2\delta_{ab}, \qquad \mathrm{Tr}(\lambda_a) = 0. \tag{A.5}$$

The commutation relations of the Gell-Mann matrices indicate the structure of the Lie group of SU(3) with

$$\left[\frac{\lambda_a}{2}, \frac{\lambda_b}{2}\right] = i f_{abc} \frac{\lambda_c}{2}, \tag{A.6}$$

where f_{abc} are the totally antisymmetric structure constants. The non-vanishing values of f_{abc} are

$$\begin{aligned} f_{123} &= 1, \\ f_{147} &= -f_{156} = f_{246} = f_{257} = f_{345} = -f_{367} = \frac{1}{2}, \\ f_{458} &= f_{678} = \frac{\sqrt{3}}{2}. \end{aligned} \tag{A.7}$$

Other important relations of the Gell-Mann matrices are their anti-commutation relations

$$\{\lambda_a, \lambda_b, \} = \frac{4}{3}\delta_{ab} + 2 d_{abc} \lambda_c, \tag{A.8}$$

where the totally symmetric real constants d_{abc} are

$$\begin{aligned} d_{118} &= d_{228} = d_{338} = -d_{888} = \frac{1}{\sqrt{3}}, \\ d_{146} &= d_{157} = -d_{247} = d_{256} = d_{344} = d_{355} = -d_{366} = -d_{377} = \frac{1}{2}, \\ d_{448} &= d_{558} = d_{668} = d_{778} = -\frac{1}{2\sqrt{3}} \ . \end{aligned} \tag{A.9}$$

Appendix B

Solutions of the Dirac equation for the effective potential

In this section we indicate the solutions to the Dirac equation with the effective potential $V_{\text{eff}}(r) = S(r) + \gamma^0 V(r)$. The scalar $S(r)$ and time-like vector $V(r)$ parts are given by

$$\begin{aligned} S(r) &= M_1 + c_1 r^2, \\ V(r) &= M_2 + c_2 r^2, \end{aligned} \tag{B.1}$$

with the particular choice

$$M_1 = \frac{1\,-\,3\rho^2}{2\,\rho R}, \qquad M_2 = \mathcal{E}_0 - \frac{1\,+\,3\rho^2}{2\,\rho R}, \qquad c_1 \equiv c_2 = \frac{\rho}{2R^3}. \tag{B.2}$$

The quark wave function $u_\alpha(\vec{r})$ in state α with eigenenergy $\mathcal{E}_\alpha$ satisfies the Dirac equation

$$[-i\vec{\alpha}\vec{\nabla} + \beta S(r) + V(r) - \mathcal{E}_\alpha]u_\alpha(\vec{r}) = 0. \tag{B.3}$$

Solutions of the Dirac spinor $u_\alpha(\vec{r})$ to Eq. (B.3) can be written in the form [97]

$$u_\alpha(\vec{r}) = N_\alpha \begin{pmatrix} g_\alpha(r) \\ i\vec{\sigma}\cdot\hat{r} f_\alpha(r) \end{pmatrix} \mathcal{Y}_\alpha(\hat{r})\chi_f\chi_c. \tag{B.4}$$

For the particular choice of the potential, the radial functions g and f satisfy the form

$$g_\alpha(r) = \left(\frac{r}{R_\alpha}\right)^l L_{n-1}^{l+1/2}\left(\frac{r^2}{R_\alpha^2}\right) e^{-\frac{r^2}{2R_\alpha^2}}, \tag{B.5}$$

where for $j = l + \frac{1}{2}$

$$f_\alpha(r) = \rho_\alpha \left(\frac{r}{R_\alpha}\right)^{l+1} \left[L_{n-1}^{l+3/2}(\frac{r^2}{R_\alpha^2}) + L_{n-2}^{l+3/2}(\frac{r^2}{R_\alpha^2})\right] e^{-\frac{r^2}{2R_\alpha^2}}, \tag{B.6}$$

and for $j = l - \frac{1}{2}$

$$f_\alpha(r) = -\rho_\alpha \left(\frac{r}{R_\alpha}\right)^{l-1} \left[(n + l - \frac{1}{2})L_{n-1}^{l-1/2}(\frac{r^2}{R_\alpha^2}) + nL_n^{l-1/2}(\frac{r^2}{R_\alpha^2})\right] e^{-\frac{r^2}{2R_\alpha^2}}. \tag{B.7}$$

The label $\alpha = (nljm)$ characterizes the state with principle quantum number $n = 1, 2, 3, ...$, orbital angular momentum l, total angular momentum $j = l \pm \frac{1}{2}$ and projection m. Due to the quadratic nature of the potential the radial wave functions contain the associated Laguerre polynomials $L_n^k(x)$ with

$$L_n^k(x) = \sum_{m=0}^{n} (-1)^m \frac{(n+k)!}{(n-m)!(k+m)!m!} x^m. \tag{B.8}$$

The angular dependence ($\mathcal{Y}_\alpha(\hat{r}) \equiv \mathcal{Y}_{lmj}(\hat{r})$) is defined by

$$\mathcal{Y}_{lmj}(\hat{r}) = \sum_{m_l, m_s} (lm_l \frac{1}{2} m_s | jm) Y_{lm_l}(\hat{r}) \chi_{\frac{1}{2}m_s} \tag{B.9}$$

where $Y_{lm_l}(\hat{r})$ is the usual spherical harmonic. Flavor and color part of the Dirac spinor are represented by χ_f and χ_c, respectively.

The normalization constant is obtained from the condition

$$\int_0^\infty d^3\vec{r} u_\alpha^\dagger(\vec{r}) u_\alpha(\vec{r}) = 1 \tag{B.10}$$

which results in

$$N_\alpha = \left[2^{-2(n+l+1/2)} \pi^{1/2} R_\alpha^3 \frac{(2n+2l)!}{(n+l)!(n-1)!} \{1 + \rho_\alpha^2 (2n + l - \frac{1}{2})\}\right]^{-1/2}. \tag{B.11}$$

The two coefficients R_α and ρ_α are of the form

$$R_\alpha = R(1+\Delta\mathcal{E}_\alpha\rho R)^{-1/4}, \tag{B.12}$$

$$\rho_\alpha = \rho\left(\frac{R_\alpha}{R}\right)^3 \tag{B.13}$$

and are related to the Gaussian parameters ρ, R of Eq. (4.17). The quantity $\Delta\mathcal{E}_\alpha = \mathcal{E}_\alpha - \mathcal{E}_0$ is the difference between the energy of state α and the ground state. $\Delta\mathcal{E}_\alpha$ depends on the quantum numbers n and l and is related to the parameters ρ and R by

$$(\Delta\mathcal{E}_\alpha + \frac{3\rho}{R})^2(\Delta\mathcal{E}_\alpha + \frac{1}{\rho R}) = \frac{\rho}{R^3}(4n+2l-1)^2. \tag{B.14}$$

Appendix C

Renormalization of the nucleon charge in the PCQM

The renormalization constant $\hat{Z}$ and Z_s can be obtained from considerations concerning the conserved nucleon charge. As discussed earlier, the role of the counterterms consequently results in a cancellation of the terms related to the diagrams (e) to (l) in Fig. 4.2. Therefore only the diagrams (a) to (d) contribute to the nucleon charges. Diagram (a) is just the $3q$-core contribution and, due to our formalism, is normalized to reproduce exactly the charge of the nucleon, i.e.

$$Q_N = {}^N\langle\phi_0| \int \delta(t) d^4x j^0_{\psi^r}(x) |\phi_0\rangle^N. \tag{C.1}$$

The three-quark counterterm diagram in Fig. 4.2(b) gives rise to

$$\begin{aligned} Q_N^{r;b} &= (\hat{Z}-1) Q_N^{r;a} \\ &= (\hat{Z}-1) Q_N. \end{aligned} \tag{C.2}$$

The contribution to the nucleon charges due to the meson cloud diagram in Fig. 4.2(c) is

$$Q_N^{r;c} = \frac{27}{400} \left(\frac{g_A}{\pi F}\right)^2 \int_0^\infty dp p^4 F^2_{\pi NN}(p^2) \sum_{\Phi=\pi,K} \frac{q_N^{\Phi;c}}{w_\Phi^3(p^2)}, \tag{C.3}$$

where

$$q_N^{\pi;c} = \begin{cases} \frac{2}{3} & \text{for} \quad N=p \\ -\frac{2}{3} & \text{for} \quad N=n \end{cases}, \qquad q_N^{K;c} = \begin{cases} \frac{4}{3} & \text{for} \quad N=p \\ \frac{2}{3} & \text{for} \quad N=n \end{cases}. \tag{C.4}$$

$F_{\pi NN}(p^2)$ is the πNN form factor normalized to unity at zero recoil,

$$F_{\pi NN}(p^2) = \exp\left(-\frac{p^2R^2}{4}\right)\left\{1+\frac{p^2R^2}{8}\left(1-\frac{5}{3g_A}\right)\right\} \tag{C.5}$$

and the meson energy is $w_\Phi(p^2) = \sqrt{M_\Phi^2 + p^2}$.

Finally, the contribution of the vertex correction diagram in Fig. 4.2(d) is given by

$$Q_N^{r;d} = \frac{27}{400}\left(\frac{g_A}{\pi F}\right)^2 \int_0^\infty dp p^4 F_{\pi NN}^2(p^2) \sum_{\Phi=\pi,K} \frac{q_N^{\Phi;d}}{w_\Phi^3(p^2)}, \tag{C.6}$$

where

$$\begin{aligned} q_N^{\pi;d} &= \begin{cases} \frac{1}{3} & \text{for} \quad N=p \\ -\frac{2}{3} & \text{for} \quad N=n \end{cases}, \qquad q_N^{K;d} = \begin{cases} -\frac{2}{3} & \text{for} \quad N=p \\ -\frac{2}{3} & \text{for} \quad N=n \end{cases}, \\ q_N^{\eta;d} &= \begin{cases} \frac{1}{9} & \text{for} \quad N=p \\ 0 & \text{for} \quad N=n \end{cases}. \end{aligned} \tag{C.7}$$

Charge conservation gives the constraint

$$Q_N^{r;b} + Q_N^{r;c} + Q_N^{r;d} \equiv 0. \tag{C.8}$$

This results in the renormalization constants

$$\begin{aligned} \hat{Z} &= 1 - \frac{27}{400}\left(\frac{g_A}{\pi F}\right)^2 \int_0^\infty dp p^4 F_{\pi NN}^2(p^2)\left[\frac{1}{w_\pi^3(p^2)} + \frac{2}{3w_K^3(p^2)} + \frac{1}{9w_\eta^3(p^2)}\right], \\ Z_s &= 1 - \frac{27}{400}\left(\frac{g_A}{\pi F}\right)^2 \int_0^\infty dp p^4 F_{\pi NN}^2(p^2)\left[\frac{4}{3w_K^3(p^2)} + \frac{4}{9w_\eta^3(p^2)}\right]. \end{aligned} \tag{C.9}$$

Appendix D

Electromagnetic $N - \Delta$ transition in the PCQM

Here we present the analytical expressions for the $N\gamma \to \Delta$ helicity amplitudes $A_{1/2}(Q^2)$ and $A_{3/2}(Q^2)$. The Feynman diagrams contributing to these amplitudes are shown in Figs. 4.3.

Ground state contributions

We first restrict to the ground state quark propagator. The three-quark diagram in Fig. 4.3(a) results in

$$A_{1/2}(Q^2)|_{3q} = A_{1/2}(Q^2)|_{3q}^{LO} + A_{1/2}(Q^2)|_{3q}^{NLO}, \tag{D.1}$$

where

$$\begin{aligned} A_{1/2}(Q^2)|_{3q}^{LO} &= -\frac{2}{3}\frac{eP^*(Q^2)}{\sqrt{2\omega_\gamma}}\rho R\frac{\exp\left(-\frac{Q^2R^2}{4}\right)}{1+\frac{3\rho^2}{2}}, \\ A_{1/2}(Q^2)|_{3q}^{NLO} &= A_{1/2}(Q^2)|_{3q}^{LO}\hat{m}_0^r\left(\frac{\rho R}{1+\frac{3\rho^2}{2}}\right)\left(\frac{Q^2R^2}{4}-\frac{2-\frac{3\rho^2}{2}}{1+\frac{3\rho^2}{2}}\right). \end{aligned} \tag{D.2}$$

$P^*(Q^2) = \sqrt{(M_\Delta^2 - M_N^2 - Q^2)^2 + 4M_\Delta^2 Q^2}/2M_\Delta$ is the absolute value of the three-momentum of the virtual photon in the Δ-rest frame and $\omega_\gamma = P^*(0)$. $\hat{m}_0^r$ is the renormalized quark mass as presented in Eq. (4.44). The three-quark counterterm (CT) diagram in Figs. 4.3(b) is

$$A_{1/2}(Q^2)|_{CT} = (\hat{Z}^0 - 1)A_{1/2}(Q^2)|_{3q}^{LO}, \tag{D.3}$$

where $\hat{Z}^0$ is the same as $\hat{Z}$ which is shown in Eq. (C.9).
The meson-cloud (MC) diagram in Figs. 4.3(c) yields

$$\begin{aligned} A_{1/2}(Q^2)|_{MC} &= -\frac{3}{200}\frac{eP^*(Q^2)}{\sqrt{2\omega_\gamma}}\left(\frac{g_A}{\pi F}\right)^2\int_0^\infty dpp^4\int_{-1}^{1}dx(1-x^2) \\ &\times\mathcal{F}_{\pi NN}(p^2,Q^2,x)t_N^{MC}(p^2,Q^2,x), \end{aligned} \tag{D.4}$$

where

$$\begin{aligned} \mathcal{F}_{\pi NN}(p^2,Q^2,x) &= F_{\pi NN}(p^2)F_{\pi NN}(p_+^2), \\ F_{\pi NN}(p^2) &= \exp\left(-\frac{p^2R^2}{4}\right)\left\{1+\frac{p^2R^2}{8}\left(1-\frac{5}{3g_A}\right)\right\}, \\ t_N^{MC}(p^2,Q^2,x) &= 2D_\pi(p^2,Q^2,x)+D_K(p^2,Q^2,x), \\ D_\Phi(p^2,Q^2,x) &= \frac{1}{w_\Phi^2(p^2)w_\Phi^2(p_+^2)}, \\ p_\pm^2 &= p^2+Q^2\pm 2p\sqrt{Q^2}x, \end{aligned} \tag{D.5}$$

with meson energy $w_\Phi(p^2)=\sqrt{M_\Phi^2+p^2}$.
The vertex-correction (VC) diagram in Figs. 4.3(d) is

$$\begin{aligned} A_{1/2}(Q^2)|_{VC} &= -\frac{1}{200}\frac{eP^*(Q^2)}{\sqrt{2\omega_\gamma}}\left(\frac{g_A}{\pi F}\right)^2\exp\left(-\frac{Q^2R^2}{4}\right)\frac{\rho R}{1+\frac{3\rho^2}{2}} \\ &\times\int_0^\infty dpp^4F_{\pi NN}^2(p^2)t_N^{VC}(p^2), \end{aligned} \tag{D.6}$$

where

$$\begin{aligned} t_N^{VC}(p^2) &= W_\pi(p^2)-\frac{1}{3}W_\eta(p^2), \\ W_\Phi &= \frac{1}{w_\Phi^3(p^2)}. \end{aligned} \tag{D.7}$$

The meson-in-flight (MF) diagram in Figs. 4.3(e) is

$$\begin{aligned} A_{1/2}(Q^2)|_{MF} &= -\frac{9}{200}\frac{eP^*(Q^2)}{\sqrt{2\omega_\gamma}}\left(\frac{g_A}{\pi F}\right)^2\int_0^\infty dpp^4\int_{-1}^{1}dx(1-x^2) \\ &\times\mathcal{F}_{\pi NN}(p^2,Q^2,x)D_\pi(p^2,Q^2,x). \end{aligned} \tag{D.8}$$

Inclusion of the excited quark state propagators

By taking into account the excited quark state propagators in the loop calculations the renormalized quark mass and the renormalization constant are modified such that $\hat{m}_0^r \to \hat{m}_F^r$ and $\hat{Z}_0^r \to \hat{Z}^F$, where

$$\begin{aligned}
\hat{m}_F^r &= \hat{m} - \sum_\alpha \frac{1}{3\gamma}\left(\frac{1}{\pi F}\right)^2 \int_0^\infty dp p^2 F_\alpha(p^2) F_\alpha^\dagger(p^2) \\
&\quad \times \left\{ \frac{9}{4}\mathcal{C}_\alpha^\pi(p^2) + \frac{3}{2}\mathcal{C}_\alpha^K(p^2) + \frac{1}{4}\mathcal{C}_\alpha^\eta(p^2) \right\}, \\
\hat{Z}^F &= 1 - \sum_\alpha \left(\frac{1}{\pi F}\right)^2 \int_0^\infty dp p^2 F_\alpha(p^2) F_\alpha^\dagger(p^2) \\
&\quad \times \left\{ \frac{3}{4}\mathcal{W}_\alpha^\pi(p^2) + \frac{1}{2}\mathcal{W}_\alpha^K(p^2) + \frac{1}{12}\mathcal{W}_\alpha^\eta(p^2) \right\},
\end{aligned} \tag{D.9}$$

where $\gamma = (1-3\rho^2/2)/(1+3\rho^2/2)$ is the relativistic reduction factor and the defined quantities are (see also Appendix B),

$$\begin{aligned}
F_\alpha(p^2) &= N N_\alpha \frac{\partial}{\partial p} \int_0^\infty dr\, r\, S(r)[g_0(r) f_\alpha(r) + g_\alpha(r) f_0(r)] \\
&\quad \times \int_\Omega d\cos\theta\, d\phi\, e^{ipr\cos\theta} C_\alpha Y_{l0}(\theta,\phi), \\
\mathcal{C}_\alpha^\Phi &= \frac{1}{w_\Phi(p^2)(w_\Phi(p^2) + \Delta\mathcal{E}_\alpha)}, \\
\mathcal{W}_\alpha^\Phi &= \frac{1}{w_\Phi(p^2)(w_\Phi(p^2) + \Delta\mathcal{E}_\alpha)^2}.
\end{aligned} \tag{D.10}$$

Therefore, the three-quark NLO and the three-quark CT are

$$A_{1/2}(Q^2)|_{3q}^{NLO} = A_{1/2}(Q^2)|_{3q}^{LO} \hat{m}_F^r \left(\frac{\rho R}{1+\frac{3\rho^2}{2}}\right)\left(\frac{Q^2R^2}{4} - \frac{2-\frac{3\rho^2}{2}}{1+\frac{3\rho^2}{2}}\right), \tag{D.11}$$

$$A_{1/2}(Q^2)|_{CT} = (\hat{Z}^F - 1) A_{1/2}(Q^2)|_{3q}^{LO}. \tag{D.12}$$

For the MC diagram we have

$$\begin{aligned} A_{1/2}(Q^2)|_{MC} &= -\frac{1}{6}\frac{eP^*(Q^2)}{\sqrt{2\omega_\gamma}}\left(\frac{1}{\pi F}\right)^2\int\limits_0^\infty dpp^3\int\limits_{-1}^{1}dx\frac{(1-x^2)}{\sqrt{p_+^2}} \\ &\times\sum_\alpha \mathcal{F}_{\alpha;MC}(p^2,Q^2,x)t_{\alpha;MC}(p^2,Q^2,x), \end{aligned} \tag{D.13}$$

where

$$\begin{aligned} t_{\alpha;MC}(p^2,Q^2,x) &= 2D_\alpha^\pi(p^2,Q^2,x)+D_\alpha^K(p^2,Q^2,x), \\ D_\alpha^\Phi(p^2,Q^2,x) &= \frac{1+\Delta\mathcal{E}_\alpha/[w_\Phi(p_+^2)+w_\Phi(p^2)]}{w_\Phi(p^2)w_\Phi(p_+^2)[w_\Phi(p^2)+\Delta\mathcal{E}_\alpha][w_\Phi(p_+^2)+\Delta\mathcal{E}_\alpha]}, \\ \mathcal{F}_{\alpha;MC}(p^2,Q^2,x) &= F_\alpha(p_+^2)F_\alpha^\dagger(p^2). \end{aligned} \tag{D.14}$$

The VC diagram is

$$\begin{aligned} A_{1/2}(Q^2)|_{VC} &= \sum_{\beta,\alpha}\frac{I_{\beta\alpha}(Q^2)}{18}\frac{eP^*(Q^2)}{\sqrt{2\omega_\gamma}}\left(\frac{1}{\pi F}\right)^2 \\ &\times\int\limits_0^\infty dpp^2\mathcal{F}_{\beta\alpha;VC}(p^2)t_{\beta\alpha;VC}(p^2), \end{aligned} \tag{D.15}$$

where

$$\begin{aligned} t_{\beta\alpha;VC}(p^2) &= \mathcal{W}_{\beta\alpha}^\pi(p^2)-\frac{1}{3}\mathcal{W}_{\beta\alpha}^\eta(p^2), \\ \mathcal{W}_{\beta\alpha}^\Phi(p^2) &= \frac{1}{w_\Phi(p^2)[w_\Phi(p^2)+\Delta\mathcal{E}_\beta][w_\Phi(p^2)+\Delta\mathcal{E}_\alpha]}, \\ \mathcal{F}_{\beta\alpha;VC}(p^2) &= F_\beta(p^2)F_\alpha^\dagger(p^2). \end{aligned} \tag{D.16}$$

We also define

$$\begin{aligned} I_{\beta\alpha}(Q^2) &= 2N_\beta N_\alpha\frac{\partial}{\partial Q^2}\int\limits_0^\infty drr[g_\beta(r)f_\alpha(r)+g_\alpha(r)f_\beta(r)] \\ &\times\int\limits_\Omega d\cos\theta d\phi e^{i\sqrt{Q^2}r\cos\theta}C_\beta Y_{l_\beta 0}(\theta,\phi)C_\alpha Y_{l_\alpha 0}(\theta,\phi). \end{aligned} \tag{D.17}$$

Appendix E

Calculational technique of quark-meson loop diagrams

In order to calculate the loop diagrams in Figs. 5.1, 5.2, 5.3 and 5.14 we refer to the technique called "the infrared dimensional regularization" (IDR) which has been discussed in detail in Refs. [13, 20]. Here the difference is that instead of working with nucleon degrees of freedom we work with the constituent quark. We briefly recall the basic ideas of this technique. In Baryon ChPT the loop integrals are non-homogeneous functions of the mesonic momenta and the quark masses due to the presence of a new scale parameter, the nucleon mass. As a result, the loop integrals contain an infrared singular part involving the fractional powers of the meson masses and an infrared regular part involving the fractional powers of the nucleon mass. The presence of the regular part in the loop integrals spoils the power counting rules since their chiral expansion starts at the same order as the tree graphs. The basic idea of the IDR method is to remove the infrared regular parts of the loop integrals from the consideration and to absorb them in the low-energy couplings of the underlying chiral Lagrangian. The IDR method is consistent with Lorentz and gauge invariance. Also, chiral power counting is preserved and the Ward identities of chiral symmetry are fulfilled.

The self-energy diagram shown in Fig. 5.3(3) can be used to demonstrate the IDR method contributing to the quark mass operator. We consider the scalar loop integral in d dimensions

$$H(p^2) = \int \frac{d^d k}{(2\pi)^d i} \frac{1}{[M^2 - k^2 - i\epsilon][m^2 - (p-k)^2 - i\epsilon]}, \tag{E.1}$$

where M and m are the meson and constituent quark masses, respectively. With

dimensional regularization the master formula in d-dimensions is

$$\int \frac{d^dk}{(2\pi)^d}\frac{k^{2n}}{[M^2-k^2]^m} = \frac{i^{2n+1}}{(4\pi)^{d/2}}\frac{\Gamma(n+d/2)\Gamma(m-n-d/2)}{\Gamma(d/2)\Gamma(m)}M^{2(n-m)+d}. \quad \text{(E.2)}$$

At threshold $p^2=(m+M)^2$, we obtain

$$H(p^2) = \underbrace{c_d\frac{M^{d-3}}{m+M}}_{=I(p^2)} + \underbrace{c_d\frac{m^{d-3}}{m+M}}_{=R(p^2)}, \quad \text{(E.3)}$$

where

$$c_d = \frac{\Gamma(2-d/2)}{(4\pi)^{d/2}(d-3)}. \quad \text{(E.4)}$$

Here $I(p^2)$ is the infrared singular piece which is characterized by fractional powers of M and generated by the loop momenta of order of the meson mass. For $I(p^2)$ the usual power counting applies. Another piece in the decomposition of $H(p^2)$ defined by $R(p^2)$ is the infrared regular part which is generated by the loop momenta of the order of the constituent quark mass m (in our counting m is of the order of $\Lambda_{\chi SB}\sim$ 1 GeV). As discussed before, we remove the regular part $R(p^2)$ by redefining the low-energy coupling constants in the chiral Lagrangian. In Ref. [13] a recipe was suggested how to split the integral $H(p^2)$ into the singular and regular parts. We use the Feynman parameterization to combine two multipliers $a=M^2-k^2-i\epsilon$ and $b=m^2-(p-k)^2-i\epsilon$ in the denominator of $H(p^2)$:

$$\int \frac{d^dk}{(2\pi)^d}\frac{1}{ab} = \int \frac{d^dk}{(2\pi)^d}\int_0^1 \frac{dx}{[a(1-x)+bx]^2}, \quad \text{(E.5)}$$

and then to write down the integral from 0 to 1 as the difference of two integrals:

$$\int_0^1 dx\ldots = \left[\int_0^\infty - \int_1^\infty\right]dx\ldots. \quad \text{(E.6)}$$

Then the integral from 0 to ∞ is exactly the infrared singular part and the integral from 1 to ∞ is the infrared regular one. This method can be applied to any general one-loop integral with adjustable number of meson and quark propagators.

The calculational technique suggests that: one should separate numerator and denominator; simplify the numerator using the standard (invariant integration) methods. Finally, the result can be reduced to the master integral $I(p^2)$ and its derivatives (like in the conventional dimensional regularization). The integrals containing only the quark propagators do not contribute to the infrared singular parts, and therefore, vanish in the IDR.

The ultraviolet divergences contained in the one-loop integrals are removed via the renormalization of the low-energy constants in the chiral Lagrangian. To perform the renormalization of the constituent quark at one loop and to guarantee charge conservation we need the Z-factor (the wave-function renormalization constant), which is determined by the derivative of the quark mass operator (generated by the diagrams in Fig.4) with respect to its momentum:

$$Z_q^{-1} = 1 - \frac{\partial \Sigma_q(\not{p})}{\partial \not{p}}\bigg|_{\not{p}=m_q}, \qquad q = u, d, s. \tag{E.7}$$

The matrix $Z_q = \mathrm{diag}\{Z_u,\, Z_d,\, Z_s\}$ with $Z_u = Z_d = Z$ is given up to fourth order by

$$Z_q = I + \sum_{P=\pi,K,\eta} \frac{1}{F_P^2}\Big[-g^2\alpha_P\Delta_P + Q_P\Big], \tag{E.8}$$

where

$$\begin{aligned}
\Delta_P &= 2M_P^2\left[\lambda(\mu) + \frac{1}{16\pi^2}\ln\left(\frac{M_P}{\mu}\right)\right],\\
\lambda(\mu) &= \frac{\mu^{d-4}}{(4\pi)^2}\left[\frac{1}{d-4} - \frac{1}{2}(\ln 4\pi + \Gamma'(1) + 1)\right],\\
Q_P &= \frac{g^2M_P^2}{24\pi^2}\alpha_P\left[-1 + \frac{3\pi}{2}\frac{M_P}{m} + \frac{3}{2}\frac{M_P^2}{m^2}\right] + \frac{3c_2M_P^4}{64\pi^2 m}\beta_P I,
\end{aligned} \tag{E.9}$$

and the corresponding coefficients for the pseudoscalar mesons are

$$\alpha_\pi = \frac{9}{2}Q + \frac{3}{2}I - \frac{9}{4}\lambda_3, \quad \alpha_K = -3Q + 2I + \frac{3}{2}\lambda_3, \quad \alpha_\eta = -\frac{3}{2}Q + \frac{I}{2} + \frac{3}{4}\lambda_3,$$
$$\beta_\pi = 1, \qquad \beta_K = \frac{4}{3}, \qquad \beta_\eta = \frac{1}{3},$$

where Q, I and λ_3 are the charge, identity and Gell-Mann matrices, respectively. For the evaluation of the form factor $f_D^q(q^2)$, the quark charge Q [diagram (1) in Fig 5.1] has to be multiplied by Z_q. For $f_P^q(q^2)$, a second-order contribution to the quark anomalous magnetic moment proportional to the c_6 [diagram (2) in Fig. 5.1 and diagram (2^*) in Fig. 5.2] has to be renormalized by the Z_q-factor. The term proportional to c_2 must be dropped, because the product $c_6 c_2$ is of higher-order when compared to the accuracy we are working in.

Appendix F

Loop Integrals

We present the loop integrals contributing to the electromagnetic transition operator between constituent quarks in the infrared regularization scheme Ref. [13]. These integrals have been introduced in ChPT in Refs. [13, 20]. The initial and final quark field momenta are denoted by p and p', respectively. The momentum of the photon field is $q = p' - p$. We also define $P = p' + p$. Since the external quarks are on the mass shell $p^2 = p'^2 = m^2$, the structure integrals can be expanded through a set of scalar functions which depend on the transverse momentum squared $t = Q^2 = -q^2$, the mass of meson M and the constituent quark mass m. Following Refs. [13, 20] the masses of particles occurring in the loop integrals are their leading order values i.e. $M_P \to \overset{\circ}{M}_P$ and $m_q \to m$. For universality, the integrals are calculated in terms of the adjustable values of the constituent quark mass inside the loop (m^*) and for the external one with mass m. In the final state of the numerical calculations we will neglect the different between m^* and m, i.e. we will set $m^* = m$.

Infrared parts of loop integrals

We deal with the following loop integrals:

$$\int_I \frac{d^dk}{(2\pi)^d i} \frac{1}{M^2 - k^2} = \Delta_M, \tag{F.1}$$

$$\int_I \frac{d^dk}{(2\pi)^d i} \frac{1}{[M^2 - k^2][M^2 - (k+q)^2]} = J^{(0)}(t, M^2), \tag{F.2}$$

$$\int_I \frac{d^dk}{(2\pi)^d i} \frac{k_\mu}{[M^2-k^2][M^2-(k+q)^2]} = -\frac{1}{2} q_\mu J^{(0)}(t, M^2), \tag{F.3}$$

$$\int_I \frac{d^dk}{(2\pi)^d i} \frac{k_\mu k_\nu}{[M^2-k^2][M^2-(k+q)^2]}$$
$$= (q_\mu q_\nu - g_{\mu\nu} t) J^{(1)}(t, M^2) + q_\mu q_\mu J^{(2)}(t, M^2), \tag{F.4}$$

$$\int_I \frac{d^dk}{(2\pi)^d i} \frac{1}{[M^2-k^2][m^{*2}-(p-k)^2]} = I^{(0)}(M^2, m^2, m^{*2}), \tag{F.5}$$

$$\int_I \frac{d^dk}{(2\pi)^d i} \frac{k_\mu}{[M^2-k^2][m^{*2}-(p-k)^2]} = p_\mu I^{(1)}(M^2, m^2, m^{*2}), \tag{F.6}$$

$$\int_I \frac{d^dk}{(2\pi)^d i} \frac{1}{[M^2-k^2][m^{*2}-(p-k)^2][m^{*2}-(p'-k)^2]}$$
$$= I_{12}^{(0)}(t, M^2, m^2, m^{*2}), \tag{F.7}$$

$$\int_I \frac{d^dk}{(2\pi)^d i} \frac{k_\mu}{[M^2-k^2][m^{*2}-(p-k)^2][m^{*2}-(p'-k)^2]}$$
$$= P_\mu I_{12}^{(1)}(t, M^2, m^2, m^{*2}), \tag{F.8}$$

$$\int_I \frac{d^dk}{(2\pi)^d i} \frac{k_\mu\, k_\nu}{[M^2-k^2][m^{*2}-(p-k)^2][m^{*2}-(p'-k)^2]}$$
$$= g_{\mu\nu} I_{12}^{(2)}(t, M^2, m^2, m^{*2}) + P_\mu P_\nu I_{12}^{(3)}(t, M^2, m^2, m^{*2})$$
$$+ q_\mu q_\nu I_{12}^{(4)}(t, M^2, m^2, m^{*2}), \tag{F.9}$$

$$\int_I \frac{d^dk}{(2\pi)^d i} \frac{1}{[M^2-k^2][M^2-(k+q)^2][m^{*2}-(p-k)^2]}$$
$$= I_{21}^{(0)}(t, M^2, m^2, m^{*2}), \tag{F.10}$$

$$\int_I \frac{d^dk}{(2\pi)^d i} \frac{k_\mu}{[M^2-k^2][M^2-(k+q)^2][m^{*2}-(p-k)^2]}$$
$$= P_\mu I_{21}^{(1)}(t, M^2, m^2, m^{*2}) - \frac{1}{2} q_\mu I_{21}^{(0)}(t, M^2, m^2, m^{*2}), \tag{F.11}$$

$$\int\limits_I \frac{d^dk}{(2\pi)^d i}\frac{k_\mu k_\nu}{[M^2-k^2][M^2-(k+q)^2][m^{*2}-(p-k)^2]}$$
$$= g_{\mu\nu}I_{21}^{(2)}(t,M^2,m^2,m^{*2}) + P_\mu P_\nu I_{21}^{(3)}(t,M^2,m^2,m^{*2})$$
$$+q_\mu q_\nu I_{21}^{(4)}(t,M^2,m^2,m^{*2})$$
$$-\frac{1}{2}(P_\mu q_\nu + P_\nu q_\mu)I_{21}^{(1)}(t,M^2,m^2,m^{*2}), \tag{F.12}$$

where the symbol $\int\limits_I$ represents the loop integration according to the infrared dimensional regularization scheme [13, 20].

Reduction formulas for loop integrals

Higher-order tensorial integrals can be reduced to the basic scalar integrals using the invariant integration [13, 20]:

$$J^{(1)}(t,M^2) = \frac{1}{4(d-1)t}\Big[(t+4M^2)J^{(0)}(t,M^2) - 2\Delta_M\Big], \tag{F.13}$$

$$J^{(2)}(t,M^2) = \frac{1}{4}J^{(0)}(t,M^2) + \frac{1}{2t}\Delta_M, \tag{F.14}$$

$$I^{(1)}(M^2,m^2,m^{*2}) = \frac{1}{2m^2}\Big[M^{*2}I^{(0)}(M^2,m^2,m^{*2}) + \Delta_M\Big], \tag{F.15}$$

$$I_{12}^{(1)}(t,M^2,m^2,m^{*2}) = \frac{1}{4m^2+t}\Big[I^{(0)}(M^2,m^2,m^{*2})$$
$$+M^{*2}I_{12}^{(0)}(t,M^2,m^2,m^{*2})\Big], \tag{F.16}$$

$$I_{12}^{(2)}(t,M^2,m^2,m^{*2}) = \frac{1}{d-2}\Big[M^2I_{12}^{(0)}(t,M^2,m^2,m^{*2})$$
$$-M^{*2}I_{12}^{(1)}(t,M^2,m^2,m^{*2})\Big], \tag{F.17}$$

$$I_{12}^{(3)}(t,M^2,m^2,m^{*2}) = \frac{1}{(d-2)(4m^2+t)}\Big[M^{*2}(d-1)I_{12}^{(1)}(t,M^2,m^2,m^{*2})$$
$$-M^2I_{12}^{(0)}(t,M^2,m^2,m^{*2})$$
$$+\frac{d-2}{2}I^{(1)}(M^2,m^2,m^{*2})\Big], \tag{F.18}$$

$$
\begin{aligned}
I_{12}^{(4)}(t,M^2,m^2,m^{*\,2}) &= \frac{1}{(d-2)\,t}\Bigg[-M^{*\,2}I_{12}^{(1)}(t,M^2,m^2,m^{*\,2}) \\
&\quad +M^2 I_{12}^{(0)}(t,M^2,m^2,m^{*\,2}) \\
&\quad +\frac{d-2}{2}I^{(1)}(M^2,m^2,m^{*\,2})\Bigg], \qquad \text{(F.19)}\\
I_{21}^{(1)}(t,M^2,m^2,m^{*\,2}) &= \frac{1}{2(4m^2+t)}\Bigg[(2M^{*\,2}+t)I_{21}^{(0)}(t,M^2,m^2,m^{*\,2}) \\
&\quad -2I^{(0)}(M^2,m^2,m^{*\,2})+2J^{(0)}(t,M^2)\Bigg], \qquad \text{(F.20)}\\
I_{21}^{(2)}(t,M^2,m^2,m^{*\,2}) &= \frac{1}{4(d-2)}\Bigg[(4M^2+t)I_{21}^{(0)}(t,M^2,m^2,m^{*\,2}) \\
&\quad -2(2M^{*\,2}+t)I_{21}^{(1)}(t,M^2,m^2,m^{*\,2}) \\
&\quad -2I^{(0)}(M^2,m^2,m^{*\,2})\Bigg], \qquad \text{(F.21)}\\
I_{21}^{(3)}(t,M^2,m^2,m^{*\,2}) &= \frac{1}{4(d-2)(4m^2+t)}\Bigg[-(4M^2+t)I_{21}^{(0)}(t,M^2,m^2,m^{*\,2}) \\
&\quad +2(d-1)(2M^{*\,2}+t)I_{21}^{(1)}(t,M^2,m^2,m^{*\,2}) \\
&\quad +2I^{(0)}(M^2,m^2,m^{*\,2}) \\
&\quad -2(d-2)I^{(1)}(M^2,m^2,m^{*\,2})\Bigg], \qquad \text{(F.22)}\\
I_{21}^{(4)}(t,M^2,m^2,m^{*\,2}) &= \frac{1}{4(d-2)}\Bigg[-(4M^2+(d-1)t)I_{21}^{(0)}(t,M^2,m^2,m^{*\,2}) \\
&\quad +2(2M^{*\,2}+t)I_{21}^{(1)}(t,M^2,m^2,m^{*\,2}) \\
&\quad -2(d-3)I^{(0)}(M^2,m^2,m^{*\,2}) \\
&\quad +2(d-2)I^{(1)}(M^2,m^2,m^{*\,2})\Bigg], \qquad \text{(F.23)}
\end{aligned}
$$

where $M^{*\,2} = M^2 + m^2 - m^{*\,2}$.

Scalar loop integrals

The scalar loop integrals are given as [13, 20]

$$\Delta_M = 2M^2\lambda_M, \tag{F.24}$$

$$J^{(0)}(t, M^2) = -2\lambda_M - \frac{1}{16\pi^2}\left[1 + k\left(\frac{t}{M^2}\right)\right], \tag{F.25}$$

$$\begin{aligned} I^{(0)}(M^2, m^2, m^{*2}) &= -\frac{M^{*2}}{m^2}\left[\lambda_M - \frac{1}{32\pi^2}\right] \\ &\quad -\frac{\mu^*}{8\pi^2} g(0, M, m, m^*)[1 - \Omega^2] r^{*3}, \end{aligned} \tag{F.26}$$

$$\begin{aligned} I^{(1)}_{12}(t, M^2, m^2, m^{*2}) &= -\frac{f\left(\frac{t}{m^2}\right)}{m^2}\left[\lambda_M + \frac{1}{32\pi^2}\right] \\ &\quad +\frac{M^{*2}}{32\pi^2 M m^3} g\left(\frac{t}{m^2}, M, m, m^*\right), \end{aligned} \tag{F.27}$$

$$\begin{aligned} I^{(1)}_{21}(t, M^2, m^2, m^{*2}) &= \frac{f\left(\frac{t}{m^2}\right)}{m^2}\left[\lambda_M + \frac{1}{32\pi^2}\right] + \frac{1}{32\pi^2 m^2}\left[h_1\left(\frac{t}{M^2}, M, m, m^*\right)\right. \\ &\quad \left. +2\left(\frac{1}{\mu^*} + \Omega\right) h_2\left(\frac{t}{M^2}, M, m, m^*\right)\right], \end{aligned} \tag{F.28}$$

where

$$\lambda_M = \frac{M^{d-4}}{(4\pi)^2}\left\{\frac{1}{d-4} - \frac{1}{2}(\ln 4\pi + \Gamma'(1) + 1)\right\},$$

$$\Omega = \frac{m^2 - m^{*2} - M^2}{2m^* M}, \qquad \mu = \frac{M}{m}, \qquad \mu^* = \frac{M}{m^*}, \qquad r^* = \frac{m^*}{m}.$$

The dimensionless functions k, f, g, h_1 and h_2 are given by the expressions

$$k(s) = \int_0^1 dx \ln(1 + x(1-x)s) = \sqrt{\frac{4+s}{s}} \ln \frac{\sqrt{4+s} + \sqrt{s}}{\sqrt{4+s} - \sqrt{s}} - 2, \tag{F.29}$$

$$f(s) = \int_0^1 dx \frac{1}{1 + x(1-x)s} = \frac{2}{\sqrt{s(4+s)}} \ln \frac{\sqrt{4+s} + \sqrt{s}}{\sqrt{4+s} - \sqrt{s}}, \tag{F.30}$$

$$g(s,M,m,m^*) = \int_0^1 dx \frac{\arccos\left[-r^*(\Omega+\mu^*)\frac{\sqrt{r^{*\,2}+x(1-x)s}}{1+x(1-x)s}\right]}{[1+x(1-x)s)]\sqrt{(1-\Omega^2)r^{*\,2}+x(1-x)s}}, \quad \text{(F.31)}$$

$$h_1(s,M,m,m^*) = \int_0^1 dx \frac{\ln[1+x(1-x)s]}{1+\mu^2 x(1-x)s}, \quad \text{(F.32)}$$

$$h_2(s,M,m,m^*) = \int_0^1 dx \arccos\left[-\frac{[\mu^*(1+x(1-x)s)+\Omega]r^*}{\sqrt{1+\mu^2 x(1-x)s}\sqrt{1+sx(1-x)}}\right] \times \frac{1}{[1+\mu^2 x(1-x)s]\sqrt{1+\Omega^2+x(1-x)s}}. \quad \text{(F.33)}$$

Appendix G

Electromagnetic meson-cloud form factors

We explicitly show the contributions of the diagrams in Fig. 5.1 and Fig. 5.2 to the Dirac and Pauli quark form factors. We use the notations $f_D^{(i)}(t)$ and $f_P^{(i)}(t)$ where the superscript i refers to the numbering of the diagrams. We expand the diagonal 3×3 matrices $f_D^{(i)}(t)$ and $f_P^{(i)}(t)$ in the basis of the 3×3 matrices Q, I, and λ_3

$$Q = \begin{pmatrix} 2/3 & 0 & 0 \\ 0 & -1/3 & 0 \\ 0 & 0 & -1/3 \end{pmatrix}, \quad I = \begin{pmatrix} 1 & 0 & 0 \\ 0 & 1 & 0 \\ 0 & 0 & 1 \end{pmatrix}, \quad \lambda_3 = \begin{pmatrix} 1 & 0 & 0 \\ 0 & -1 & 0 \\ 0 & 0 & 0 \end{pmatrix},$$

and in terms of the convergent parts of the structure integrals

$$\begin{aligned}
\bar{J}^{(1)}(t, M^2) &= -\frac{1}{576\pi^2 t}\left[t + 3k(t)\left(t + 4M^2\right)\right], \\
\bar{I}^{(1)}(M^2, m^2, m^2) &= \frac{\mu^3}{64\pi^2}[\mu - g(0, M, m, m)(4 - \mu^2)], \\
\bar{I}_{12}(t, M^2, m^2, m^2) &= \frac{1}{32\pi^2 m^2}[g(t, M, m, m)\mu - f(t)], \\
\bar{I}_{12}^{(2)}(t, M^2, m^2, m^2) &= \frac{\mu^3}{256\pi^2}\Big[-2\mu D_\tau + g(t, M, m, m)(4 - \mu^2 D_\tau) \\
&\quad + g(0, M, m, m)(4 - \mu^2) D_\tau\Big],
\end{aligned}$$

$$
\begin{aligned}
\bar{I}_{12}^{(3)}(t,M^2,m^2,m^2) &= \frac{\mu^3 D_\tau}{1024\pi^2 m^2}\Big[2\mu\,(1+2D_\tau)-\mu f(t) \\
&\quad -g(t,M,m,m)(4-3\mu^2 D_\tau) \\
&\quad +g(0,M,m,m)(4-\mu^2)(2+3D_\tau)\Big], \\
\bar{I}_{12}^{(4)}(t,M^2,m^2,m^2) &= \frac{\mu^3}{512\pi^2 m^2\tau}\Big[\mu\tau D_\tau - 2g(t,M,m,m)(1-\mu^2 D_\tau) \\
&\quad -g(0,M,m,m)(8-4\mu^2+(\mu^2-4)D_\tau)\Big], \\
\bar{I}_{21}^{(2)}(t,M^2,m^2,m^2) &= \frac{1}{512\pi^2}\Big[2D_\tau\mu(\mu^2-2)(2\mu-g(0,M,m,m)(4-\mu^2)) \\
&\quad +k(t)(2+(\mu^2-2)D_\tau) \\
&\quad +2H_{12}(t,M,m,m)(4-(2-\mu^2)^2 D_\tau)\Big], \\
\bar{I}_{21}^{(3)}(t,M_P^2,m^2,m^2) &= \frac{D_\tau}{1024\pi^2 m^2}\Big[2(4+6\mu^2-\mu^4+2(\mu^2-2)(\mu^2+1)D_\tau) \\
&\quad -6k(t)(2+(\mu^2-2)D_\tau)+2f(t)(2+(\mu^2-2)D_\tau)^2 \\
&\quad +g(0,M,m,m)\mu(4-\mu^2)[2(\mu^2+2)+3(\mu^2-2)D_\tau] \\
&\quad -H_{12}(t,M,m,m)(12-8\mu^2+2\tau-3(\mu^2-2)^2 D_\tau)\Big],
\end{aligned}
$$

where

$$
\begin{aligned}
H_{12}(t,M,m,m) &= h_1(t,M,m,m)+h_2(t,M,m,m)\left(\frac{2-\mu^2}{\mu}\right), \\
D_\tau &= \frac{1}{1+\tau/4}.
\end{aligned}
$$

Pseudoscalar mesons contribution

The contributions of the diagrams in Fig. 5.1 to the Dirac form factors of the u, d, and s quark are

$$\begin{aligned}
f_D^{(1)}(t) &= Q\bar{Z}_q, \\
f_D^{(2)}(t) &= f_D^{(4)}(t) = f_D^{(8)}(t) = f_D^{(12)}(t) = 0, \\
f_D^{(3)}(t) &= 2t\bar{d}_{10}Q\,, \\
f_D^{(i)}(t) &= \sum_{P=\pi,K,\eta} \lambda_i^P \epsilon_i^P\,, \qquad i = 5,6,7,9,10,11\,,
\end{aligned} \tag{G.1}$$

where $\bar{Z}_q$ is the finite part of the renomalization matrix Z_q defined in Eq. (E.8) and

$$\begin{aligned}
&\lambda_5^\pi = Q + \frac{1}{3}I - \lambda_3, \quad \lambda_5^K = -\frac{8}{3}Q - \frac{2}{9}I + \frac{4}{3}\lambda_3, \quad \lambda_5^\eta = Q - \frac{1}{9}I - \frac{1}{3}\lambda_3, \\
&\lambda_6^\pi = \lambda_7^\pi = \lambda_9^\pi = \lambda_3, \quad \lambda_6^K = \lambda_7^K = \lambda_9^K = 3Q - \lambda_3, \quad \lambda_6^\eta = \lambda_7^\eta = \lambda_9^\eta = 0, \\
&\lambda_{10}^\pi = c_6\left(Q + \frac{1}{3}I - \lambda_3\right), \quad \lambda_{10}^K = c_6\left(-\frac{8}{3}Q - \frac{2}{9}I + \frac{4}{3}\lambda_3\right), \\
&\lambda_{10}^\eta = c_6\left(Q - \frac{1}{9}I - \frac{1}{3}\lambda_3\right), \\
&\lambda_{11}^\pi = Q, \quad \lambda_{11}^K = \frac{4}{3}Q, \quad \lambda_{11}^\eta = \frac{1}{3}Q,
\end{aligned} \tag{G.2}$$

and

$$\begin{aligned}
\epsilon_5^P &= -\frac{g^2m^2}{F_P^2}\Big\{\bar{I}^{(1)}(M_P^2,m^2,m^2) + M_P^2\bar{I}_{12}^{(0)}(t,M_P^2,m^2,m^2) - 2\bar{I}_{12}^{(2)}(t,M_P^2,m^2,m^2) \\
&\quad -8m^2\bar{I}_{12}^{(3)}(t,M_P^2,m^2,m^2)\Big\}, \\
\epsilon_6^P &= \frac{g^2}{F_P^2}\Big\{t\bar{J}^{(1)}(t,M_P^2) - 4m^2\bar{I}_{21}^{(2)}(t,M_P^2,m^2,m^2) - 16m^4\bar{I}_{21}^{(3)}(t,M_P^2,m^2,m^2)\Big\}, \\
\epsilon_7^P &= -\frac{2g^2m^2}{F_P^2}\bar{I}^{(1)}(M_P^2,m^2,m^2), \\
\epsilon_9^P &= -\frac{t}{F_P^2}\bar{J}^{(1)}(t,M_P^2,m^2,m^2),
\end{aligned}$$

$$\begin{aligned}
\epsilon_{10}^P &= -\frac{2tg^2m^2}{F_P^2}\bar{I}_{12}^{(3)}(t, M_P^2, m^2, m^2), \\
\epsilon_{11}^P &= -\frac{3c_2}{64\pi^2 m F_P^2}M_P^4.
\end{aligned} \tag{G.3}$$

For the Pauli form factors of the u, d and s quarks we have

$$\begin{aligned}
f_P^{(1)}(t) &= f_P^{(7)}(t) = f_P^{(8)}(t) = f_P^{(9)}(t) = 0, \\
f_P^{(2)}(t) &= \bar{Z}_q c_6 Q, \\
f_P^{(3)}(t) &= -2t\bar{d}_{10}Q, \\
f_P^{(4)}(t) &= -4mt\bar{e}_{10}Q - 16m\left[M^2\bar{e}_6 Q + \frac{1}{3}(M_K^2 - M_\pi^2)(\bar{e}_7[Q - \lambda_3 - I/3] - \bar{e}_8 I)\right], \\
f_P^{(i)}(t) &= \sum_{P=\pi,K,\eta} \lambda_i^P m_i^P, \qquad i = 5, 6, 10, 11, 12,
\end{aligned} \tag{G.4}$$

where

$$\lambda_{12}^\pi = \lambda_3, \quad \lambda_{12}^K = 3Q - \lambda_3, \quad \lambda_{12}^\eta = 0,$$

and

$$\begin{aligned}
m_5^P &= -\frac{8g^2m^4}{F_P^2}\bar{I}_{12}^{(3)}(t, M_P^2, m^2, m^2), \\
m_6^P &= \frac{16g^2m^4}{F_P^2}\bar{I}_{21}^{(3)}(t, M_P^2, m^2, m^2), \\
m_{10}^P &= \frac{g^2m^2}{F_P^2}\Big\{\bar{I}^{(1)}(M_P^2, m^2, m^2) - M_P^2\bar{I}_{12}(t, M_P^2, m^2, m^2) + 4\bar{I}_{12}^{(2)}(t, M_P^2, m^2, m^2) \\
&\quad +2t\left(\bar{I}_{12}^{(3)}(t, M_P^2, m^2, m^2) - \bar{I}_{12}^{(4)}(t, M_P^2, m^2, m^2)\right)\Big\}, \\
m_{11}^P &= \frac{3c_2}{64\pi^2 m F_P^2}M_P^4, \\
m_{12}^P &= \frac{4mtc_4}{F_P^2}\bar{J}^{(1)}(t, M_P^2, m^2, m^2).
\end{aligned} \tag{G.5}$$

Vector mesons contribution

The contributions of the diagrams in Fig. 5.2 (vector mesons contributions) to the Dirac and Pauli form factors of the u, d and s quark are

$$
\begin{aligned}
f_D^{(2^*)}(t) &= f_D^{(11^*)}(t) = f_D^{(12^*)}(t) = 0, \\
f_D^{(3^*)}(t) &= -\frac{t}{2}\left\{\lambda_\rho D_\rho(t) + \frac{1}{3}\lambda_\omega D_\omega(t) + \frac{2}{3}\lambda_\phi D_\phi(t)\right\}, \\
f_D^{(10^*)}(t) &= \frac{k_V}{2}\left\{[\lambda_\omega D_\omega(t) - \lambda_\rho D_\rho(t)]\epsilon_{10}^\pi - \frac{4}{3}[\lambda_\phi D_\omega(t) + \lambda_\omega D_\phi(t)]\epsilon_{10}^K \right. \\
&\quad \left. + \frac{1}{9}[3\lambda_\rho D_\rho(t) + \lambda_\omega D_\omega(t) + 8\lambda_\phi D_\phi(t)]\epsilon_{10}^\eta\right\}, \\
f_P^{(2^*)}(t) &= \frac{k_V}{2}\left\{\bar{Z}\lambda_\rho D_\rho(t) + \frac{1}{3}\bar{Z}\lambda_\omega D_\omega(t) + \frac{2}{3}\bar{Z}_s\lambda_\phi D_\phi(t)\right\}, \\
f_P^{(3^*)}(t) &= f_P^{11^*}(t) = 0, \\
f_P^{(10^*)}(t) &= \frac{k_V}{2}\left\{[\lambda_\omega D_\omega(t) - \lambda_\rho D_\rho(t)]m_{10}^\pi - \frac{4}{3}[\lambda_\phi D_\omega(t) + \lambda_\omega D_\phi(t)]m_{10}^K \right. \\
&\quad \left. + \frac{1}{9}[3\lambda_\rho D_\rho(t) + \lambda_\omega D_\omega(t) + 8\lambda_\phi D_\phi(t)]m_{10}^\eta\right\}, \\
f_P^{(12^*)}(t) &= -\frac{t}{2}k_V\left\{\lambda_\rho D_\rho(t)\left[\frac{2}{F_\pi^2}\bar{J}^{(1)}(t, M_\pi^2) + \frac{1}{F_K^2}\bar{J}^{(1)}(t, M_K^2)\right]\right. \\
&\quad \left. + \frac{\lambda_\omega}{F_K^2}D_\omega(t)\bar{J}^{(1)}(t, M_K^2) + \frac{2\lambda_\phi}{F_K^2}D_\phi(t)\bar{J}^{(1)}(t, M_K^2)\right\},
\end{aligned}
\tag{G.6}
$$

where

$$
\lambda_\rho = \lambda_3, \quad \lambda_\omega = 2Q + 2I/3 - \lambda_3, \quad \lambda_\phi = 2Q - I/3 - \lambda_3,
$$

and

$$
D_V(t) = 1/(M_V^2 + t). \tag{G.7}
$$

Expansion for the practical calculation

In the practical calculation, we keep the exact form of the function $f(t)$, while we expand the functions $k(t)$, $g(t, M, m, m)$, $h_1(t, M, m, m)$ and $h_2(t, M, m, m)$ in powers of θ and μ with $\theta = t/M^2$ and $\mu = M/m$.

Finally, we keep our expressions for ϵ_i^P, and m_i^P up to $O(\theta_P, \mu_P^4)$ which are explicitly given as

$$
\begin{aligned}
\epsilon_5^P &= \frac{g^2 m^2 \mu_P^2}{32\pi^2 F_P^2}\Bigg[f(t)\left(1-\frac{3}{4}\mu_P^2 D_\tau^2\right)+\pi\mu_P\left(1-\frac{D_\tau}{2}-2D_\tau^2\right) \\
&\quad +\frac{\mu_P^2}{2}(1-D_\tau-\frac{3}{2}D_\tau^2)\Bigg], \\
\epsilon_6^P &= \frac{g^2 m^2}{16\pi^2 F_P^2}\Bigg[\mu_P^2\left(1-\frac{5\pi}{2}\mu_P-2\mu_P^2\right) \\
&\quad +\tau\left(\frac{7}{2}-\frac{35\pi}{24}\mu_P-\frac{13}{6}\mu_P^2+\frac{105\pi}{64}\mu_P^3+\frac{107}{72}\mu_P^4\right)\Bigg], \\
\epsilon_7^P &= \frac{g^2 m^2 \mu_P^3}{16\pi^2 F_P^2}\left(\pi+\frac{\mu_p}{2}\right), \\
\epsilon_9^P &= \frac{t}{192\pi^2 F_P^2}, \\
\epsilon_{10}^P &= \frac{g^2 m^2 \mu_P^3}{32\pi^2 F_P^2}(1-D_\tau)\left[\pi(1+2D_\tau)+\frac{\mu_P}{2}\left(1+\frac{3}{2}D_\tau\right)+\frac{3}{4}\mu_P D_\tau f(t)\right], \\
\epsilon_{11}^P &= -\frac{3c_2 m^3 \mu_P^4}{64\pi^2 F_P^2}, \\
m_5^P &= \frac{g^2 m^2 \mu_P^3}{16\pi^2 F_P^2}\left\{\frac{3}{8}\mu_P f(t) D_\tau^2 + D_\tau\left[\pi\left(\frac{1}{2}+D_\tau\right)+\frac{3}{8}\left(\frac{2}{3}+D_\tau\right)\right]\right\}, \\
m_6^P &= -\frac{g^2 m^2}{\pi F_P^2}\Bigg[\frac{\mu_P}{8}\left(\pi+\mu_P-\frac{15}{8}\pi\mu_P^2-\frac{4}{3}\mu_P^3\right) \\
&\quad +\frac{\tau}{96\mu_P}\left(\pi+8\mu_P-\frac{105\pi}{8}\mu_P^2-\frac{52}{3}\mu_P^3+\frac{1575\pi}{128}\mu_P^4+\frac{107}{10}\mu_P^5\right)\Bigg], \\
m_{10}^P &= \frac{g^2 m^2 \mu_P^2}{32\pi^2 F_P^2}\Bigg\{f(t)\left[1-\frac{3}{4}D_\tau\mu_P^2(1-D_\tau)\right]-\pi\mu_P\left(1+\frac{1}{2}D_\tau-2D_\tau^2\right) \\
&\quad -\frac{1}{2}\mu_P^2\left(1+\frac{1}{2}D_\tau-\frac{3}{2}D_\tau^2\right)\Bigg\}, \\
m_{11}^P &= \frac{3c_2 m^3 \mu_P^4}{64\pi^2 F_P^2}, \\
m_{12}^P &= \frac{c_4 m t}{48\pi^2 F_P^2}.
\end{aligned}
$$

Renormalization of LECs

After absorbing the divergences coming from the vector meson-exchange diagrams the renormalized LECs are written as

$$\begin{aligned}
\bar{d}_{10} &= d_{10}^r(\mu) - \frac{\beta_{d_{10}}}{32\pi^2 F_K^2} \ln \frac{M_K^2}{\mu^2}, \\
\bar{e}_{10} &= e_{10}^r(\mu) - \frac{\beta_{e_{10}}}{32\pi^2 F_K^2} \ln \frac{M_K^2}{\mu^2}, \\
\bar{e}_6 &= e_6^r(\mu) - \frac{\beta_{e_6}}{32\pi^2 F_\pi^2} \ln \frac{M_\pi^2}{\mu^2}, \\
\bar{e}_7 &= e_7^r(\mu) - \frac{\beta_{e_7}}{32\pi^2 F_\pi^2} \ln \frac{M_\pi^2}{\mu^2}, \\
\bar{e}_8 &= e_8^r(\mu) - \frac{\beta_{e_8}}{32\pi^2 F_\pi^2} \ln \frac{M_\pi^2}{\mu^2}
\end{aligned} \tag{G.8}$$

where the β-coefficients with taking into account the vector mesons are given by

$$\begin{aligned}
\beta_{d_{10}} &= -\frac{1+5g^2}{4}, \\
\beta_{e_{10}} &= \frac{1}{8m}\left(1 - 7g^2 + k_V + 4mc_4\right), \\
\beta_{e_6} &= -\frac{35}{144m}(c_6 g^2 + k_V) - \frac{1}{16m}(c_6 - 4c_4 m) - \frac{5g^2}{9m}, \\
\beta_{e_7} &= -\frac{11}{48m}(c_6 + k_V)g^2 - \frac{3}{16m}(c_6 - 4c_4 m) - \frac{7g^2}{6m}, \\
\beta_{e_8} &= -\frac{1}{16m}(c_6 + k_V)g^2 + \frac{1}{16m}(c_6 - 4c_4 m) + \frac{g^2}{4m},
\end{aligned} \tag{G.9}$$

and

$$M^2 = M_\pi^2 - M_K^2 + \frac{3}{2}M_\eta^2. \tag{G.10}$$

Appendix H

Meson-nucleon sigma-terms

Two important identities are involved in the evaluation of the meson-nucleon sigma-terms. In particular, the derivatives with respect to the current quark masses are equivalent to the ones with respect to the meson masses [140]

$$\hat{m}\frac{\partial}{\partial\hat{m}}\Sigma_q = M_\pi^2\left(\frac{\partial}{\partial M_\pi^2}+\frac{1}{2}\frac{\partial}{\partial M_K^2}+\frac{1}{3}\frac{\partial}{\partial M_\eta^2}\right)\Sigma_q\,, \tag{H.1}$$

$$\hat{m}_s\frac{\partial}{\partial\hat{m}}\Sigma_q = M_{K\eta}^2\left(\frac{\partial}{\partial M_\pi^2}+\frac{1}{2}\frac{\partial}{\partial M_K^2}+\frac{1}{3}\frac{\partial}{\partial M_\eta^2}\right)\Sigma_q\,, \tag{H.2}$$

$$\hat{m}\frac{\partial}{\partial\hat{m}_s}\Sigma_q = M_\pi^2\left(\frac{1}{2}\frac{\partial}{\partial M_K^2}+\frac{2}{3}\frac{\partial}{\partial M_\eta^2}\right)\Sigma_q\,, \tag{H.3}$$

$$\hat{m}_s\frac{\partial}{\partial\hat{m}_s}\Sigma_q = M_{K\eta}^2\left(\frac{\partial}{\partial M_K^2}+\frac{4}{3}\frac{\partial}{\partial M_\eta^2}\right)\Sigma_q\,, \tag{H.4}$$

with $M_{K\eta}^2 = -M_K^2 + 3M_\eta^2/2\,.$

Below we give the exact expression for the typical type of derivatives

$$\begin{aligned}\hat{m}\frac{\partial}{\partial\hat{m}}\bar{\Sigma} = {} & \hat{m} - \frac{9g^2M_\pi^2}{64\pi}\left\{\frac{M_\pi}{F_\pi^2}+\frac{M_K}{3F_K^2}+\frac{M_\eta}{27F_\eta^2}\right\} - \frac{3g^2M_\pi^2}{32\pi^2 m}\left\{\frac{M_\pi^2}{F_\pi^2}+\frac{M_K^2}{3F_K^2}+\frac{M_\eta^2}{27F_\eta^2}\right\} \\ & -4c_1M_\pi^2 + \frac{3c_2}{64\pi^2}\left\{\frac{M_\pi^4}{F_\pi^2}+\frac{2}{3}\frac{M_K^4}{F_K^2}+\frac{M_\eta^4}{9\,F_\eta^2}\right\} - \frac{2}{3}c_5M_\pi^2 + 2\bar{e}_1M_\pi^2M^2 \\ & -\frac{\bar{e}_3}{6}M_\pi^2(M_K^2-M_\pi^2) + \frac{5}{12}\bar{e}_4M_\pi^4 - \frac{\bar{e}_5}{36}M_\pi^2(M_K^2-M_\pi^2)\,.\end{aligned} \tag{H.5}$$

One should note that there are additional useful relations between different sigma-terms [29, 35]. In particular, with the definitions of y_N and $\sigma_{KN}^{I=1}$ we can relate

KN and ηN sigma-terms to the πN sigma-term as

$$\sigma_{KN}^{u} = \sigma_{\pi N}(1+y_N)\frac{\hat{m}+m_s}{4\hat{m}} + \sigma_{KN}^{I=1}, \tag{H.6}$$

$$\sigma_{KN}^{d} = \sigma_{KN}^{u} - 2\sigma_{KN}^{I=1}, \tag{H.7}$$

$$\sigma_{\eta N} = \sigma_{\pi N}\frac{\hat{m}+2y_N m_s}{3\hat{m}}. \tag{H.8}$$

List of Figures

3.1 Lowest-order electron-nucleon scattering 21

3.2 G_E^p/G_D and $G_M^p/(\mu_p G_D)$ obtained by the Rosenbluth method . . . 25

3.3 The ratio $\mu_p G_E^p/G_M^p$ obtained from the Rosenbluth separation . . . 26

3.4 The ratio $\mu_p G_E^p/G_M^p$ obtained from polarization transfer measurements 27

3.5 Feynman diagrams for the two-photon exchange 27

3.6 The ratio $G_M^n/(\mu_n G_D)$ 28

3.7 The charge form factor of the neutron 28

4.1 Diagrams contributing to the mass shift of the nucleon 37

4.2 Diagrams contributing to the nucleon charge 47

4.3 Diagrams contributing to the charge and magnetic form factors of the baryon octet 48

4.4 Charge form factors $G_E^B(Q^2)$ for $B = p$, Σ^+, Σ^- and Ξ^- for a size parameter $R = 0.6$ fm compared to the dipole fit $G_D(Q^2)$ 53

4.5 Results for the neutron charge form factor $G_E^n(Q^2)$ for different values of $R = 0.55$, 0.6, and 0.65 fm 53

4.6 The charge form factors $G_E^B(Q^2)$ for $B = n$, Σ^0, Λ and Ξ^0 for $R =$ 0.6 fm 54

4.7 The magnetic form factors $G_M^B(Q^2)/\mu_B$ for $B = p$, Σ^+, Σ^- and Ξ^- at $R = 0.6$ fm 54

4.8 The magnetic form factors $G_M^B(Q^2)/\mu_B$ for $B = n$, Σ^0, Λ and Ξ^0 at $R = 0.6$ fm 55

4.9 Q^2 dependence of the transverse helicity amplitude $A_{1/2}(Q^2)$ for the case where the quark propagator is truncated to the ground state (GS) contribution 59

4.10 Q^2 dependence of the total transverse helicity amplitude $A_{1/2}(Q^2)$. 60

4.11 Total results for the transverse helicity amplitudes $A_{1/2}(Q^2)$ and $A_{3/2}(Q^2) = \sqrt{3}\, A_{1/2}(Q^2)$ 60

5.1 Diagrams including pseudoscalar meson contributions to the EM quark transition operator up to fourth order 70

5.2 Diagrams including vector-meson contributions to the EM quark transition operator 71

5.3 Diagrams contributing to the mass operator of the quark at one loop 78

5.4 Ratio $G_E^p(Q^2)/G_D(Q^2)$ 95

5.5 Ratio $G_M^p(Q^2)/(\mu_p\, G_D(Q^2))$ 95

5.6 Ratio $G_M^n(Q^2)/(\mu_n\, G_D(Q^2))$ 96

5.7 Ratio $\mu_p G_E^p(Q^2)/G_M^p(Q^2)$ 96

5.8 The charge and magnetic form factors of the nucleon and the contribution due to the meson cloud 97

5.9 The meson cloud contribution to the nucleon charge and magnetic form factors 98

5.10 The charge density of the nucleon $\rho_E^N(r)$ and $r^2\, \rho_E^N(r)$ 99

5.11 The magnetization density of the nucleon $\rho_M^N(r)$ and $r^2\, \rho_M^N(r)$ . . . 100

5.12 The charge density of meson cloud contribution to the nucleon $\rho_E^{N,\mathrm{cloud}}(r)$ and $r^2\, \rho_E^{N,\mathrm{cloud}}(r)$ 101

5.13 The magnetization density of meson cloud contribution to the nucleon $\rho_M^{N,\mathrm{cloud}}(r)$ and $r^2\, \rho_M^{N,\mathrm{cloud}}(r)$ 102

5.14 Diagrams contributing to the quark operator describing the stong interaction of vector mesons with quarks 103

List of Tables

4.1 Results for the magnetic moments μ_B of the baryon octet (in units of the nucleon magneton μ_N) 51

4.2 Results for the charge radii squared $\langle r_E^2 \rangle^B$ of the baryon octet (in units of fm^2) 51

4.3 Results for the magnetic radii squared $\langle r_M^2 \rangle^B$ of the baryon octet (in units of fm^2) 52

4.4 Contributions of the individual diagrams to the transverse helicity amplitudes for $Q^2 = 0$ (in units of 10^{-3} GeV$^{-1/2}$) 58

4.5 Absolute contributions of π, K and η to $A_{1/2}(Q^2 = 0)$ for the meson-cloud (MC) and vertex-correction (VC) diagrams 58

4.6 Total result for the helicity amplitudes $A_{1/2}(Q^2 = 0)$ and $A_{3/2}(Q^2 = 0)$ in comparison to other theoretical models 59

5.1 SU(6) couplings α_E^{Bi} and α_M^{Bi} 87

5.2 Magnetic moments of the baryon octet (in units of the nucleon magneton μ_N) 89

5.3 Comparison of the parameters of phenomenological ansatz in Ref. [131] 94

Bibliography

[1] M. K. Jones *et al.* [Jefferson Lab Hall A Collaboration], Phys. Rev. Lett. **84**, 1398 (2000) [arXiv:nucl-ex/9910005].

[2] O. Gayou *et al.* [Jefferson Lab Hall A Collaboration], Phys. Rev. Lett. **88**, 092301 (2002) [arXiv:nucl-ex/0111010].

[3] V. Punjabi *et al.*, Phys. Rev. C **71**, 055202 (2005) [Erratum-ibid. C **71**, 069902 (2005)] [arXiv:nucl-ex/0501018];

[4] M. Gell-Mann, Phys. Lett. **8**, 214 (1964).

[5] G. Zweig, CERN-8419-TH-412, 1964.

[6] A. Pich and J. Prades, Nucl. Phys. Proc. Suppl. **86**, 236 (2000) [arXiv:hep-ph/9909559].

[7] K. Maltman, Phys. Lett. B **462**, 195 (1999) [arXiv:hep-ph/9904370].

[8] S. Weinberg, PhysicaA **96**, 327 (1979).

[9] J. Gasser and H. Leutwyler, Annals Phys. **158**, 142 (1984);

[10] J. Gasser and H. Leutwyler, Nucl. Phys. B **250**, 465 (1985).

[11] J. Gasser, M. E. Sainio and A. Švarc, Nucl. Phys. B **307** 779 (1988).

[12] E. Jenkins and A. V. Manohar, Phys. Lett. B **255** 558 (1991); V. Bernard, N. Kaiser, J. Kambor and U. G. Meissner, Nucl. Phys. B **388** 315 (1992).

[13] T. Becher and H. Leutwyler, Eur. Phys. J. C **9** 643 (1999) [arXiv:hep-ph/9901384]; JHEP **0106** 017 (2001) [arXiv:hep-ph/0103263].

[14] P. J. Ellis and H. B. Tang, Phys. Rev. C **57** 3356 (1998) [arXiv:hep-ph/9709354] H. B. Tang, arXiv:hep-ph/9607436.

[15] J. Gegelia and G. Japaridze, Phys. Rev. D **60**, 114038 (1999) [arXiv:hep-ph/9908377].

[16] M. R. Schindler, J. Gegelia and S. Scherer, Phys. Lett. B **586**, 258 (2004) [arXiv:hep-ph/0309005].

[17] T. Fuchs, J. Gegelia, G. Japaridze and S. Scherer, Phys. Rev. D **68**, 056005 (2003) [arXiv:hep-ph/0302117]; Eur. Phys. J. A **19**, 35 (2004) [arXiv:hep-ph/0309234].

[18] T. Fuchs, M. R. Schindler, J. Gegelia and S. Scherer, Phys. Lett. B **575**, 11 (2003) [arXiv:hep-ph/0308006].

[19] M. R. Schindler, J. Gegelia and S. Scherer, Eur. Phys. J. A **26**, 1 (2005) [arXiv:nucl-th/0509005].

[20] B. Kubis and U. G. Meissner, Nucl. Phys. A **679** 698 (2001) [arXiv:hep-ph/0007056].

[21] B. Kubis and U. G. Meissner, Eur. Phys. J. C **18** 747 (2001) [arXiv:hep-ph/0010283].

[22] J. L. Goity, D. Lehmann, G. Prezeau and J. Saez, Phys. Lett. B **504** 21 (2001) [arXiv:hep-ph/0101011]; D. Lehmann and G. Prezeau, Phys. Rev. D **65** 016001 (2002) [arXiv:hep-ph/0102161].

[23] A. Chodos, R. L. Jaffe, K. Johnson, C. B. Thorn and V. F. Weisskopf, Phys. Rev. D **9**, 3471 (1974).

[24] S. Théberge, A. W. Thomas and G. A. Miller, Phys. Rev. D **22** 2838 (1980) [Erratum-ibid. D **23** 2106 (1981)]; Phys. Rev. D **24** 216 (1981); S. Théberge and A. W. Thomas, Nucl. Phys. A **393** 252 (1983); A. W. Thomas, Adv. Nucl. Phys. **13** 1 (1984).

[25] E. Oset, R. Tegen and W. Weise, Nucl. Phys. A **426** 456 (1984) [Erratum-ibid. A **453** 751 (1986)]; R. Tegen, Annals Phys. **197** 439 (1990); S. A. Chin, Nucl. Phys. A **382** 355 (1982).

[26] T. Gutsche and D. Robson, Phys. Lett. B **229**, 333 (1989);

[27] D. Diakonov and V. Y. Petrov, Nucl. Phys. B **245** 259 (1984); Nucl. Phys. B **272** 457 (1986); D. Diakonov, V. Y. Petrov and M. Praszalowicz, Nucl. Phys. B **323** 53 (1989).

[28] T. Gutsche, Ph.D. thesis, Florida State University, 1987.

[29] V. E. Lyubovitskij, T. Gutsche, A. Faessler and E. G. Drukarev, Phys. Rev. D **63**, 054026 (2001) [arXiv:hep-ph/0009341].

[30] V. E. Lyubovitskij, T. Gutsche and A. Faessler, Phys. Rev. C **64** 065203 (2001) [arXiv: hep-ph/0105043].

[31] V. E. Lyubovitskij, T. Gutsche, A. Faessler and R. Vinh Mau, Phys. Lett. B **520** 204 (2001) [arXiv:hep-ph/0108134];

[32] V. E. Lyubovitskij, P. Wang, T. Gutsche and A. Faessler, Phys. Rev. C **66** 055204 (2002) [arXiv:hep-ph/0207225];

[33] K. Pumsa-ard, V. E. Lyubovitskij, T. Gutsche, A. Faessler and S. Cheedket, Phys. Rev. C **68**, 015205 (2003) [arXiv:hep-ph/0304033].

[34] S. Cheedket, V. E. Lyubovitskij, T. Gutsche, A. Faessler, K. Pumsa-ard and Y. Yan, Eur. Phys. J. A **20**, 317 (2004) [arXiv:hep-ph/0212347].

[35] T. Inoue, V. E. Lyubovitskij, T. Gutsche and A. Faessler, Phys. Rev. C **69**, 035207 (2004) [arXiv:hep-ph/0311275].

[36] K. Khosonthongkee, V. E. Lyubovitskij, T. Gutsche, A. Faessler, K. Pumsa-ard, S. Cheedket and Y. Yan, J. Phys. G **30**, 793 (2004) [arXiv:hep-ph/0403119].

[37] Y. B. Dong, A. Faessler, T. Gutsche, J. Kuckei, V. E. Lyubovitskij, K. Pumsa-ard and P. Shen, J. Phys. G **32**, 203 (2006) [arXiv:hep-ph/0507277].

[38] A. Faessler, T. Gutsche, V. E. Lyubovitskij and K. Pumsa-Ard, Prog. Part. Nucl. Phys. **55**, 12 (2005).

[39] A. Faessler, T. Gutsche, V. E. Lyubovitskij and K. Pumsa-ard, Phys. Rev. D **73**, 114021 (2006) [arXiv:hep-ph/0511319].

[40] R. Frisch and O. Stern, Z. Phys. **85**, 4 (1933).

[41] I. Estermann and O. Stern, Z. Phys. **85**, 17 (1933).

[42] J. M. B. Kellogg, I. I. Rabi, N. F. Ramsey and J. R. Zacharias, Phys. Rev. **56** 728 (1939).

[43] S. Eidelman *et al.* [Particle Data Group Collaboration], Phys. Lett. B **592** 1 (2004).

[44] M. N. Rosenbluth, Phys. Rev. **79** 615 (1950).

[45] R. Hofstadter, F. Bumiller and M. Croissiaux, Phys. Rev. Lett. **5** 263 (1960).

[46] L. N. Hand, D. G. Miller and R. Wilson, Rev. Mod. Phys. **35**, 335 (1963).

[47] L. Andivahis *et al.*, Phys. Rev. D **50**, 5491 (1994).

[48] R. C. Walker *et al.*, Phys. Rev. D **49** 5671 (1994).

[49] G. Hohler, E. Pietarinen, I. Sabba Stefanescu, F. Borkowski, G. G. Simon, V. H. Walther and R. D. Wendling, Nucl. Phys. B **114**, 505 (1976).

[50] L. E. Price, J. R. Dunning, M. Goitein, K. Hanson, T. Kirk and R. Wilson, Phys. Rev. D **4**, 45 (1971).

[51] A. F. Sill *et al.*, Phys. Rev. D **48**, 29 (1993).

[52] D. Day, Nucl. Phys. A **755**, 151 (2005) [arXiv:nucl-ex/0502003].

[53] A. I. Akhiezer, L. N. Rozentsweig and I. M. Shmushkevich, Sov. Phys. JETP **6**, 588 (1958).

[54] R. G. Arnold, C. E. Carlson and F. Gross, Phys. Rev. C **23**, 363 (1981).

[55] T. Janssens, R. Hofstadter, E. B. Hughes and M. R. Yearian, Phys. Rev. **142**, 922 (1966).

[56] W. Bartel *et al.*, Phys. Rev. Lett. **17**, 608 (1966).

[57] J. Litt *et al.*, Phys. Lett. B **31**, 40 (1970).

[58] C. Berger, V. Burkert, G. Knop, B. Langenbeck and K. Rith, Phys. Lett. B **35**, 87 (1971).

[59] C. E. Hyde-Wright and K. de Jager, Ann. Rev. Nucl. Part. Sci. **54**, 217 (2004) [arXiv:nucl-ex/0507001].

[60] B. D. Milbrath *et al.* [Bates FPP collaboration], Phys. Rev. Lett. **80**, 452 (1998) [Erratum-ibid. **82**, 2221 (1999)] [arXiv:nucl-ex/9712006].

[61] T. Pospischil *et al.* [A1 Collaboration], Eur. Phys. J. A **12**, 125 (2001).

[62] S. Dieterich *et al.*, Phys. Lett. B **500**, 47 (2001) [arXiv:nucl-ex/0011008].

[63] J. Arrington, Phys. Rev. C **68**, 034325 (2003) [arXiv:nucl-ex/0305009].

[64] M. E. Christy *et al.* [E94110 Collaboration], Phys. Rev. C **70**, 015206 (2004) [arXiv:nucl-ex/0401030].

[65] I. A. Qattan *et al.*, Phys. Rev. Lett. **94**, 142301 (2005) [arXiv:nucl-ex/0410010].

[66] L. W. Mo and Y. S. Tsai, Rev. Mod. Phys. **41**, 205 (1969).

[67] P. G. Blunden, W. Melnitchouk and J. A. Tjon, Phys. Rev. Lett. **91**, 142304 (2003) [arXiv:nucl-th/0306076].

[68] Y. C. Chen, A. Afanasev, S. J. Brodsky, C. E. Carlson, and M. Vanderhaeghen, Phys. Rev. Lett. **93**, 122301 (2004).

[69] H. Anklin *et al.*, Phys. Lett. B **336**, 313 (1994).

[70] H. Anklin *et al.*, Phys. Lett. B **428**, 248 (1998).

[71] G. Kubon *et al.*, Phys. Lett. B **524**, 26 (2002) [arXiv:nucl-ex/0107016].

[72] E. E. W. Bruins *et al.*, Phys. Rev. Lett. **75**, 21 (1995).

[73] H. Gao *et al.*, Phys. Rev. C **50**, 546 (1994);

[74] W. Xu *et al.*, Phys. Rev. Lett. **85**, 2900 (2000) [arXiv:nucl-ex/0008003].

[75] W. Xu *et al.* [Jefferson Lab E95-001 Collaboration], Phys. Rev. C **67**, 012201 (2003) [arXiv:nucl-ex/0208007].

[76] S. Galster, H. Klein, J. Moritz, K. H. Schmidt, D. Wegener and J. Bleckwenn, Nucl. Phys. B **32**, 221 (1971).

[77] R. G. Arnold *et al.*, Phys. Rev. Lett. **61**, 806 (1988).

[78] S. Rock *et al.*, Phys. Rev. D **46**, 24 (1992).

[79] A. Lung *et al.*, Phys. Rev. Lett. **70**, 718 (1993).

[80] P. Markowitz *et al.*, Phys. Rev. C **48**, 5 (1993).

[81] T. Eden *et al.*, Phys. Rev. C **50**, 1749 (1994).

[82] I. Passchier *et al.*, Phys. Rev. Lett. **82**, 4988 (1999) [arXiv:nucl-ex/9907012].

[83] C. Herberg *et al.*, Eur. Phys. J. A **5**, 131 (1999).

[84] M. Ostrick *et al.*, Phys. Rev. Lett. **83**, 276 (1999).

[85] R. Madey *et al.* [E93-038 Collaboration], Phys. Rev. Lett. **91**, 122002 (2003) [arXiv:nucl-ex/0308007].

[86] D. I. Glazier *et al.*, Eur. Phys. J. A **24**, 101 (2005) [arXiv:nucl-ex/0410026].

[87] G. Warren *et al.* [Jefferson Lab E93-026 Collaboration], Phys. Rev. Lett. **92**, 042301 (2004) [arXiv:nucl-ex/0308021].

[88] H. Zhu *et al.* [E93026 Collaboration], Phys. Rev. Lett. **87**, 081801 (2001) [arXiv:nucl-ex/0105001].

[89] C. E. Jones-Woodward *et al.*, Phys. Rev. C **44**, 571 (1991).

[90] J. Becker *et al.*, Eur. Phys. J. A **6**, 329 (1999).

[91] J. Golak, G. Ziemer, H. Kamada, H. Witala and W. Gloeckle, Phys. Rev. C **63**, 034006 (2001) [arXiv:nucl-th/0008008].

[92] J. Bermuth *et al.*, Phys. Lett. B **564**, 199 (2003) [arXiv:nucl-ex/0303015].

[93] D. Rohe *et al.*, Phys. Rev. Lett. **83**, 4257 (1999).

[94] M. Gell-Mann and F. Low, Phys. Rev. **84**, 350 (1951).

[95] J. Goldstone, Proceed. Roy. Soc. A **239**, 267 (1957).

[96] J. Hubbard, Proceed. Roy. Soc. A **240**, 539 (1957).

[97] R. Tegen, R. Brockmann and W. Weise, Z. Phys. A **307**, 339 (1982).

[98] K. Hagiwara *et al.* [Particle Data Group], Phys. Rev. D **66**, 010001 (2002).

[99] M. Gell-Mann and M. Levy, Nuovo Cim. **16**, 1729 (1960).

[100] I. Eschrich *et al.* [SELEX Collaboration], Phys. Lett. B **522**, 233 (2001) [arXiv:hep-ex/0106053].

[101] G. G. Simon, F. Borkowski, C. Schmitt and V. H. Walther, Z. Naturforsch. **35A**, 1 (1980).

[102] M. Meyerhoff *et al.*, Phys. Lett. B **327**, 201 (1994).

[103] L. A. Copley, G. Karl and E. Obryk, Nucl. Phys. B **13**, 303 (1969).

[104] R. Koniuk and N. Isgur, Phys. Rev. D **21**, 1868 (1980) [Erratum-ibid. D **23**, 818 (1981)].

[105] M. M. Giannini, Rept. Prog. Phys. **54**, 453 (1990).

[106] A. J. Buchmann, E. Hernandez and A. Faessler, Phys. Rev. C **55**, 448 (1997) [arXiv:nucl-th/9610040].

[107] A. J. Buchmann, Z. Naturforsch. A **52**, 877 (1997).

[108] G. Kaelbermann and J. M. Eisenberg, Phys. Rev. D **28** (1983) 71.

[109] K. Bermuth, D. Drechsel, L. Tiator and J. B. Seaborn, Phys. Rev. D **37**, 89 (1988).

[110] D. H. Lu, A. W. Thomas and A. G. Williams, Phys. Rev. C **55**, 3108 (1997) [arXiv:nucl-th/9612017].

[111] Y. B. Dong, K. Shimizu and A. Faessler, Nucl. Phys. A **689**, 889 (2001).

[112] N. Isgur, G. Karl and R. Koniuk, Phys. Rev. D **25**, 2394 (1982).

[113] S. S. Gershtein and G. V. Jikia, Sov. J. Nucl. Phys. **34**, 870 (1981) [Yad. Fiz. **34**, 1566 (1981)].

[114] D. Drechsel and M. M. Giannini, Phys. Lett. B **143**, 329 (1984).

[115] E. Jenkins, X. d. Ji and A. V. Manohar, Phys. Rev. Lett. **89**, 242001 (2002) [arXiv:hep-ph/0207092].

[116] C. Dib, A. Faessler, T. Gutsche, S. Kovalenko, J. Kuckei, V. E. Lyubovitskij and K. Pumsa-ard, J. Phys. G **32**, 547 (2006) [arXiv:hep-ph/0601144].

[117] T. Inoue, V. E. Lyubovitskij, T. Gutsche and A. Faessler, Int. J. Mod. Phys. E **14**, 995 (2005) [arXiv:hep-ph/0407305].

[118] T. Inoue, V. E. Lyubovitskij, T. Gutsche and A. Faessler, Int. J. Mod. Phys. E **15**, 121 (2006) [arXiv:hep-ph/0404051].

[119] V. E. Lyubovitskij, T. Gutsche, A. Faessler and R. Vinh Mau, Phys. Rev. C **65**, 025202 (2002) [arXiv:hep-ph/0109213].

[120] A. Manohar and H. Georgi, Nucl. Phys. B **234** 189 (1984).

[121] B. Kubis, T. R. Hemmert and U. G. Meissner, Phys. Lett. B **456**, 240 (1999) [arXiv:hep-ph/9903285].

[122] N. Fettes, U. G. Meissner and S. Steininger, Nucl. Phys. A **640** 199 (1998) [arXiv:hep-ph/9803266].

[123] G. Ecker, J. Gasser, A. Pich and E. de Rafael, Nucl. Phys. B **321** 311 (1989); G. Ecker, J. Gasser, H. Leutwyler, A. Pich and E. de Rafael, Phys. Lett. B **223** 425 (1989).

[124] R. L. Jaffe and X. D. Ji, Phys. Rev. Lett. **67**, 552 (1991);

[125] M. A. B. Bég and A. Zepeda, Phys. Rev. D **6** 2912 (1972).

[126] H. Hellmann, Einführung in die Quantenchemie (Deuticke Verlag, Leipzig, 1937); R. P. Feynman, Phys. Rev. **56** 340 (1939).

[127] S. Weinberg, Phys. Rev. Lett. **67**, 3473 (1991); **65**, 1181 (1990); S. Peris, Phys. Rev. D **46**, 1202 (1992); D. A. Dicus, D. Minic, U. van Kolck and R. Vega, Phys. Lett. B **284**, 384 (1992); S. Peris and E. de Rafael, Phys. Lett. B **309**, 389 (1993) [arXiv:hep-ph/9304262]; W. Broniowski, A. Steiner and M. Lutz, Phys. Rev. Lett. **71** 1787 (1993) [arXiv:hep-ph/9304292].

[128] B. Borasoy and U. G. Meissner, Annals Phys. **254**, 192 (1997) [arXiv:hep-ph/9607432].

[129] M. Frink, U. G. Meissner and I. Scheller, Eur. Phys. J. A **24**, 395 (2005) [arXiv:hep-lat/0501024].

[130] J. J. Kelly, Phys. Rev. C **66** 065203 (2002) [arXiv:hep-ph/0204239].

[131] J. Friedrich and T. Walcher, Eur. Phys. J. A **17** 607 (2003) [arXiv:hep-ph/0303054].

[132] S. J. Brodsky, J. R. Hiller, D. S. Hwang and V. A. Karmanov, Phys. Rev. D **69**, 076001 (2004) [arXiv:hep-ph/0311218].

[133] A. V. Belitsky, X. d. Ji and F. Yuan, Phys. Rev. Lett. **91**, 092003 (2003) [arXiv:hep-ph/0212351].

[134] I. Sick, Phys. Lett. B **576**, 62 (2003) [arXiv:nucl-ex/0310008].

[135] G. G. Simon, C. Schmitt, F. Borkowski and V. H. Walther, Nucl. Phys. A **333**, 381 (1980).

[136] K. M. Hanson, J. R. Dunning, M. Goitein, T. Kirk, L. E. Price and R. Wilson, Phys. Rev. D **8**, 753 (1973).

[137] W. Bartel *et al.*, Nucl. Phys. B **58**, 429 (1973).

[138] S. Rock *et al.*, Phys. Rev. Lett. **49**, 1139 (1982).

[139] R. Schiavilla and I. Sick, Phys. Rev. C **64**, 041002 (2001) [arXiv:nucl-ex/0107004].

[140] J. Gasser, Annals Phys. **136**, 62 (1981).

[141] J. J. de Swart, Rev. Mod. Phys. **35**, 916 (1963).

Acknowledgement

I am extremely grateful to Prof. Dr. Dr. h. c. mult. Amand Faessler for his guidance and support of my work. Special thanks go to, particularly, Prof. Dr. Thomas Gutsche and Dr. Valery Lyubovitskij for their constant guidance and substantial discussions. I would like to acknowledge my former colleagues, Dr. Sampart Cheedket, Dr. Khanchai Khosonthongkee and Dr. Ping Wang for their constructive discussions. I am grateful to the Development and Promotion of Science and Technology talents project (DPST) scholarship conducted jointly by the Royal Thai Government Agencies and the Institute for the Promotion of teaching Science and Technology (IPST) Thailand for financial support. I would like to give my special thanks to Asien-Haus Tübingen shop and all the staff there for always providing good Thai food and for all their support. Finally, I would like to deeply thank my family for all the support and cheerfulness.

Curriculum Vitae

KEM PUMSA-ARD

Institut für Theoretische Physik
Universität Tübingen
Auf der Morgenstelle 14
D-72076 Tübingen, Germany
E-mail: pumsa@tphys.physik.uni-tuebingen.de

Personal Particulars

Date of Birth:	July 22, 1975
Place of Birth:	Bangkok, Thailand
Marital Status:	Single

Education

May 1982 - Feb. 1988	Anubal Phra Nakorn Sri Ayutthaya School (Ayutthaya, Thailand)
May 1988 - Feb. 1991	Ayutthaya Teacher College Demonstration School (Ayutthaya, Thailand)
May 1991 - Feb. 1994	Samsen Witthayalai School (Bangkok, Thailand)
July 1994 - March 1998	Department of Physics, Mahidol University (Bangkok, Thailand) B.Sc. Degree in Physics
May 1998 - Aug. 2000	School of Physics, Suranaree University of Technology (Nakorn Ratchasima, Thailand) M.Sc. Degree in Physics *Proton-Proton High-Energy Elastic Scattering in Meson Exchange Model*
Feb. 2001 - July 2006	Institute of Theoretical Physics, University of Tübingen, Ph.D thesis title: *Chiral Dynamics of Baryons in the Perturbative Chiral Quark Model* (advisors Prof. Dr. Dr. h. c. mult. Amand Faessler and Prof. Dr. Thomas Gutsche)

Scholarships and Employment

May 1991 - Oct. 2005	The Development and Promotion of Science and Technology talents project (DPST) scholarship conducted jointly by the Royal Thai Government Agencies and the Institute for the Promotion of teaching Science and Technology (IPST) Thailand
Jan. 2006 - May 2006	Employment through EU-Project I3HP

Academic Teachers

Physics	T. Boonyarith, R. Hoonsawat, S. Leelaprute, K. Arayathanitkul, P. Sithikong, S. Varamit, S. Chollatharnrat, T. Kerdcharoen, W. Prachyabrued, C. Laowattanakul, S. Wangsuya, I-Ming Tang, M. A. Allen, Y. Yan, E. B. Manoukian, S. Phatisena, Amand Faessler, Th. Gutsche, V. E. Lyubovitskij, P. Grabmayr

List of Publications

- K. Pumsa-ard, V. E. Lyubovitskij, T. Gutsche, A. Faessler and S. Cheedket, "Electromagnetic nucleon Delta transition in the perturbative chiral quark model," Phys. Rev. C **68**, 015205 (2003) [arXiv:hep-ph/0304033].
- Y. Yan, K. Pumsa-ard, R. Tegen, T. Gutsche, V. E. Lyubovitskij and A. Faessler, "Nucleon nucleon high-energy scattering," Int. J. Mod. Phys. E **12** (2003) 367.
- S. Cheedket, V. E. Lyubovitskij, T. Gutsche, A. Faessler, K. Pumsa-ard and Y. Yan, "Electromagnetic form factors of the baryon octet in the perturbative chiral quark model," Eur. Phys. J. A **20**, 317 (2004) [arXiv:hep-ph/0212347].
- K. Khosonthongkee, V. E. Lyubovitskij, T. Gutsche, A. Faessler, K. Pumsa-ard, S. Cheedket and Y. Yan, "Axial form factor of the nucleon in the perturbative chiral quark model," J. Phys. G **30**, 793 (2004) [arXiv:hep-ph/0403119].
- Y.B. Dong, A. Faessler, T. Gutsche, J. Kuckei, V. E. Lyubovitskij, K. Pumsa-ard and P. Shen, "Nucleon polarizabilities in the perturbative chiral quark model," J. Phys. G **32**, 203 (2006) [arXiv:hep-ph/0507277].
- A. Faessler, T. Gutsche, V. E. Lyubovitskij and K. Pumsa-ard, "Chiral dynamics of baryons in a covariant quark model," Prog. Part. Nucl. Phys. **55**, 12 (2005).
- C. Dib, A. Faessler, T. Gutsche, S. Kovalenko, J. Kuckei, V. E. Lyubovitskij and K. Pumsa-ard, "The neutron electric dipole form factor in the perturbative chiral quark model," J. Phys. G **32**, 547 (2006) [arXiv:hep-ph/0601144].
- K. Pumsa-ard, W. Uchai and Y. Yan, "Meson exchange theory for high energy proton-proton scattering," Int. J. Mod. Phys. E **15**, 109 (2006).
- A. Faessler, T. Gutsche, M. A. Ivanov, J. G. Korner, V. E. Lyubovitskij, D. Nicmorus and K. Pumsa-ard, "Magnetic moments of heavy baryons in the relativistic three-quark model," Phys. Rev. D **73**, 094013 (2006) [arXiv:hep-ph/0602193].
- J. Kuckei, C. Dib, A. Faessler, T. Gutsche, S. Kovalenko, V. E. Lyubovitskij and K. Pumsa-ard, "Strong CP violation and the neutron electric dipole form factor," to be published in Phys. Atom. Nucl. [arXiv:hep-ph/0510116].
- A. Faessler, T. Gutsche, V. E. Lyubovitskij and K. Pumsa-ard, "Chiral dynamics of baryons in a Lorentz covariant quark model," Phys. Rev. D **73**, 114021 (2006) [arXiv:hep-ph/0511319].